The Development of Molecular Probes for the *in vitro* and *in vivo* Study of Glucocerebrosidase

By

Daniel Tesolin

A Thesis submitted to

The Department of Chemistry

Faculty of Science and Environmental Studies

Lakehead University

In partial fulfillment of the requirements for the degree of

Master of Science

March 2017

Abstract

Parkinson's Disease (PD) is one of the most common neurodegenerative diseases in the world. Despite its prevalence, the disease is difficult to diagnose early with the vast majority of individuals already having significant neuronal death prior to therapeutic intervention. PD is characterized by the lysosome's unusual inability to dispose of α-synuclein in areas of the brain that primarily control motor function. Recently, studies have shown that in post-mortem brain samples from suspected PD patients, there is a deficiency in the activity of the lysosomal enzyme glucocerebrosidase (GCase). GCase is a retaining β-glucosidase that hydrolyzes glucosylceramide in the lysosomes of normal cells. Interestingly, deficiency in enzyme activity was found in both early or late stages of the disease suggesting that GCase could be a biomarker of early PD. To validate GCase as a potential biomarker this thesis focuses on the development of molecular probes for the detection of GCase activity in biological systems. Recently the Phenix lab has developed a class of *N*-alkylated conduritol aziridines that were shown to be potent and selective irreversible inhibitors of GCase *in vitro*. A new synthesis pathway has been developed to synthesize these compounds more efficiently and which can be adaptable for producing fluorescent derivatives for *in vitro* imaging and radioactive derivatives for *in vivo* imaging. Two new fluorescent derivatives have been developed as well two fluorinated derivatives for future radiolabelling. The development of techniques to radiolabel these compounds is shown in this work. Future work will be done to optimize radiolabelling and test these molecular probes for imaging GCase in biologically relevant systems to validate it as a biomarker for PD.

Acknowledgements

I would like to thank my supervisor Dr. Chris Phenix for his generous teaching and guidance over the many years I have known him. He is always available to have a discussion about my results and point me in the right direction. He treated me with respect and was always more confident in my abilities than I was. I would especially like to thank him for not giving up on me even amongst the transitionary period that occurred as his group moved across the country.

I would like to thank my fellow lab members for their assistance and willingness to always help. They were always available to ask questions and give me the time I needed to learn. Especially appreciated is the guidance of Dr. Morshed Chowdhury and Dr. Shusheng Wang for their vast knowledge of chemistry and biology. Dr. Shusheng Wang deserves particular thanks for doing some cell studies with my compounds for me. Thank you to Brady Vigliarolo for helping me understand the graduate student experience and for always keeping me positive when things were not working out. Also thanks to Ashley Esarik for teaching me how to operate the automatic synthesis units at the cyclotron and for helping me with my enzyme kinetics.

Thank you to all the staff at the Cyclotron facility for helping me troubleshoot and for always trying to help my research go as smoothly as possible. You never asked for anything but always gave me all you could. Especially Dr. Michael Campbell for many hours assisting me troubleshoot the automated synthesis units and my radiochemical reactions. I know a lot of experiments failed but I learned so much. Thank you also Dr. Campbell for being on my committee.

Thank you to my other committee member Dr. Christine Gottardo for her amazing compassion and guidance during my graduate student experience. She truly helped me feel part of the community despite my lab's physical detachment from the University. Her Organic Chemistry class did more for me than I think she knows and she was always available for answering chemistry or degree related questions.

I would also like to thank Benjamin Adams for his work on the *N*-alkylated conduritol aziridines. Without his hard work I would not have a lead compound to work from or a synthesis to base mine off of. You truly laid down the ground work for my project.

Thank you to all other TBRHRI and Lakehead University students and staff that became my friends, mentors and colleagues over the years. My experience was enriched because of you all.

Table of Contents

List of Tables

List of Figures

List of Schemes

List of Abbreviations

^{18}F	Fluorine – 18
2,4-DNP-β-D-Glc	2,4-dinitrophenyl-β-D-glucose
Ac	Acetate
BBB	Blood brain barrier
Bn	Benzyl ether
Bz	Benzoate
Calcd	Calculated
CBE	Conduritol-B-Epoxide
CD_3OD	Deuterated Methanol
$CDCl_3$	Deuterated Chloroform
CH_2Cl_2	Dichloromethane
CH_3CN	Acetonitrile
$CHCl_3$	Chloroform
CT	Computed Tomography
DMF	Dimethylformamide
DMSO	Dimethyl sulfoxide
Em_{max}	Emission Maximum Wavelength
ER	Endoplasmic Reticulum
ESI	Electrospray Ionisation
EtOAc	Ethyl Acetate
EtOH	Ethanol
Ex_{max}	Excitation Maximum Wavelength
FDG	2-deoxy-2-fluoro-D-glucose
FIB	4-fluoro-iodobenzene
GBA1	Gene expressing GCase
GBA2	β-glucosidase cousin of GCase compartmentalized in the cytoplasm
GBA3	β-glucosidase cousin of GCase compartmentalized in the cytoplasm

GCase	Glucocerebrosidase
GBq	Giga Becquerel
Glu	Glutamic Acid
HCl	Hydrochloric acid
Hex	Hexanes
HPLC	High Performance Liquid Chromatography
HRMS	High Resolution Mass Spectrometry
IC_{50}	Concentration of inhibitor required to reduce a enzymatic activity by half
K2.2.2	4,7,13,16,21,24-Hexaoxa-1,10-diazabicyclo[8.8.8]hexacosane (Kryptofix®)
K_2CO_3	Potassium Carbonate
K_i	Dissociation constant for the enzyme-inhibitor complex
k_i	Rate constant of inactivation
k_i/K_i	Overall measure of the efficiency of an inhibitor
k_{obs}	Observed pseudo-first order rate constant
$LiAlH_4$	Lithium Aluminum Hydride
LIMP2	Lysosome Membrane Protein 2
LRMS	Low Resolution Mass Spectrometry
MeOH	Methanol
Mesyl	Methanesulfonyl
MOM	Methoxymethyl ether
MRI	Magnetic Resonance Imaging
mRNA	Messenger Ribonucleic Acid
Na_2SO_4	Sodium Sulfate
$NaHCO_3$	Sodium Bicarbonate
NaN_3	Sodium Azide
NaOH	Sodium Hydroxide
NMR	Nuclear Magnetic Resonance
PD	Parkinson's Disease

Pd/C	Palladium over Carbon support
PET	Positron Emission Tomography
Ph_3P	Triphenylphosphine
QMA	Quaternary Ammonium Exchange Column
R_f	Retention factor
SDS	Sodium Dodecyl Sulfate
SDS-PAGE	Sodium Dodecyl Sulfate Polyacrylamide Gel Electrophoresis
S_N2	Nucleophilic bimolecular reaction
SPECT	Single Photon Emission Computed Tomography
TBAF	Tetrabutyl ammonium fluoride
TBS	tert-Butyldimethylsilyl ether
TBSCl	tert-Butyldimethylsilyl chloride
TBSOTf	tert-Butyldimethylsilyl triflate
TEA	Triethylamine
TEAB	Tetraethyl ammonium bicarbonate
TEAF	Tetraethyl ammonium fluoride
TFA	Trifluoroacetic Acid
THF	Tetrahydrofuran
TLC	Thin Layer Chromatography
TMSBr	Bromotrimethylsilane
TOF	Time of Flight
Tosyl	4-Toulenesulfonyl
UV	Ultraviolet

Introduction

Glucocerebrosidase

Glucocerebrosidase (GCase) is a lysosomal enzyme that catalyzes the hydrolysis of the β-glucosyl linkage in the natural substrate glucosylceramide (Figure 1). GCase is classified as a retaining β-glucosidase meaning it has specificity for cleaving β-glucosyl linkages and the β configuration of the resulting glucose is retained after cleavage.[1]

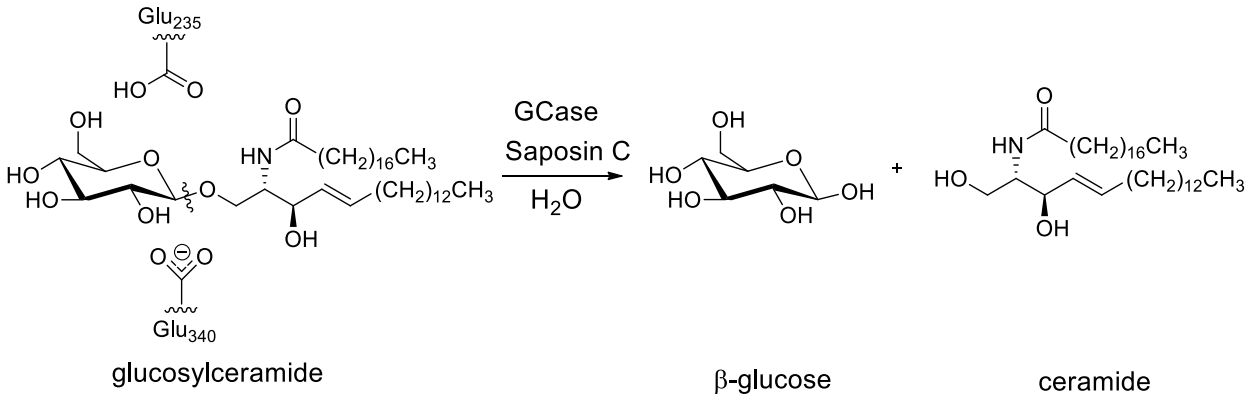

Figure 1: The hydrolysis of glucosylceramide by lysosomal retaining β-glucosidase GCase. The hydrolysis is catalyzed by glutamic acid residues 235 and 340. A complex with co-enzyme Saposin C is required for catalysis.

The mechanism of action for substrate hydrolysis by GCase has been elucidated through the study of X-ray crystal structures and studies done with irreversible active site inhibitors.[2] Studies have shown that the active site of GCase contains two catalytic glutamic acid residues, Glu_{235} and Glu_{340}, which are involved in a two-step double displacement mechanism for the hydrolysis of glucosylceramide (Figure 2). In the first step of the mechanism, upon substrate binding with the enzyme's active site, Glu_{340} performs a nucleophilic attack on the anomeric carbon in glucosylceramide. This nucleophilic substitution reaction is catalyzed by Glu_{235} acting as a general acid protonating the displaced ceramide. This S_N2 reaction has been shown to proceed through an oxycarbenium ion-like transition state stabilized through hydrogen bonding and various electrostatic interactions with active site residues.[3] The first step results in cleavage of the β-glycosidic bond in glucosylceramide, release of ceramide and the formation of a covalent glucosyl-enzyme intermediate. In the last step, which also proceeds through a oxocarbenium-ion like transition state, the glucosyl-enzyme intermediate is hydroyzled to release β-glucose whilst regenerating GCase back into its active form. Retention of the β conformation in glucose further supports the double displacement mechanism.

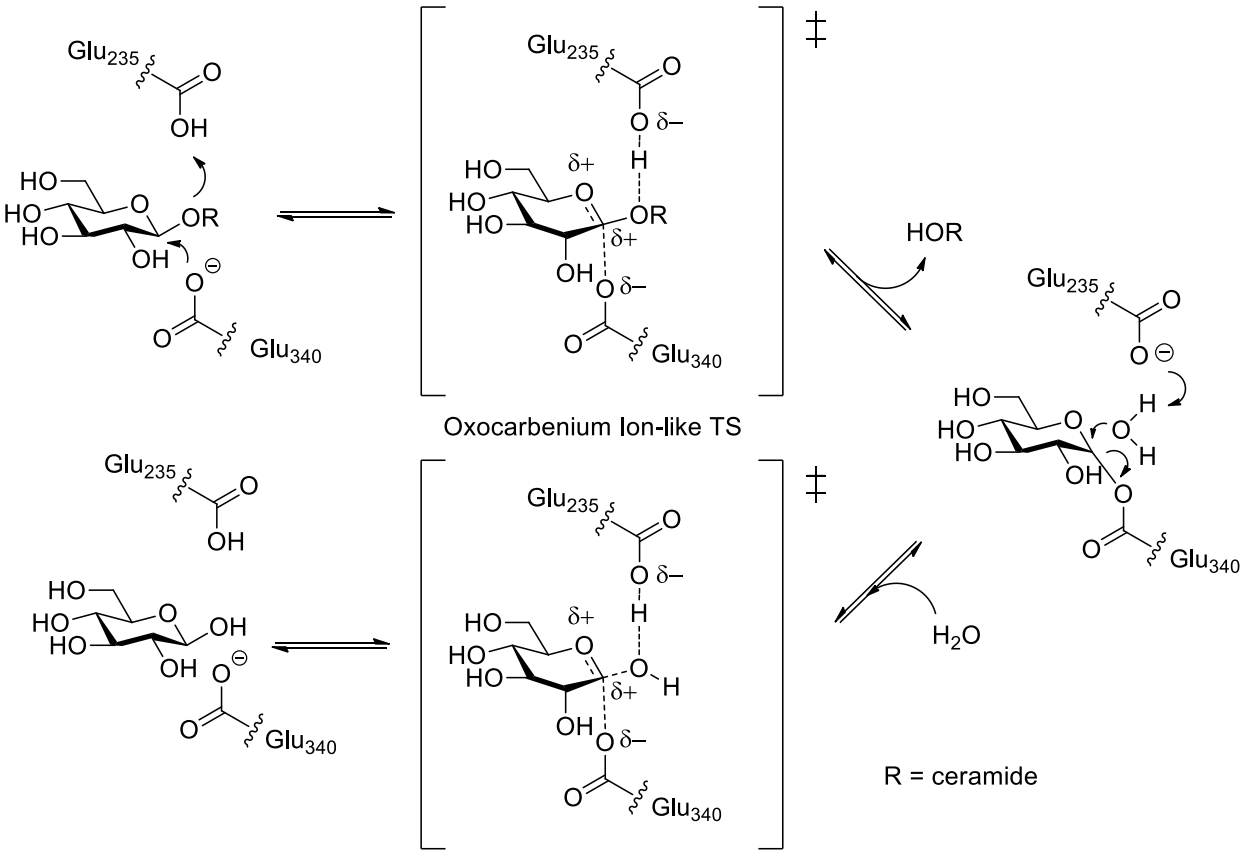

Figure 2: The catalytic mechanism of glucosylceramide hydrolysis by GCase. Glutamic acid residue 340 performs a nucleophilic attack on the β-glyosidic linkage. This reaction is catalyzed by Glutamic acid residue 235, forming a oxocarbenium ion like transition state which collapses to give a covalent glucosyl-enzyme intermediate. This intermediate is converted back to its starting configuration upon hydrolysis to yield β-glucose.

Evidence of the existence of a glucosyl-enzyme intermediate in the double displacement mechanism comes from X-ray cyrstallography and spectrocopic studies using active site inhibitors such as 2-deoxy-2-fluoro-D-glucosyl fluorides[2] or conduritol-B-epoxide (CBE)[4] through trapping of the covalent inhibitor-enzyme intermediate. An X-ray crystal structure showed CBE to be covalently bound to Glu_{340} of GCase and can be seen later in this thesis in Figure 7B.

GCase is expressed from the GBA1 gene and is translated in the cytosol of the cell.[5] GCase is a lysosomal enzyme so for proper function it must be relocated. After translation the protein is recognized by trafficking receptor LIMP2 and packaged in a vesicle.[6] This is all facilitated in the endoplasmic reticulum. GCase is trafficked from the endoplasmic reticulum to the Golgi for further processing and will finally reach the lysosome where the vesicle empties its cargo[7] (Figure 3). Once GCase reaches the lysosome it forms a complex with co-activator Saposin C and hydrolyzes its substrate glucosylceramide

on the surface of the lysosomal membrane. The exact mechanism by which this complex forms remains controversial but it is known that Saposin C is required for GCase enzymatic function[8].

Glucosylceramide hydrolysis is important in the production of ceramide for cells. Ceramide is a required precursor for many lipid metabolic pathways and its production has a large impact on cellular membrane structure as well as many signalling pathways.[9] Ceramide can alternatively be generated through *de novo* synthesis and through the breakdown of sphingomyelin but in some cells[10], like neurons, glucosylceramide hydrolysis accounts for 50-90% of sphingolipid production.[11] Deficiencies in GCase can therefore have a large impact in cellular ceramide levels. Deficiencies in GCase can also result in harmful accumulation of glucosylceramide in the lysosome as seen in Figure 3. Severe GCase enzyme deficiency, which can occur from the inheritance of mutated GBA1 genes, will result in a lysosomal storage disorder known as Gaucher Disease. Interestingly, mutation of the GBA1 gene and Gaucher Disease have recently been implicated as strong risk factors for developing Parkinson's Disease.[36-39]

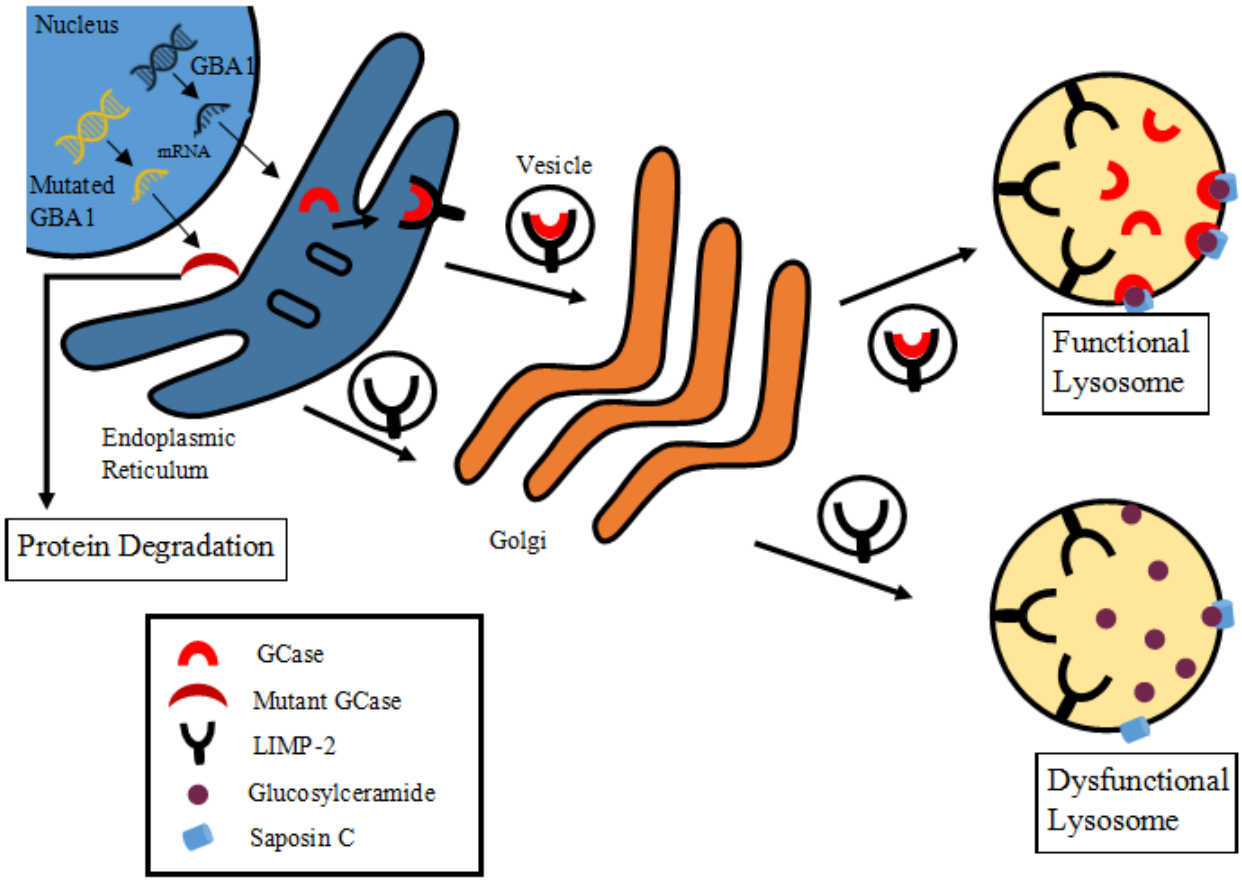

Figure 3: Upon expression of GCase from the GBA1 gene, GCase is packaged up into a vesicle for transport to the Golgi. This transport is mediated by transport receptor LIMP-2. In the Golgi GCase is processed so that it may be suitable to function once it gets to the lysosome. In the lysosome GCase forms complexes with Saposin C on the lysosomal membrane and glucosylceramide is hydrolyzed. In the case where a mutated GBA1 gene expresses improperly folded enzyme the mutant GCase becomes ubiquitinated and targeted for protein degradation. This deficiency in lysosomal GCase activity results in a build up of glucosylceramide that eventually will cause symptoms associated with Gaucher Disease.

Gaucher Disease: a Lysosomal Storage Disorder

The lysosome is a single membraned organelle found in most eukaryotic cells.[12] It is known as the digestive or recycling organelle because of its enzymatic contents. These can include acid phosphatases ribonucleases, deoxyribonucleases, cathepsins, glycosidases and sulfatases.[12] Deficiencies in any of these enzymes can result in lysosome dysfunction causing disruptions in natural metabolic pathways, destruction of some signalling pathways or lysosomal membrane leakage causing intracellular damage.[9] Depending on which enzyme, many different diseases can arise from enzyme deficiency (Figure 4).[13]

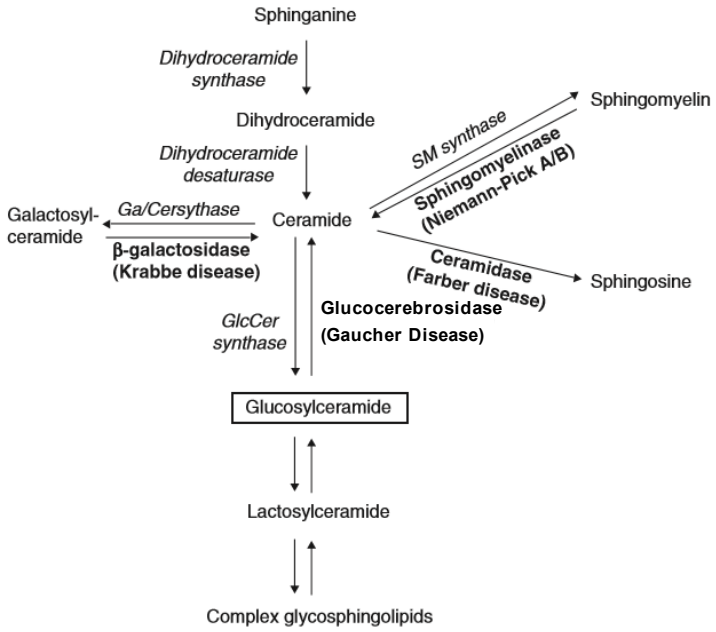

Figure 4: Common lysosomal storage diseases and the enzymes involved in their pathogenicity. A deficiency in GCase results in Gaucher Disease.[14]

The most common lysosomal storage disease is Gaucher Disease where 1 in 40,000-50,000 live births will be born with the disease.[15] The Ashkenazi Jews are an ethnic group with the highest risk of developing Gaucher Disease with 1 in 800 people inheriting the disease.[16] The disease is a recessive genetic disorder where a number of mutations in the GBA1 gene can cause a dysfunctional GCase enzyme to be expressed.[17] In these cases, the mutant enzyme does not fold properly preventing trafficking across the endoplasmic reticulum or the mutation disrupts its ability to interact with Saposin C.[18] As can be inferred from Figure 4, lysosomal GCase deficiency will result in lysosome dysfunction after accumulation of glucosylceramide begins. Significant reduction in ceramide production results and in turn reduction in sphingolipid synthesis will occur having severe pathological implications.[14]

In Type I Gaucher Disease, the main symptoms are chronic pain resulting from inflammation and enlargement of the spleen and liver (splenomegaly, hepatomegaly), blood related problems (anaemia, thrombocytopenia) and chronic bone pain (osteopenia, osteonecrosis and skeletal deformities)[19] resulting from deficient GCase activity primarily in macrophages.[14] These symptoms, with the addition of severe neurological symptoms effect patients with Type II (acute neurological) and Type III (chronic neurological) Gaucher Disease, both of which are deadly forms.[20]

Currently the most effective form of therapy for Gaucher Disease is through Enzyme Replacement Therapy. This involves injections of exogenously produced enzyme to increase otherwise deficient levels of GCase activity in a patient.[21] This recombinant form of GCase is produced by

Genzyme under the market name of Cerezyme®. Enzyme Replacement Therapy with Cerezyme® is an extremely expensive option so research has recently focused on the discovery of small molecular chaperones that can help traffic mutated GCase to the lysosome through binding to the active site stabilizing the folded tertiary structure and thus escaping ubiquination and degradation in the ER.[22] Discovery of such molecular chaperones for GCase has gained increased importance due to new evidence suggesting the heavy involvement of GCase in the progression of Parkinson's Disease as described below.

GCase as a Potential Biomarker of Parkinson's Disease

Parkinson's Disease (PD) is one of the most common neurodegenerative diseases in the world.[23] Its symptoms are clinically characterised by bradykinesia (slowness of movement), resting tremor, postural instability and eventually, cognitive impairment such as dementia.[24] The underlying pathology in PD involves the abnormal accumulation of α-synuclein protein fibrils. Normally α-synuclein is highly soluble in the cell but in PD this protein forms highly ordered insoluble aggregates in the neurons of the brain.[25] Large aggregates, otherwise known as Lewy Bodies, form in the lysosomes of dopaminergic neurons.[24] The eventual result of Lewy Body growth is the death of dopaminergic neurons in the brain.[26] Dopaminergic neurons are those involved in the transmission of dopamine throughout the brain, an important neurotransmitter required for normal brain function.[27] In PD, Lewy Body formation occurs primarily within neurons of the substantia nigra region of the brain, a region responsible for the motor impairment symptoms that are classic to PD. As PD progresses to advanced stages of the disease, Lewy Body formation can spread to neocortical regions of the brain, as it does with 80% of patients, producing severe cognitive impairments such as Lewy Body dementia.[28]

PD is a disease without a cure. The most effective treatment for PD to date is treatment through dopamine replacement therapy. This therapy includes the replacement of dopamine by the administration of levodopa, dopamine agonists or by using monoamine oxidase B inhibitors.[29] Artificial dopamine replacement helps alleviate the loss of dopamine caused by the death of dopaminergic neurons. Unfortunately, this does not slow the progression of the disease but only helps patients manage PD symptoms related to the loss of dopaminergic neurons.[30] However, sometimes patients feel that the side effects from these therapies can be worse than the disease itself.[30] Since it is often worse to receive unnecessary dopamine replacement therapy rather than begin therapy early, clinical diagnosis of PD takes around two years before treatment begins.[31] This results in a large use of healthcare resources and can be very stressful for the patient. Not to mention the patient has to go this entire time without treatment.

Clinical diagnosis of PD relies on the presence of the motor impairment symptoms described above and the absence of other features indicative of similar neurodegenerative disorders.[24] When clear signs of these symptoms are present it is estimated that the accuracy of a clinical diagnosis is 76 to 92%.[32] The issue is, as stated in most reviews, motor symptoms only present themselves after 50% of dopaminergic neurons in the substantia nigra are already dead.[33] It is early diagnosis which is difficult because early clinical symptoms overlap with other diseases like multiple system atrophy, corticobasal degeneration and progressive supranuclear palsy.[24] These diseases all share common physical symptoms and mainly differ in their pathophysiology. Currently, no blood test or imaging agent exists for the biochemical diagnosis of PD or the detection of Lewy Bodies *in vivo*.[24] Indeed, neuronal Lewy Body formation can only be confirmed during post-mortem brain tissue examination.[34]

Since Lewy Body pathophysiology is a very early indicator of PD, detection of α-synuclein levels in the brain could potentially accurately diagnose early PD compared to clinical diagnosis through expert symptom assessment. Efforts have been made to image α-synuclein using Positron Emission Tomography (PET) but the inability to develop imaging probes that specifically bind to α-synuclein over other neuronal fibrils has been a major set-back in probe development.[24] Imaging dopamine uptake is the only current imaging method used to gather biochemical information about PD. Through the use of DaTscan® clinicians are able to visualize uptake of a radioactively labelled dopamine to gather molecular information about the disease characterized by the loss of dopaminergic neurons.[35] The problem with this technique is the loss of dopaminergic neurons is not specific to PD so DaTscans can only help confirm a diagnosis not make one by themselves. Neurologists currently have to use a "wait and watch" philosophy when it comes to accurately diagnosing and treating PD.[29] Surely waiting for a disease to progress until severe symptoms appear is not an ideal strategy for disease management. The early stages of PD may provide the most opportune time for intervention although it remains the most difficult time to diagnosis. By having a tool to detect early Lewy Body formation, through either direct or indirect detection, neurologists may be able to extend the quality of life of their patients by influencing what therapies a patient receives and when they receive them while researchers may be equipped with a better tool for developing a cure.

Interestingly, GCase may be an effective target for developing such a tool. Recently, studies have shown that patients with Gaucher Disease are at a higher risk of developing PD compared to a healthy control. One study of nearly 6000 patients showed that Type I Gaucher Disease patients are 6 to 17 fold more likely to develop PD compared to a healthy group of patients.[36] Although Gaucher Disease patients have homozygous mutations of the GBA1 gene, other studies have shown that that even heterozygous carriers of GBA1 mutations are at higher risk than the general population. A study of large cohorts of PD

patients showed 4-7% were found to carry heterozygous GBA1 mutations.[37] A different study looking at 57 post-mortem brain samples from PD patients demonstrated 12% carried at least one mutation in the GBA1 gene which is a higher GBA1 mutation frequency than within the at risk Ashkenazi Jewish population.[38] One of the most surprising discoveries was that in a group of 5000 patients it had been demonstrated that there was a greater than 1 in 5 chance for a PD patient to carry a GBA1 mutation thus making genetic defects in the GBA1 gene the most significant genetic risk factor for PD identified to date.[39]

It is clear that there is a strong correlation between GBA1 mutations and the occurrence of PD but further investigation in cells, animals and humans was required to understand the role that GCase has in the progression of the disease. The most obvious trend to investigate was the correlation between GCase and Lewy Body formation. A dementia study has shown that of 95 patients with pathological Lewy Body findings, 28% of them had GBA1 mutations.[40] When another group examined post-mortem brain samples from PD patients, they found that from the patients that were homozygous and heterozygous for GBA1 mutations, 80% and 75% respectively showed that the GCase protein was co-localized within the Lewy Bodies.[39] In fact it was demonstrated that in cell lines with a GBA1 deficiency, global lysosomal dysfunction was correlated with α-synuclein aggregation.[41] This suggests that the expression of mutant GCase can lead to increased formation of Lewy Bodies.

Increased α-synuclein levels were not only shown to occur in cell lines with GBA1 knockouts but also *in vivo* with GBA1 mutant mouse models of Gaucher Disease. It has been shown over the course of the mouse's life, increases in α-synuclein levels were directly correlated to decreases in GCase enzymatic activity.[13] Interestingly, mice receiving injections of exogenous recombinant GCase enzyme were found to have reduced levels of α-synuclein, fewer pathological Lewy Bodies and ameliorated cognitive symptoms associated with PD.[13] This data is consistent with results obtained from experiments using cell lines having GBA1 deficiency and lysosomal dysfunction that promoted α-synuclein aggregation but recovered normal lysosomal function with the addition of exogenous GCase.[41] This suggests that GCase activity alone is able to mitigate the aggregation of α-synuclein in the formation of Lewy Bodies presumably due to normal lysosomal function.

The most perplexing data reported in the literature is that of observable decreases in GCase activity in PD patients without any GBA1 mutations. This was perplexing because it was initially thought that the decrease in GCase activity in PD patients was directly a consequence of mutant enzyme that was unable to reach the lysosome. One thorough investigation evaluated 19 post-mortem brain samples from patients confirmed of having PD but no GBA1 mutations.[42] The patients varied from being afflicted by early to late stages of progression of PD. Neuronal death was only present in the late stage samples,

although, sodium dodecyl sulphate (SDS) soluble α-synuclein levels were elevated in all samples. SDS-soluble refers to proteins that are largely insoluble in water but will only dissolve in the presence of strong detergents like SDS. This includes samples containing insoluble α-synuclein aggregates (Lewy Body) or GCase. There was a strong negative correlation shown between the levels of SDS-soluble α-synuclein increasing and the SDS-soluble GCase levels decreasing. Lysosomal GCase enzyme activity was also shown to decrease. This observation was seen in both early and late stages of the disease. This is interesting because GCase activity is shown to decrease even in early stages of the disease before neuronal death has occurred. Furthermore, these results were taken from patients without GBA1 mutations who expressed the wild type enzyme suggesting that GCase activity may decrease in all patients with PD. These two facts together highlight the significant impact GCase may have as a biomarker for the progression of PD or a therapeutic target. Indeed, lysosomal activity and cellular levels of GCase are shown to be decreased early on in the disease, before neuronal death has occurred and in patients without any GBA1 mutations suggesting that GCase activity may be a universal biomarker for PD patients.

It is also interesting to note that there were reductions in GCase concentration, both in the cytoplasm and lysosome, in the early stages of the disease. Despite this early reduction, GCase concentration in the cytoplasm seemed to remain at this level, even in the late stage PD samples.[42] GCase mRNA levels also appeared to remain constant throughout the progression of the disease. Lysosomal GCase enzymatic activity, however, seemed to drop continuously as the disease progressed from early to late.[42] (This information is summarized in Table 1). This suggests that in PD there is not a reduction in the GCase being produced but rather the amount that is reaching the lysosome. A separate study has demonstrated that there is some kind of bidirectional pathogenic loop in PD where α-synuclein accumulation reduces GCase trafficking to the lysosome while trafficking of GCase to lysosome reduces α-synuclein levels (Figure 5).[43] This suggests GCase also presents a therapeutic target through promotion of its trafficking to the lysosome as it may reduce α-synuclein aggregation.

Table 1: Summarization of GCase and α-synuclein level analysis in post-mortem human neurons affected by PD. The + symbols represent an arbitrary increase or decrease and are not set to any scale but are used to demonstrate that GCase levels are decreased in early PD before neuronal death has occurred.[42]

	GCase mRNA levels	Lewy Body Formation	GCase Levels		Neuronal death
			Cytoplasm	Lysosome	
Healthy	+++		+++	+++	No
Early PD	+++	+	++	++	No
Late PD	+++	+++	++	+	Yes

In conclusion, this evidence demonstrates GCase activity levels are directly correlated with the accumulation of α-synuclein, the formation of Lewy Bodies and thus the pathogenicity of PD. The disease is promoted by the inheritance of mutant forms of GCase but can still progress regardless of the existence of GBA1 mutations. The exact reason GCase activity levels drop in PD patients is still unknown and is thought to be part of some negative feedback loop between α-synuclein aggregation and GCase trafficking to the lysosome. More importantly it has been shown that lysosomal GCase activity decreases occur early on in the progression of PD and can be detected before neuronal death occurs. These data conclude that GCase is an attractive potential biomarker for detecting the early and accurate onset of PD and as a potential therapeutic target for drug development in patients with or without GBA1 mutations. Further studies are required to test these assumptions through the design of molecular tools that are able to track and measure GCase activity *in vitro* and *in vivo*.

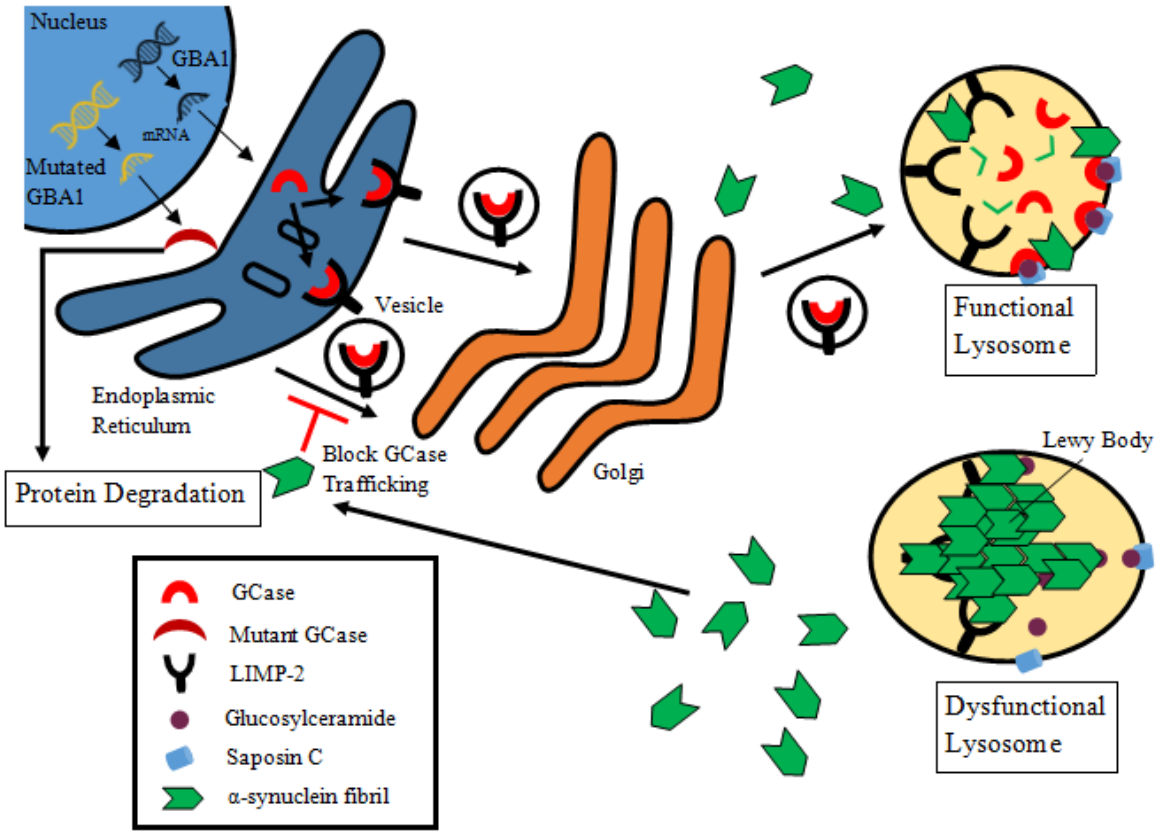

Figure 5: GCase is thought to be important in the degradation of α-synuclein in the lysosome. When GCase levels in a functioning lysosome are high, α-synuclein aggregation is not seen. In the case of PD GCase levels in the lysosome appear to be low and α-synuclein levels increase until large aggregates form in the lysosome (Lewy Body). It is thought when α-synuclein levels are high they somehow have a negative impact on GCase trafficking to the lysosome, increasing further their aggregation. Mutant GCase is also unable to travel to the lysosome making GBA1 mutations strong risk factors for developing Lewy Body formation.[7]

GCase Molecular Probe Design

To validate GCase as a biomarker for PD molecular tools need to be developed to study its activity *in vitro* and *in vivo*. Since activity of GCase is shown to be decreased in patients with PD it is desirable to develop activity-based probes in order to detect activity and track GCase biodistribution within a biological system.

Activity-based protein profiling enlists the help of a small molecule that is designed to interact with the active site of a particular enzyme. These activity-based probes take advantage of an enzyme's catalytic mechanism in order to irreversibly bind within the active site.[44] Probes can be developed by taking a compound that binds well to the active site of an enzyme and coupling to this compound a detectable tag such as a fluorescent molecule or a radioactive isotope. Typically, these probes must have 3 characteristics in order for them to be excellent activity based probes; 1) high affinity for the active site so they can bind to the enzyme at biologically significant concentrations, 2) high selectivity to the target enzyme so they produce a signal for only one target, 3) a "warhead" that does not reduce active site binding and forms an irreversible covalent bond at some point during the enzyme's catalytic mechanism.[45] Two off-site targets to be concerned with for the production of GCase activity based probes are GBA2 and GBA3 which are β-glucosidases from the same family as GCase. These glucosidases are found in the cytosol rather than the lysosome.[46] Often compounds that are potent binders of GCase also bind well with GBA2 or GBA3. To design an activity-based probe that is specific for GCase it is necessary to consider what compounds have already been shown to be potent and selective inhibitors of the enzyme.

One of the first and obvious structures to mimic for an activity based probe is GCase's natural substrate glucosylceramide. The structure of the natural substrate of an enzyme is often used as a starting point in the design of inhibitors but glucosylceramide is not simple to synthesize in large amounts or simple to chemically modify. One way of circumventing this issue is by replacing the ceramide moiety with a different leaving group while keeping the glucose moiety intact considering glucose's natural affinity for GCase.

A

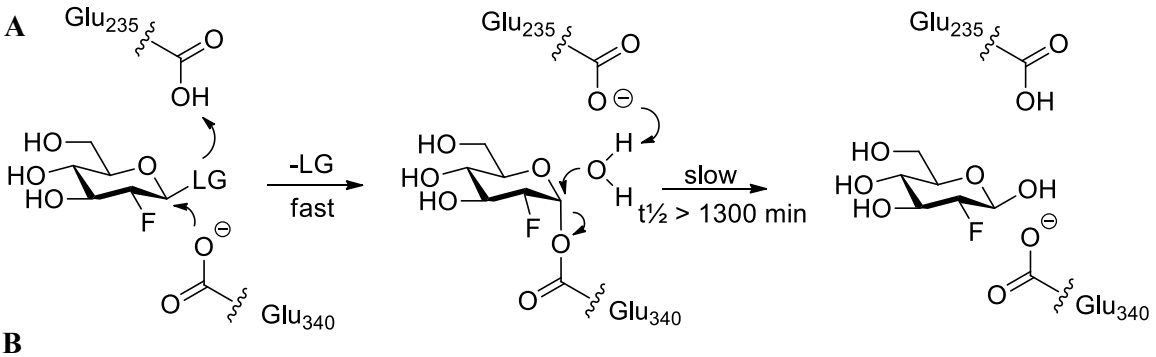

B

LG	IC_{50} (μM)
F	>1000
2,4-DNP	>1000
STol	>1000
S(O)Tol	>1000
$O(NPh)CF_3$	5.5
$OP(O)(OPh)_2$	>1000

Figure 6: 2-deoxy-2-fluoroglucoside as mechanism based inhibitors of GCase. A) By replacing the 2 position on glucose with electron withdrawing fluorine it is possible to deactivate the transition state during glycosylation so that its deglycosylation has a half life of greater than 1300 min. **B)** Table shows the IC_{50} values associated with different 2-deoxy-2-fluoroglucoside leaving groups.

Interestingly, Withers *et al.* has shown that if you replace one of the hydroxyls on glucose with an electronegative fluorine and install a good leaving group at the anomeric carbon, this generates a mechanism-based inhibitor where the glucosyl-enzyme intermediate is rapidly formed but only slowly hydrolyzed, especially when the fluorine is in the 2 position (Figure 6A).[47] There are several examples of this type of activity-based probe with fluorine in the 2 position and a good leaving group on the anomeric oxygen of glucose (Figure 6B).[44] For example, Phenix *et al.* synthesized a β-2,4-Dinitrophenyl-fluorodeoxyglucose **1.1** (Figure 8) for the purpose of labelling Cerezyme®, a recombinant form of GCase used for treating Gaucher Disease.[48] They successfully synthesized the compound with radioactive fluorine-18 (^{18}F) showing the glucosyl-enzyme is extremely stable (t½ > 1300 min). Despite a very stable glucosyl-enzyme intermediate, as can be seen from IC_{50} values in Figure 6B, these 2-fluoroglucose probes suffer from terrible binding affinities that are probably attributed to the loss of a crucial hydroxyl group required for binding and deactivation of the probe as a whole by fluorine making it less reactive for the glycosylation step.

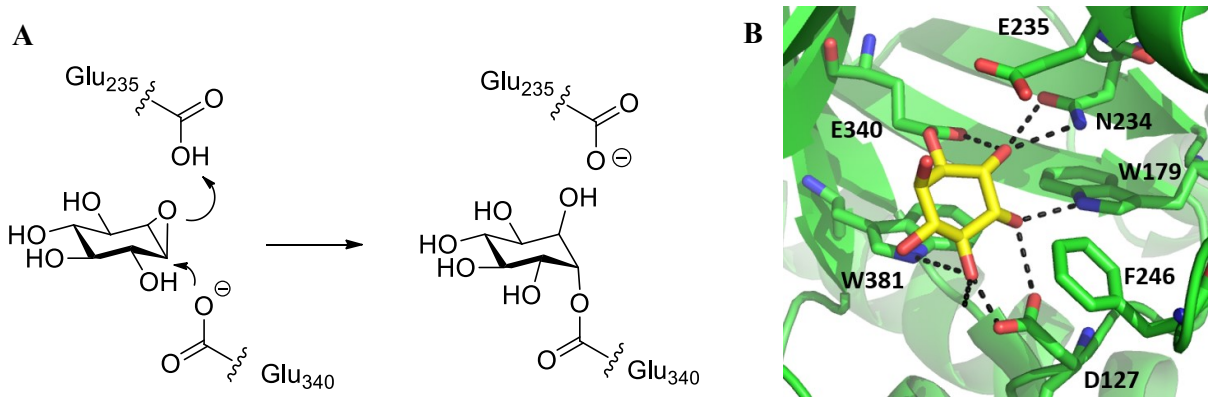

Figure 7: Inactivation of mechanism based inhibitor conduritol-B-epoxide (CBE). A) Proposed mechanism of GCase inactivation. **B)** Crystal structure of CBE covalently bound to GCase (PDB: 1Y7V)[4] shows extensive hydrogen bonding and a covalent bond between CBE and glutamic acid 340.

One of the first and most widely available irreversible inhibitors of GCase is conduritol-B-epoxide (CBE) **1.2** having a Ki value of ~140 μM.[49] Unlike the fluorosugar inhibitors that are pyranohexoses, CBE is an inositol based compound whose polyhydroxyl cyclohexane conformation demonstrates excellent GCase active site recognition. Unlike glucose of the natural substrate, CBE is not an pyranose and as a result cannot be efficiently hydrolyzed from the active site of the covalent inhibitor-enzyme complex. The covalent complex has been shown to form through nucleophilic attack from glutamic acid residue 340 on the epoxide of CBE (Figure 7A). In 2005 Premkumar *et al.* published a crystal structure of CBE covalently bound to GCase (Figure 7B) proving that the hydroxyl groups of the conduritol backbone formed hydrogen bonds within the active site and that the epoxide did indeed open to form a covalent bond with the nucleophilic glutamic acid 340.[4]

CBE is a relatively poor inhibitor of GCase but it exhibits preferential binding of GCase over GBA2 and GBA3.[4] In addition, this inhibitor is a poor scaffold to build upon and explore new derivatives of this type of inhibitor because it lacks any obvious handles to install a radiolabel or fluorescent reporter necessary to track GCase in biological experiments.

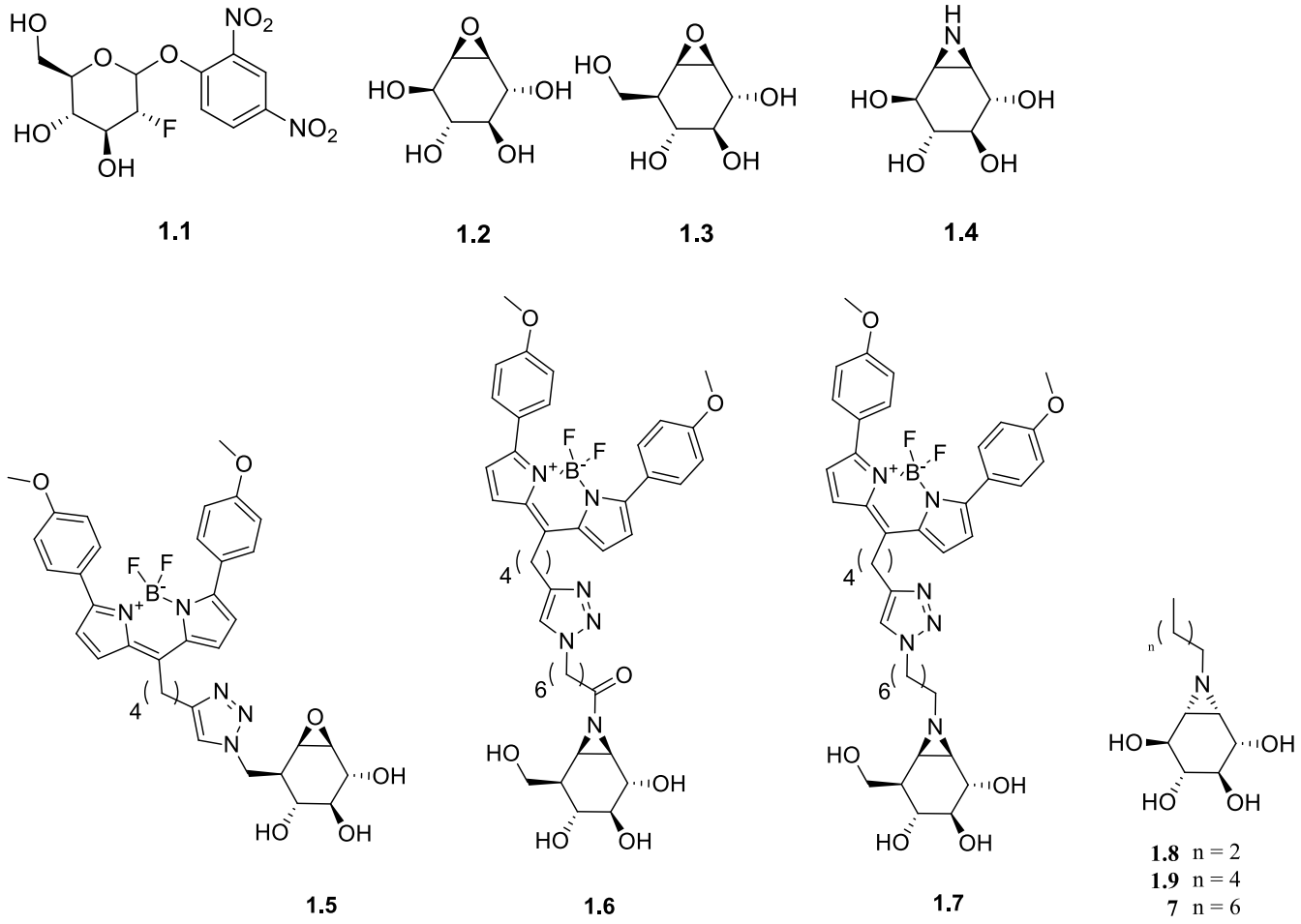

Figure 8: Structures of selected mechanism based inhibitors of GCase.

Table 2: Summarized kinetic data on compounds 1.1 to 7 for inhibition of GCase.

Compound	IC_{50} (μM)	K_i (μM)	k_i (min^{-1})	k_i/K_i ($\mu M^{-1}/min^{-1}$)	Reference
1.1	>1000	-	-	12.00	[48]
1.2	9.49	140	0.590	4.20×10^{-4}	[49]
1.3		0.152	0.078	0.514	[50]
1.5	0.00194	0.008	0.208	25.10	[50]
1.6	0.00115	-	-	-	[53]
1.7	0.00145	-	-	-	[53]
1.8	-	2.40	0.140	0.058	[46]
1.9	-	0.050	0.140	2.80	[46]
7	-	0.005	0.120	25.0	[46]

Recently, Aerts and Overkleeft have taken the principles learned from these two activity based inhibitors and have developed several cyclophellitol and aziridine-type cyclophellitol based probes with fluorescent and biotin tags.[51] The cyclophellitol based inhibitors contain the electrophilic epoxide warhead and, like CBE, form non-hydrolysable inhibitor-enzyme complexes. The structure of cyclophellitol **1.3** (Figure 8) is a compromise between that of glucose and CBE but unlike the Withers fluoro-glucose based inhibitors, in which carbon 2 was modified, a modification was made in compound **1.5** to mimic a carbon 6 modification on glucose (Figure 8).[52] This was done because, from structural biology studies, it is known modifications at carbon 2 prevent important enzyme-substrate interactions while bulky hydrophobic modifications at carbon 6 are tolerated, and in fact, enhance active site binding.[44] Aerts and Overkleeft have also made *N*-acylated aziridine **1.6** and *N*-alkylated aziridine **1.7** versions of epoxide **1.5** keeping all hydroxyl positions free.[53] These probes might have been inspired by Withers' conduritol aziridine glucosidase inhibitor **1.4** published in 1989. The activity probes were tagged with hydrophobic fluorescent reporter BODIPY and used to image GCase in cellular based assays. These probes exhibited very high binding affinities and stable enzyme-inhibitor complexes. In fact, these probes are some of the most potent inhibitors of GCase reported in the literature. The combination of a cyclophellitol backbone linked with an electrophilic epoxide warhead and hydrophobic tail make them very effective activity based probes for GCase.

All of the Aerts and Overkleeft activity based probes show high efficiencies for labelling GCase *in vitro* (Figure 8). Acyl aziridine **1.6** however, suffers from selectivity issues, having low nanomolar IC_{50} values for GBA2 and GBA3 making it a broad spectrum β-glucosidase probe.[52] The acylated aziridine in **1.6** is also quite a powerful electrophile rendering it prone to decomposition and high reactivity towards other human enzymes. Alkyl aziridine **1.7** was developed after **1.6** because alkylated aziridines are more stable then acylated ones. Although more stable, there is no information on its selectivity but conceivably **1.7** has similar selectivity issues to its acylated cousin. Epoxide **1.5**, however, shows excellent selectivity for GCase over GBA2 and GBA3.[52] This is probably due to its different carbohydrate ring substitution pattern. The issue with epoxide **1.5**, however, is its inability to penetrate the blood brain barrier (BBB) rendering it useless as an activity based probe for studying PD *in vivo*. The other issue with compounds **1.5**, **1.6** and **1.7** is the rather long and difficult synthesis associated with these compounds making their scaffolds unattractive for development of new derivatives.

Keeping in mind all the aspects of the previous activity-based inhibitors mentioned, an inhibitor with a simplified structure was synthesized and characterized by previous graduate student, Benjamin Adams, from the Phenix lab (Figure 8).[46] The structure of this activity-based irreversible inhibitor is essentially an alkylated form of conduritol aziridine **1.4** and was easily prepared in 8 steps from

commercially available *myo*-inositol. Alkylation of the aziridine was chosen instead of acylation because alkylated aziridines tend to be more stable allowing for longer shelf life, less off-site reactions in a biological system and easier synthesis. Adams *et al.* was able to show that by lengthening the alkyl chain on the aziridine the potency of the inhibitor increased.[46] The octyl-aziridine derivative **7** interestingly has a potency greater than any known inhibitor of GCase in the literature. Furthermore, it has been shown that **7** has excellent *in vitro* characteristics in terms of its cell permeability and selective inhibition of GCase over GBA2 and GBA3. Also its inositol backbone may potentially allow it to be a substrate for inositol transporters promoting its passage across the Blood Brain Barrier (BBB). These desirable *in vitro* characteristics make compound **7** the lead compound for the development of GCase activity based probes in this thesis work.

Probe Synthesis: Protecting Group Optimization

Despite these desirable *in vitro* characteristics, lead compound octyl aziridine **7** suffers from a synthesis that limits the types of derivatives that can be prepared and explored as activity based-probes. The synthesis includes a harsh $LiAlH_4$ reduction to form the aziridine and employs Birch Reduction to remove the Benzyl ether (Bn) protecting groups.[46] $LiAlH_4$ cannot be used with easily reducible protecting groups and the Birch Reduction requires avoidance of aromatic fluorescent tags or radiochemical handles. Birch reduction is not easily compatible with radiochemistry considering the time constraints of radiochemistry and the shielding requirements associated with radiation (see Radiopharmaceuticals and PET Imaging). As a consequence, the synthesis of **7** will need to be modified in order to improve the flexibility of the synthetic chemistry to be amenable to the preparation of fluorescent or ^{18}F labeled aziridines.

To improve the flexibility for the synthesis of aziridine **7**, optimization of aziridine formation and final deprotection is required. Bn deprotection should be done rapidly and by using a technique that is amenable to radiochemistry and derivative production. Alternatively, new protecting groups should also be explored that can be easily incorporated, survive the entire course of the synthesis and can be quickly removed. The deprotection must also keep the aziridine and any fluorescent or radiochemical label intact. There are few protecting groups that can be used for this type of synthesis but three groups were chosen based on their promising stability to the synthesis and easy removal in the final steps. These groups are the tert-butyl dimethyl silyl ether (TBS), benzoate (Bz) or methoxy-methyl acetal (MOM) protecting groups with their chemical features summarized in (Figure 9).[54] An improved synthesis will allow fluorescent aziridine derivatives to be developed for the study of GCase *in vitro* using appropriate cells lines while radioactive derivatives can be used to study of GCase *in vivo* using animal models of PD.

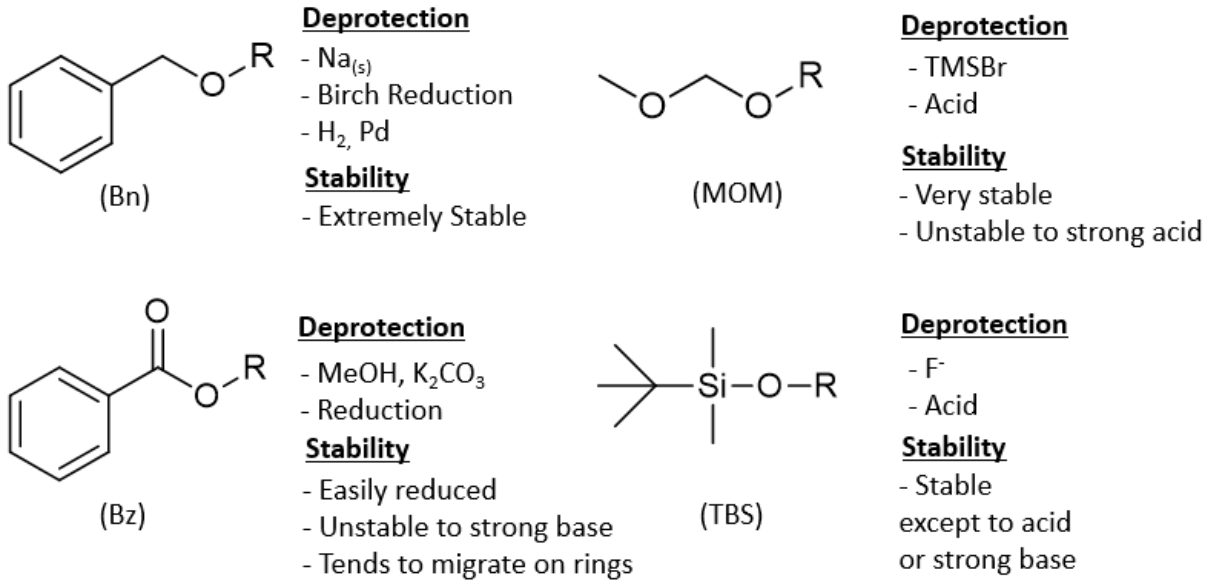

Figure 9: Summarization of potential protecting groups and their stability for synthesis of n-alkylated conduritol aziridines.[54]

Imaging GCase *in vitro*: Development of Fluorescent Derivatives

As described above, fluorescent activity based probes for GCase have already been developed and used for studying GCase activity *in vitro*.[53] These derivatives can be visualized by using fluorescent microscopy to produce colourful images showing where the probe accumulates in a cell while providing information on the activity and location of GCase inside living healthy cells or cell lines that mimic a diseased state.

Despite the development of the cyclophellitol activity-based fluorescent probes **1.5**, **1.6**, and **1.7** for GCase reported by the Aerts and Overkleeft groups, we wanted to prepare fluorescent derivatives of *N*-alkyl conduritol aziridines. The epoxide cyclophellitol-based probes required lengthy and laborious synthesis while the N-acetylated cyclophellitols were found to be non-specific binders of GBA2 and GBA3. In contrast, synthesis of the conduritol aziridine scaffold for **7** requires fewer chemical steps and initial experiments suggest that the *N*-alkyl aziridine scaffold is a potent and selective binder of GCase. Indeed, a fluorescent conduritol aziridine would prove valuable to determine the *in cellulo* specificity of these inhibitors since the probe would irreversibly label any related enzymes inside living cells. Cell lysates can be easily extracted and the proteins separated by SDS-PAGE followed by analysis with a fluorescent imaging system to detect fluorescently labeled enzymes. In addition, convenient synthetic routes for preparing efficient, selective and fluorescent *N*-alkylated aziridines would be useful for unraveling the biological role that GCase has in α-synuclein aggregation and could be used track the

enzyme activity in cells models of PD. Further, a fluorescent derivative can be used to help evaluate new chaperone therapies for improving GCase trafficking to the lysosome, a tool that would be beneficial for Gaucher Disease and PD research.

The death of many drugs that targets proteins in the brain result from their inability to cross the BBB. The BBB is a selective membrane, comprised of tightly joined endothelial cells, that selectively allow certain small lipophilic molecules to passively enter the brain and express proteins that actively transport hydrophilic substances.[55] Considering the structure of compound **7,** it cannot be considered a highly lipophilic compound and is unlikely to passively cross the BBB. This means that more lipophilic derivatives having fewer hydrogen bond acceptors or donors are needed to improve BBB permeability or find a derivative that is actively transported across the BBB. Luckily, aziridine **7** has been shown to be cell permeable by Adams *et al.* while recent and unpublished experiments performed by Dr. Shusheng Wang in the Phenix lab suggest that the conduritol aziridines are a substrate of the inositol transporters that are expressed in the BBB.[46] To study BBB permeability *in vitro* and to reveal the compounds that are highly unlikely to enter the brain, it is possible to set up a trans-well assays that employ canine kidney cell lines that overexpress important protein pumps while also forming a tight monolayer of cells that mimics the BBB.[81] Such as an assay would be valuable to identify those fluorescent and non-fluorescent aziridine derivatives that are efficient substrates in order to learn about the selectivity of these compounds towards p-Glycoprotein and multi-drug resistance protein pumps. Both of these proteins are highly expressed in the BBB and are largely responsible for preventing moderately lipophilic molecules from entering the brain due to their pumping action.

To produce a fluorescent probe, a suitable fluorophore must be chosen that is compatible with the synthetic methods employed to prepare the compound. Since GCase is usually located in the lysosome, the fluorophore must also be stable at low pH (around 5) and maintain high fluorescence in the acidic environment if the probe is to be used to image living cells.[12] Previous reports have shown that GCase readily accepts bulky and hydrophobic moieties within carbohydrate-based inhibitors or substrates so the structure of the fluorophore was not considered an important factor for binding affinity.[56] For this project, three fluorophores were chosen to be investigated: BODIPY, Acridine and Dichlorofluorescein (Figure 10). Each of these fluorophores are commonly used in cell biology studies, are highly fluorescent and are stable, even at low pH. By preparing derivatives of **7** coupled to these fluorophores we can potentially develop powerful molecular tools that can give insight into the location, function and activity of GCase inside living cells.

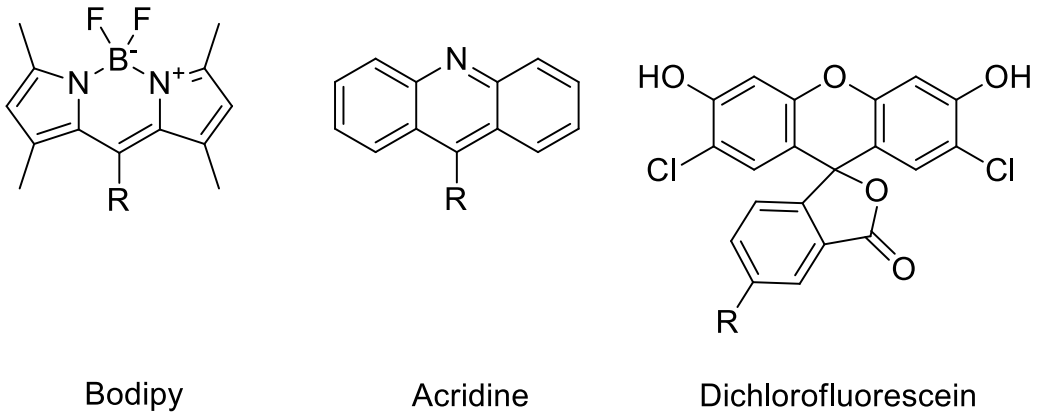

Figure 10: Fluorophores that were chosen for labeling the conduritol aziridines based on their chemical stability and intense fluorescence at low pH values. Conduritol aziridines bearing these fluorophores would be well adapted to fluorescent imaging of GCase activity within the lysosomes of living cells.

Imaging GCase *in vivo:* Development of Radiopharmaceuticals for PET Imaging

In medical imaging there exists two main types of imaging techniques; anatomical imaging and functional imagining. Anatomical images are obtained when using imaging modalities like Computed Tomography (CT), Magnetic Resonance Imaging (MRI) or Ultrasound. These techniques detect changes in tissue density and structure to produce high contrast images. Functional images are obtained when using molecular imaging modalities like functional MRI (fMRI), Single Photon Emission CT (SPECT) or Positron Emission Tomography (PET). These techniques produce images that reflect biochemical functions thus providing functional data instead of revealing the structures of tissues and organs.[57]

For imaging GCase activity in the brain, the correct imaging modality must be chosen. CT, MRI and ultrasound can only give structural images so they cannot give any information of GCase activity on the molecular level.[58] MRI contrast agents that are capable of imaging enzyme activity do exist, however no specific agents for GCase have been developed. Furthermore, MRI has very low sensitivity requiring the injection of high amounts of contrast agent meaning toxicity of the MRI active probe can preclude human use. The blood brain barrier (BBB) also represents an enormous challenge since most contrast agents require the use of heavy metals like gadolinium and are unlikely to enter the brain. Indeed, techniques have been improved to use functional MRI (fMRI) to study brain activity by measuring blood oxygen level dependent responses associated with neuron activity but this cannot give us a direct indication of GCase activity on the molecular level.[57]

SPECT is a widely used functional imaging technique but is not the modality of choice for imaging the brain. It is about 10 fold less sensitive than PET and requires the use of single-photon-

emitting nuclides like ^{99m}Tc, ^{123}I and ^{111}In.[59] These nuclides are difficult to incorporate into small molecular probes that would be expected to cross the BBB.[60] With the exception of ^{123}I, nuclides like ^{99m}Tc and ^{111}In are not commonly used to label small molecule tracers due to their large size lowering the affinity of potential tracers to the target enzymes. This reduction in binding affinity is attributed to the nuclides rather large size or their requirement to be chelated by a bulky chelating groups. These aspects make SPECT imaging agents inadequate for imaging the brain, especially when measuring enzyme activity that require a small molecule to enter a binding or active site within the interior of a protein.[57]

PET imaging has a rich history in imaging enzyme and receptor activity in the brain of humans and animals.[61] PET imaging uses radiotracers labeled with positron emitting nuclides like ^{11}C, ^{131}I and ^{18}F. Non-radioactive versions of these nuclides are commonly found in biological compounds, metabolites and many pharmaceuticals, so they can be incorporated into potential PET imaging agents without significant change to their biological properties, chemical properties or molecular weight. Indeed, many PET imaging agents intended to image targets in the brain have been developed using these nuclides. PET imaging agents for the brain are usually either small lipophilic molecules that passively diffuse across the BBB or molecules that mimic natural products that are actively transported across the BBB.[57] Once in the brain, the emission of positrons can be detected with extremely high sensitivity allowing for microscopic amounts of radioactive tracer to be used.

Positrons emitted by these isotopes *in vivo* will travel a very short distance before their momentum becomes essentially zero and they annihilate with an electron. This distance is called the positron range and is on average 0.3 mm for ^{18}F in water. When a positron eventually makes contact with an electron they annihilate, producing two high-energy 511 keV photons released approximately 180° from each other. A PET camera works by detecting these coincident 511 keV photons with a circular ring of detectors positioned around the source in order to map out in 3 dimensions the location of the annihilation (Figure 11).[59] By combining PET with a structural CT image it is possible to overlay anatomical images with the radioactive signal thus allowing researchers or physicians the ability to identify the precise tissue or organ location of tracer uptake with a high degree of accuracy. In a full body Philips Gemini TF PET/CT scanner the resolution is approximately 1 cm after including all possible inaccuracies involved with the detector, patient scanning and other physical fundamental limitations of PET while microPET instruments typically have 1 mm resolution for small animal imaging.[62]

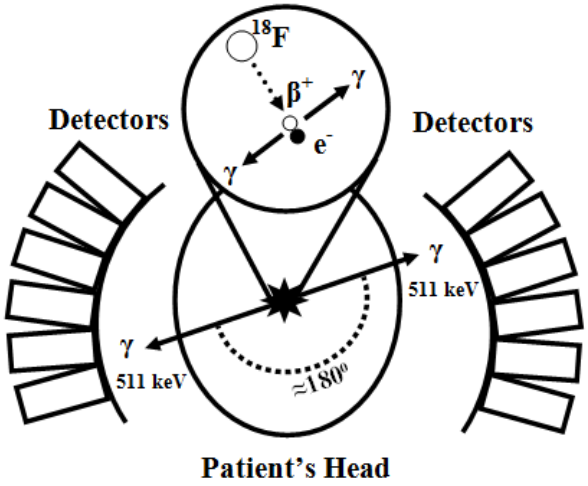

Figure 11: Schematic diagram showing an ^{18}F PET radiotracer used for functional imaging of the brain. Accumulation of the ^{18}F labeled radio tracer in specific areas of the brain result in the emission of positrons that travel a short distance before annihilating with an electron to release 2 coincident 511 keV photons. After many decay events are detected, an image is produced that quantitatively reflects the tracer uptake in specific areas of the brain.

The high sensitivity of PET allows the micro dosing of the radiotracer in the microgram - nanogram range thus avoiding concerns of chemical toxicity of the imaging probe. For example, in an ^{18}F-FDG PET scan for the average adult, 2-3 μg of imaging agent is required for a full body scan.[63] Compare that amount to Ricin, a protein that is 6000 times more toxic than cyanide but still requires at least 500 μg to kill an adult man.[64] At the micro dosing levels of the injected radiotracer, even drug candidates that were proven to be too toxic as pharmaceuticals can be radioactively labeled and used safely as PET imaging probes in humans and animals.

The most harmful component of a PET imaging scan is the radioactive dose to which the patient is exposed to. When a ^{18}F-FDG PET/CT is performed, most of the radioactive exposure comes from the anatomical CT scan when compared to the dose from the PET tracer, cumulatively resulting in about 14 mSv of dose in total.[63] With more sensitive PET cameras coming onto the market, as well as new PET/MR instruments, exposure to ionizing radiation is becoming even less of a concern. To put this dose into perspective, the annual background radiation exposure of an average person without additional exposure from manmade sources is approximately 4 mSv. Compare that to an airline crew that is estimated to receive an extra 2.19 mSv/y just from cosmic radiation.[65] These values demonstrate that a PET/CT scan exposes a patient to about 10 times more radiation than what they would normally receive from annual background levels but overall, this dose is only moderately harmful to a patient since

multiple scans are not typically performed. The risk of damage from radiation is small considering the beneficial information a scan can provide to a physician for a patient.

There are several positron emitting isotopes available for the production of radiopharmaceuticals. The most commonly used positron emitting isotopes are ^{11}C, ^{131}I and ^{18}F. To choose the best radionuclide for a GCase radiotracer two main things must be considered; 1) half-life of the nuclide and 2) the effects the radioactive atom will have on the probe's biological activity. For this thesis work the isotope that will be incorporated for producing a GCase PET tracer will be ^{18}F. This isotope is considered the isotope of choice for PET since it has the best image resolution and a sufficiently long 109.8 minute half-life compared to the short half life of ^{11}C (20 minutes) and long half life of ^{131}I (8 days). Having a longer half life helps enable radiochemical synthesis as reaction times can be increased as well as allowing time for purification, quality control and shipping to the small animal imaging facility. If the half life is too long, however, radioactive safety risks are higher because the injected animal or human remains radioactive for longer periods of time. ^{18}F is also well suited for the labeling a drug or probe without affecting its biological activity greatly. This is because ^{18}F is an isostere of both hydrogen and hydroxyl groups thus allowing great flexibility for its incorporation into biologically active molecules.[61]

Nucleophilic ^{18}F is produced by a cyclotron, an instrument has the ability to accelerate a hydride anion by using alternating electromagnets called dees. The negatively charged particle travels in a circular motion until the particle has enough kinetic energy to reach the outer diameter of the cyclotron chamber. Once traveling at sufficient speeds, the hydride ion is stripped of its electrons and the positively charged proton rapidly bombards a target made of highly pure materials. For a source of nucleophilic ^{18}F-fluoride, ^{18}O enriched water is used as the target material. Upon proton bombardment the ^{18}O is converted into ^{18}F after releasing a neutron. Production of radiopharmaceuticals with these isotopes has many challenges that have to be overcome compared with the production of regular pharmaceuticals. There are 3 major things to consider when preparing radiopharmaceuticals:

1) **Safety**: In the case of a positron emitting isotope like ^{18}F, high energy (511 keV) gamma rays will be consistently produced as positrons annihilate with surrounding electrons. These gamma rays are harmful to humans in high doses and reasonable measures should be taken to limit exposure to this ionizing energy. This means using proper shielding (lead blocks) and manually handling low amounts of activity. Working around shielding or in an automated synthesis module obviously produces many obstacles that are non-existent in a regular chemistry laboratory. This limits the types of chemical techniques and specific reactions that can be utilized for the synthesis of compounds.

2) **Time**: All radioactive isotopes have a characteristic half-life limiting the length of time for your chemical reactions. In the case of ^{18}F the half-life is 109.8 minutes meaning the total reaction and purification time should not exceed one half life ideally. Incorporation of the ^{18}F isotope should be done within the last steps of your synthesis and the reaction should be completed very quickly. Sometimes harsh reaction conditions are required to achieve this, potentially dramatically reducing yields.

3) **Concentration**: In radiopharmaceutical production, stoichiometry is much different than in a typical organic reaction. For example, 1.5 mg of ^{18}F would amount to approximately 5.5 million GBq. This amount of activity would be extremely harmful to people working with it and require enormous amounts of energy to produce. Luckily since PET detectors are the most sensitive of the molecular imaging modalities, the amount of ^{18}F required for a PET scan is less than 1 GBq. Although this is beneficial for limiting exposure to radioactivity it effects how the radiopharmaceuticals are produced. A typical production of 5.5 GBq of ^{18}F equates to only 1.5 ng of isotope. This means that stoichiometric ratios of ^{18}F to the chemical precursor is $1:10^4$ or $1:10^5$. Using such a dilute reactant makes it difficult to practically simulate the reaction in an organic chemistry lab using non-radioactive versions of the isotopes and clearly affects the rate of a reaction under pseudo-first order kinetics. Working on a ng scale with respect to ^{18}F also means that even tiny amounts of impurities in the chemical precursors can react with the radionuclide and these side products, as well as the radiochemical product, cannot be characterized using traditional methods like NMR spectroscopy or TLC staining. Mass spectrometry is usually not an option as well because of the radioactivity involved. Characterization relies solely on the detection of radioactivity on a TLC or HPLC column and comparing its retention factor to that of a non-radioactive standard.

Keeping these principles in mind it is first necessary to attempt to synthesize some fluorinated derivatives using non-radioactive ^{19}F in order to prove the radiochemical reaction is potentially possible and can be done in a reasonable time frame. This is also necessary to have authentic samples for comparison on radio-TLC and radio-HPLC.

Research Objectives

It is clear from the literature that further studies are required to validate GCase as an attractive biomarker for detecting the early and accurate onset of PD and as a potential therapeutic target for drug development in patients with or without GBA1 mutations. To accomplish this the development of molecular tools is required to study GCase *in vitro* and *in vivo*. In this thesis, lead compound **7** will be used to develop synthetic routes to prepare activity based probes as molecular tools for studying GCase by completing the following objectives:

- Optimize the synthesis of octyl aziridine **7** using an improved protecting groups strategy that is more flexible and suited for future probe development in terms of preparing aziridines having structural diversity, generating fluorescent derivatives and radiolabelling studies.
- Synthesize fluorescently labelled derivatives of **7** that potently and irreversibly label GCase.
- Synthesize non-radioactive ^{19}F-labeled derivatives of **7** as PET tracer candidates and use them for enzyme kinetic studies to measure inactivation rates and authentic standards to determine TLC R_f and HPLC retention times for future radiolabeling experiments.
- Develop radiochemical procedures for ^{18}F labeling derivatives of **7** at the cyclotron facility.

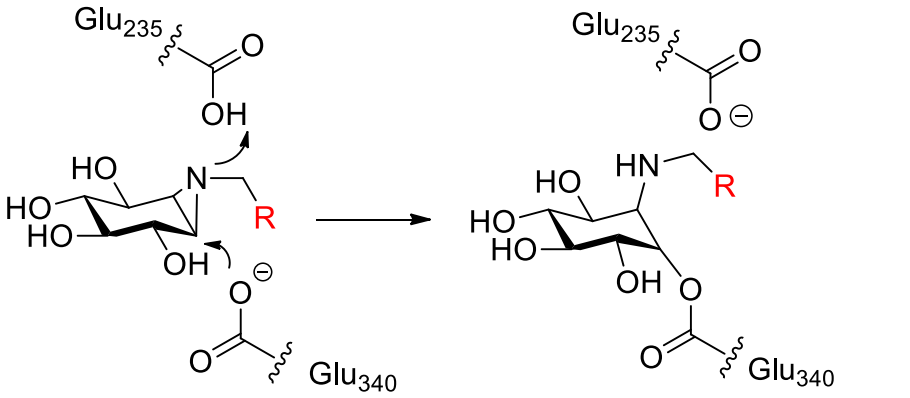

GCase Active Site Labelled

R= Fluorescent or Radioactive Tag

Figure 12: N-alkylated conduritol aziridines bearing either a fluorescent moiety or an ^{18}F tag for future imaging studies. The hypothesized mechanism of action for labelling the active site of GCase is likely to occur through covalent attachment of the cylitol ring to glutamic acid 340.

Results and Discussion

Previous Synthesis

The synthesis of racemic *N*-alkylated conduritol aziridines was previously established by Adams *et al* as shown in Scheme I.[46] This synthesis was concise and effective for obtaining the desired alkylated products to test these compounds as potent and irreversible inhibitors of GCase. Developing simple and efficient chemistry, starting from inexpensive starting materials, is noteworthy considering the numerous stereochemical issues that surround carbohydrate and inositol synthesis as well as stability issues and protecting group compatibility with the formation of aziridine rings. The synthesis begins with regioselective isopropylidene protection of the hydroxyls on the C1 and C2 carbons of commercially available *myo*-inositol using a known procedure to obtain **1**.[66] Although compound **1** is produced in a regioselective manner the resulting procedure unavoidably forms a racemic mixture. Next, per-benzylation of **1** into tetrabenzyl **2** and subsequently deprotection the isopropylidene under acidic conditions gave diol **3**, both in quantitative yields (Scheme 1). The harsh acidic deprotection of isopropylidene is possible due to the great stability of the Bn protecting group in acid. After complete mesylation of **3**, regioselective azidolysis of the mesyl group on the C2 carbon of inositol can be accomplished in DMF using NaN_3. This selectivity is thought to arise from the bulky Bn protecting groups forcing the inositol ring to configure in such a way that the benzyl groups are positioned equatorial thus having the mesyl group at the C2 carbon axial while the mesyl at the C1 carbon remains equatorial (Figure 13). This is the thermodynamically favoured ring conformation and promotes S_N2 substitution at the C2 position because the antibonding orbital of the leaving group is open for nucleophilic attack while in the C1 position the orbital is blocked inside the inositol ring. Despite this thermodynamic favourability, the overall yield from **3** to **4** is only 44%. Azide displacement rates of secondary mesylates are slow at low temperatures coupled with the presence of steric hindrance presented by the neighbouring multiple bulky Bn groups. High temperatures are required to compensate for slow conversion which increases the ability of the ring to flip and thus azidolysis of the C1 position to form a diazide by-product unavoidably

limits the yield of this step.

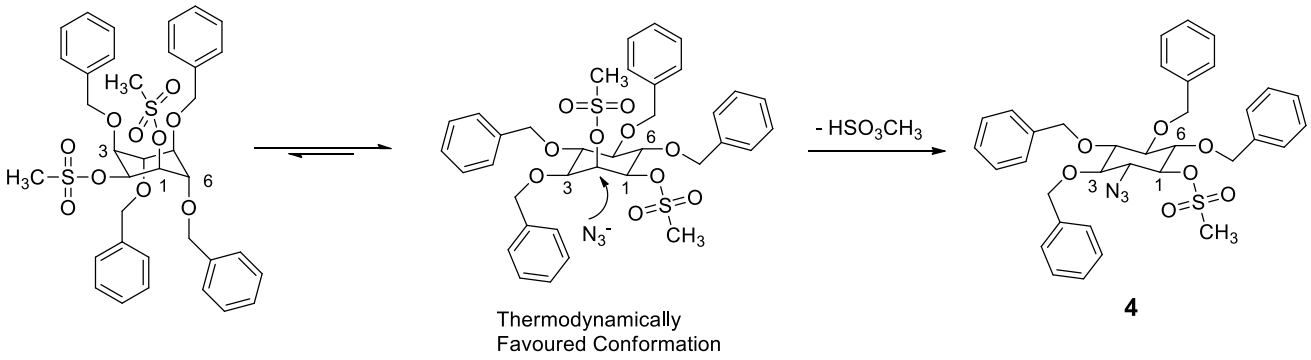

Figure 13: Tetrabenzylated inositol 3 after mesylation is thought to prefer a chair conformation where the Bn groups are predominately equatorial because of the reduction in steric hindrance. This is proven by reaction with sodium azide giving predominantly monoazide **4**.

Azide **4** is reduced with $LiAlH_4$ to form aziridine **5** in a 60% yield. This step, although effective for forming the aziridine, reduces the scope of different functional and protecting groups that can be used to prepare new derivatives and activity-based probes as many groups will not survive this powerful reducing agent. After reduction, the aziridine can be alkylated by simply heating **5** with K_2CO_3 and an iodo-alkane of differing length in DMF to yield various alkylated aziridines including **6**. For final deprotection, although hydrogenolysis using Pd and H_2 is not compatible with aziridines, tetra-benzylated **6** can be deprotected successfully into lead compound **7** using Birch reduction. It was uncertain if the aziridine ring would survive Birch reduction conditions but Adams showed the ring to be stable under Birch conditions at -78°C.[46] At this temperature conversion of **6** into unprotected aziridine **7** did not occur as quickly as anticipated but showed good conversion after 4 hours giving the final product in 55% yield. Adams has thus successfully demonstrated the ability to synthesize lead compound **7** which will act as the scaffold, in this thesis, to produce fluorescent and fluorinated derivatives as activity based probes to study GCase in biological systems.

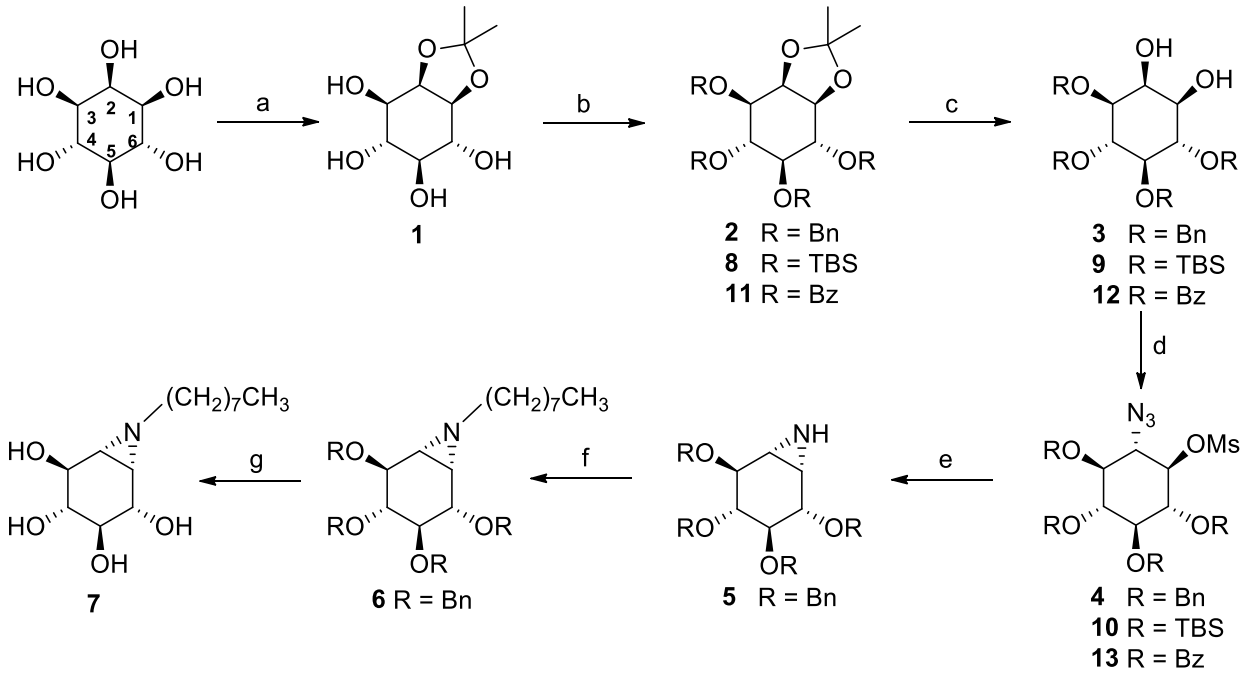

Scheme 1: Protecting group discovery. (a) 2,2-Dimethoxypropane, pTsOH, DMSO, 90°C, 69%; (b) BnBr, NaH, DMF, 0°C – rt, 89% for 2; 1)TBSCl,, imidazole, DMF, 80°C, 2) TBSOTf, 2,6-lutidine, DMF, 80°C,55% for 8;, BzCl, DMAP, pyridine, rt, 95%, for 11; (c) 80% AcOH(aq), reflux, 95% for 3 and 12; TFA: CH_2Cl_2: H_2O 4:4:1, 0°C, 63% for 9; (d) i) MsCl, pyridine, 0°C – rt; ii) NaN_3, DMSO, 75°C, 42%, (e) $LiAlH_4$ 0°C – rt, 60% for 5; Ph_3P, TEA, THF: H_2O (10:1), rt – reflux for 14; (f) iodooctane, K_2CO_3, DMF, 50°C, 59%; (g) $Na_{(s)}$, $NH_{3(l)}$, THF, -78°C, 4 h, 55%;

Protecting Group Optimization

Adams' attempted Bn deprotection with standard hydrogenolysis conditions using hydrogen gas with a pallidum catalyst but was never successful in obtaining **7** as the desired product.[46] This is probably because these standard hydrogenolysis conditions have been shown to either open,[67] rearrange[68] or dealkylate[69] an aziridine ring. To circumvent these issues, the Birch reduction was utilized instead. Removal of the Bn protecting groups is the biggest limitation in Adams' synthesis for the diversity of future fluorescent and radiochemical derivatives because of the Birch reduction step. This deprotection method works well for producing the deprotected aziridine **7** as well as other alkylated compounds but it would not be compatible with any derivatives containing reducible functional groups like alkenes, alkynes and some aromatic groups like the kinds typically found in fluorescent probes. Furthermore, this technique would be very difficult to replicate in a cyclotron facility because of the complex setup and lengthy reaction times required to remove the Bn groups. Radiochemical reactions involving ^{18}F are typically those that are less than 2 hours in total and whose protocol can eventually be adapted for an

automated synthesis module. Discovery of a faster and more versatile Bn deprotection method was required to generate a more diverse library of compounds based on lead compound **7**.

Different Bn deprotection strategies were investigated that were shown to be more versatile and quicker than Birch reduction in the literature. Reductive cleavage using $Li_{(s)}$ with naphthalene in THF at -20°C was employed because of previous reports in the literature where many functional groups that become reduced by Birch reduction still survive these conditions.[70] After monitoring the reaction it was shown to have very low conversion rates from **6** to **7** even after long reaction times with no detectable product formed by TLC. Hydrogenolysis was attempted using triethylsilane as a different source of hydrogen compared to hydrogen gas.[71] Using a less abundant source of hydrogen was thought to remove the Bn groups before a reaction with the aziridine ring occurred but conversion of starting material was not seen. $FeCl_3$ in CH_2Cl_2 has been used for the deprotection of Bn groups but for **6** the strong Lewis acid produced a compound that did not move off the baseline on TLC suggesting decomposition of the aziridine.[72] Despite testing several different conditions, an alternative Bn deprotection method was not discovered. This suggested that other protecting groups should be explored.

There are several different hydroxyl protecting groups available but not all groups possess the qualities desired for this synthesis. The protecting groups must be installed onto neighbouring hydroxyl groups on an inositol ring, must survive the entire synthesis and must be removed easily when required. In addition, they must remain stably attached to the desired hydroxy group since some protecting groups are known to transfer to adjacent hydroxyls making them inappropriate for inositol chemistry. The TBS group was the first alternative protecting group chosen to incorporate onto compound **2** because of its stability to $LiAlH_4$, the reagent used in the aziridine formation step. Also its simplistic removal using TBAF was considered to be favoured for the final deprotection step. TBS is one of the bulkier silyl protecting groups, giving it enhanced stability. However, the steric bulk of the TBS group appeared to be a problem early on in the synthesis. Interestingly, treatment of isopropylidene **1** with an excess of imidazole and TBSCl yielded a tri-silyated compound instead of desired tetra-silyated **8**. Installing the fourth TBS group was extremely difficult due to steric crowding. Although tetra TBS **8** could be obtained using the expensive TBSOTf instead of TBSCl a more potent electrophile, the isolated yields were not ideal considering this is only the second step in the synthesis. Despite having concerns that the TBS group would be removed under harsh acidic conditions, short treatment of **8** using TFA: CH_2Cl_2: H_2O 4:4:1 at 0°C allowed the isopropylidene to remain intact in order to get **9** in 63% yield. Mesylation of diol **9** was found to proceed smoothly, however, azidolysis, was unsuccessful as conversion of the mesylate into **10** was not possible. Increasing temperature was not sufficient to enable conversion into **10.** This is thought to be because of the extreme bulkiness of the TBS groups crowding the site of nucleophilic attack.

Inability to form the azide **10** using sodium azide led to the discard of this protecting group strategy for preparing fluorescent or radioactive derivatives.

Another protecting group that seemed like an obvious choice was the Bz ester protecting group. The Bz protecting group is the ester cousin of the Bn ether protecting group having similar size and structure but much higher lability to basic conditions. This conceivably would allow for efficient deprotection without destroying the acid labile aziridine group. Reaction of isopropylidene **1** with benzoyl chloride in presence of DMAP successfully generated tetrabenzoyl **11** using a published procedure [83] and deprotection of the acetal using acidic conditions proceeded smoothly to yield the tetrabenzoyl **12** in quantitative yield**.** However, reaction of the dimesylate with NaN_3 yielded many side products resulting in low isolated yield. The formation of many different products during this reaction could be due to the Bz group's tendency to migrate to neighbouring hydroxyl groups or its propensity to act as an electrophile towards, for example, a nucleophile like sodium azide.[54]

From these experiments it was clear that careful choice of the protecting group is required taking into account steric bulk and chemical reactivity. Although the silyl ethers were stable, they were too bulky leading to difficulty in preparing the tetra TBS inositol **8** and unsuccessful preparation of azide **10**. The Bz ester protecting groups appeared to produce many side products upon reaction with higher temperatures and nucleophilic azide present. Since the ether based Bn protecting group strategy was successful for the synthesis of the *N*-alkyl aziridines prepared by Adams, we decided to explore other ether-based protecting groups. The MOM protecting group is another ether based protecting group that is highly stable to basic, reducing and oxidizing conditions while still being mildly stable to acidic conditions.[54] To avoid any potential issues of acidic lability of the MOM ethers, benzaldehyde acetal was used to protect *myo*-inositol regioselectively forming **15** using a known literature protocol[74] instead of forming the isopropylidene. The MOM group was easily installed in quantitative yield to get **16** and the benzaldehyde acetal was removed using hydrogenolysis with hydrogen gas and palladium catalyst to yield the diol **17** also quantitatively (Scheme 2). Mesylation of the diol into **18** proceeded smoothly followed by azidolysis performed in DMF to form the expected mono azide that was difficult to isolate by traditional methods like silica gel chromatography or recrystallization. This is most likely due to the smaller size of the MOM group not delivering the same reaction selectivity and chromatographic separation as with the Bn group as a result of the decreased steric hindrance and increased conformation flexibility of the ring. Formation of additional side products associated with this reaction have increased and may be very similar in polarity to the desired product making purification more difficult. Despite not being able to characterize the reaction products using NMR spectroscopy, the crude materials were used directly for azide reduction to form aziridine **19**. Instead of using $LiAlH_4$ we opted to use Ph_3P and added

water to perform a Staudinger reduction of the azide to subsequently obtain aziridine **19**. Compound **19** was successfully isolated in 58% yield over 2 steps. Considering safety, the reaction efficiency and simplicity of the Staudinger reaction for forming the aziridine ring, it was deemed the new standard compared to using $LiAlH_4$ reduction which is water sensitive, more difficult to work-up and much more dangerous to handle.

N-alkylation of the aziridine was performed using iodooctane and *N,N*-diisopropylethylamine proceeding smoothly to obtain **20** in 55% yield. Global deprotection of **20** was difficult under acidic conditions such as with TFA or HCl because high concentrations of acid were required to remove all MOM groups in a reasonable time frame but we observed by TLC the conversion rate to product to be just as quick as the decomposition of the product. This is probably due to acid catalyzed opening of the aziridine ring. As anticipated, MOM groups can also be removed using a strong Lewis acid like TMSBr. By using 20 equivalents of TMSBr, anhydrous acetonitrile and an inert atmosphere at 0°C, deprotection of fully protected **20** into *N*-alkylated aziridine **7** occurred at an impressive 83% yield. More interestingly this reaction could be completed in about 30 - 40 minutes. Careful workup of this reaction was important as saturated $NaHCO_3$ was required to hydrolyze the bromo intermediate formed during this reaction and to eliminate any HBr that may form. The MOM protecting group demonstrated to be an adequate substitute for the Bn group for carrying out the complete synthesis of an *N*-alkylated conduritol aziridine. It also proved to be superior to the Bn group because of its quick and simple deprotection. Synthesis with MOM as the protecting group is anticipated to yield a large diversity of derivatives and to be much more suitable for radiolabeling reactions using the short-lived ^{18}F isotope.

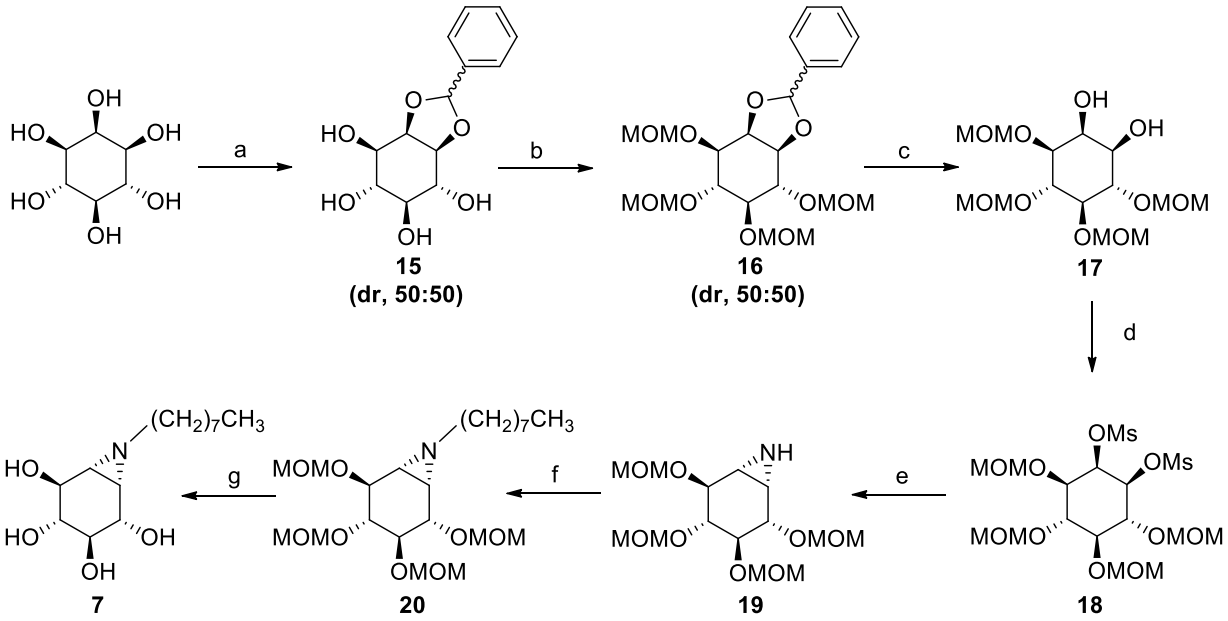

Scheme 2: Complete synthesis of 7 using the MOM protecting group. (a) Dimethoxy toluene, pTsOH, DMF, 120°C, 70%; (b) MOMCl, DIPEA, DMF, 65°C, 95%; (c) $H_{2\,(g)}$ (1 atm), Pd/C, EtOAc 95%; (d) MsCl, pyridine, 0°C – rt, 95%; (e) i) NaN_3, DMF, 80°C, ii) Ph_3P, TEA, THF: H_2O (10:1), rt – reflux, 58% over 2 steps; (f) iodooctane, DIPEA, acetonitrile, reflux, 55%; (g) TMSBr, acetonitrile, 0°C, 30 min, 83%;

Fluorescent Derivatives

Having established a new synthetic method for generating racemic *N*-alkylated conduritol aziridines through utilization of the MOM protecting group, the synthesis of fluorescent derivatives that are able to probe GCase activity was pursued next. Indeed, any fluorescent microscopy techniques that could track GCase location and activity in live cells is important for studying its involvement in PD since trafficking of the enzyme to the lysosome is apparently disrupted. We envisioned that attaching a fluorescent reporter molecule appended to the aziridine ring would result in an efficient activity-based probe that would irreversibly and selectively bind to GCase inside living cells. Additionally, recent reports in the literature have shown that bulky groups are well-tolerated and even preferred in the hydrophobic binding pocket of GCase.[56] Consequently, it is not unreasonable to assume that the potent GCase binding affinity and selectivity of the *N*-octyl conduritol aziridine **7** should be retained after incorporation of a fluorescent reporter. As mentioned before it is important to choose a molecule that maintains high fluorescence at the low pH present in the lysosome. This is why BODIPY, Acridine and Dichlorofluorescein were chosen as the fluorophores used to prepare the fluorescent aziridine derivatives.

BODIPY is a hydrophobic fluorophore that has a large quantum yield and has strong fluorescence that is insensitive to changes in pH. LysoTracker® is a BODIPY derivative designed to accumulate in the

acidic lysosomes and is the gold standard routinely used for fluorescent tracking of the organelle in live cell studies. As shown in Scheme 3, we found that alkylation of **19** with bromo-BODIPY **21a** under basic conditions and sodium iodide effectively produced **21** with a 50% yield (Scheme3). Although this was a highly encouraging result that produced the first fluorescent derivative in our lab, deprotection of the MOM ethers of **21** into the aziridine **22** was unsuccessful. Deprotection with TMSBr yielded an insoluble, non-fluorescent compound that that remained at the baseline of a TLC. The formation of an insoluble product is probably due to the strong Lewis Acid nature of TMSBr and its ability to react with the boron difluoride component in BODIPY. Other deprotection conditions were investigated to remove the MOM ethers such as various combinations of TFA and HCl in different solvents like CH_2Cl_2, THF and Dioxane. The various experimental conditions were found to either yield complex mixtures of partially deprotected compounds or non-fluorescent derivatives resulting from degradation of the BODIPY fluorophore. Since MOM deprotection in the presence of BODIPY was not compatible, coupling of BODIPY after deprotection was attempted. Alkyne **35** was synthesized (discussed later) and used for Sonogashira coupling by using 4-iodo-BODIPY-benzene **23a** to make **23**. Only starting material remained, despite trying both anhydrous and refluxing conditions. **35** was also used to attempt a Huisgen 1,3-Dipolar copper catalyzed cycloaddition using BODIPY-azide **24a** to obtain **24**. Despite several solvent combinations with DMF, H_2O or tert-Butanol along with different catalyst concentrations of $CuSO_4$, sodium ascorbate and tris-(benzyltriazolylmethyl)amine (TBTA) **24** was not synthesized.

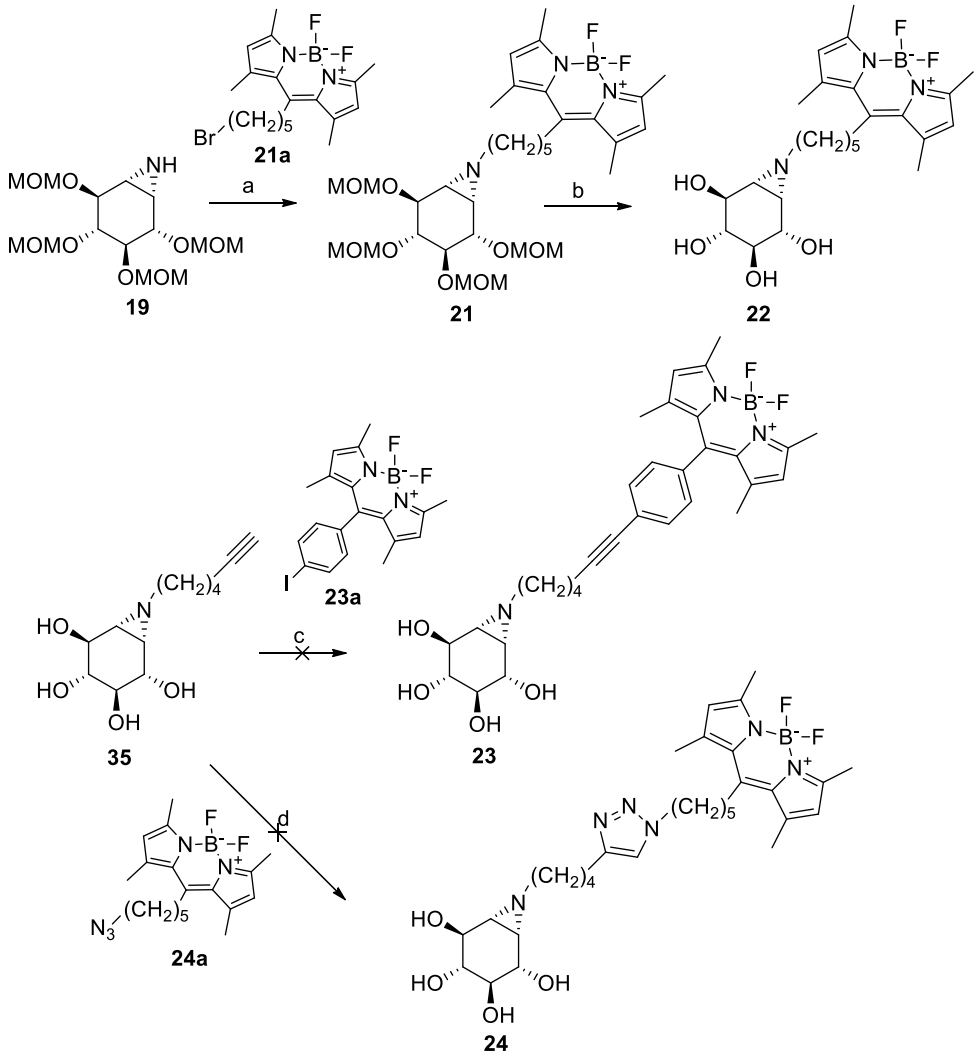

Scheme 3: Towards BODIPY inspired fluorescent derivatives. (a) **21a**, DIPEA, NaI, acetonitrile, reflux, 50%; (b) TMSBr, acetonitrile, 0°C; (c) **23a**, $Pd(PPh_3)_4$, CuI, TEA, DMF, reflux; (d) **24a**, $CuSO_4$, sodium ascorbate, TBTA, DMF: H_2O (4:1).

Since all attempts to incorporate BODIPY onto the aziridine scaffold failed, a new fluorescent reporter molecule was chosen. Acridine Orange is a versatile dye used for staining DNA, RNA in eukaryotes and prokaryotes.[73] It is highly fluorescent at low pH which also makes it useful for studying the acidic environment of the lysosome. 9-amino-Acridine (not shown) is commercially available and has been used as a nucleophile for coupling Acridine to certain drug-like molecules. These reactions, however, require harsh reaction conditions because of the poor nucleophilicity of the primary amine connected to the Acridine backbone and the delocalization of the non-bonding electrons into the aromatic rings. 9-amino-Acridine heated at 90°C with mesylated aziridine **37** (Scheme 5) and under basic conditions (NaH or $CsCO_3$) showed no reaction as 9-amino-Acridine remained and **37** was hydrolyzed.

Since the nucleophilic substitution reaction of mesylated aziridine did not produce the desired fluorescent compound, Sonogashira coupling was attempted instead. 9-iodo-Acridine **28a** was prepared from 9-chloro-Acridine and immediately reacted with the MOM protected alkyne **32** under Sonogashira conditions successfully producing fluorescent aziridine **28** in 68% yield (Scheme 4). MOM deprotection using standard TMSBr conditions gave the deprotected fluorescent aziridine **29** in 66% yield, the first fluorescent *N*-alkylated conduritol aziridine derivative synthesized in our lab. The excitation and emission maxima were found to be 355 nm and 455 nm respectively, giving **29** fluorescence in the blue range of the visible light spectrum (Figure 14).

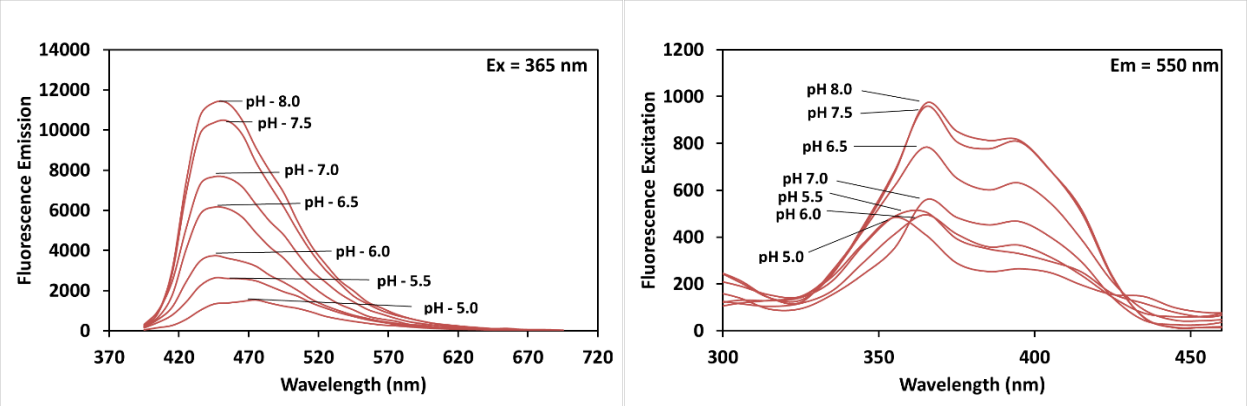

Figure 14: Emission and excitation spectra for 29 measured in a 96 well plate using a Biotek Synergy 4 hybrid multi-mode reader. Fluorescence was measured using 1 µM final concentration of compound **29** in 50 mM NaOAc buffer at various pH. Fluorescence from buffer without any compound was used as a blank and subtracted from all measurements. The sensitivity of the instrument was set at 100 and the measurements were done in 10 nm increments. The Ex_{max} = 355 nm and the Em_{max} = 455 nm at pH 5.

Due to the success of the Sonogashira coupling to prepare the Acridine labeled aziridine as described above, similar chemistry was utilized for coupling of another fluorophore, Dichlorofluorescein. This fluorophore is more photostable than fluorescein and the electron withdrawing halogens reduce the pKa of the phenolic protons thus allowing the compound to be highly fluorescent at low pH. The Dichlorofluorescein was acetylated prior to Sonogashira coupling to prevent the opening and closing of its lactone ring and increase its solubility in organic solvent. An acetylated iodo derivative of Dichlorofluorescein **30a** was prepared as a 5(6) isomer in the interest of available resources and time using a known protocol.[80] **31** was coupled with alkyne **32** using Sonogashira conditions (Scheme 4)**.** The reaction proved to be slower than in the similar reaction with the 9-iodo-Acridine but the coupling was successful nonetheless to produce compound **30** in a 31% yield. Upon MOM deprotection with TMSBr, the reaction solution became very fluorescent, suggesting the acetate groups were also being removed. Nevertheless, acetate removal was assured by stirring the crude product mixture in MeOH and K_2CO_3 for

1 hour after quenching. After silica gel column purification, the second fluorescent derivative **31** was obtained in 90% yield. The excitation and emission maximums were found to be 510 nm and 525 nm respectively, giving **31** fluorescence in the green range of the visible light spectrum (Figure 15).

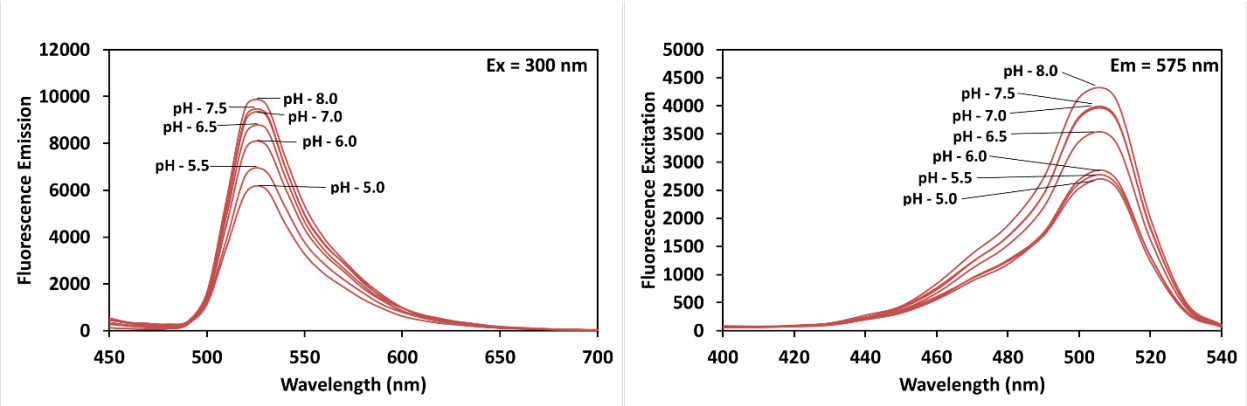

Figure 15: Emission and excitation spectra for 31 measured in a 96 well plate using a Biotek Synergy 4 hybrid multi-mode reader. Fluorescence was measured using 1 µM final concentration of compound **31** in 50 mM NaOAc buffer at various pH. Fluorescence from buffer without any compound was used as a blank and subtracted from all measurements. The sensitivity of the instrument was set at 100 and the measurements were done in 10 nm increments. The Ex_{max} = 510 nm and the Em_{max} = 525 nm at pH 5.

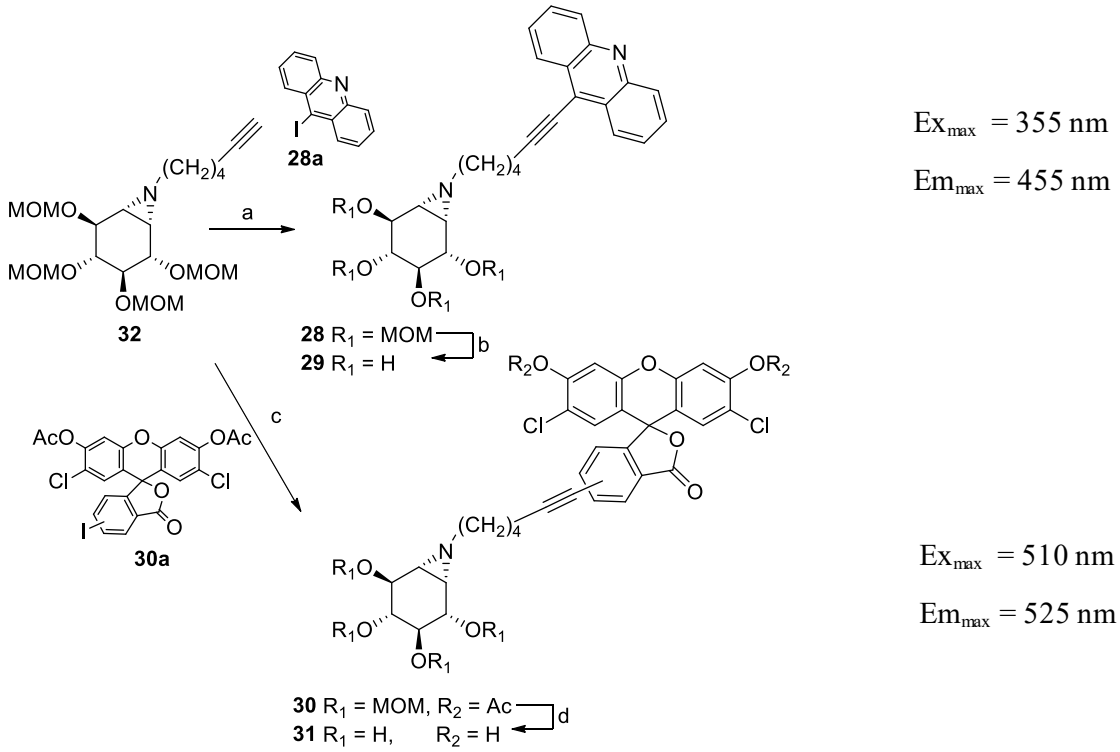

Scheme 4: Successful synthesis of Acridine and Dichlorofluorescein inspired conduritol aziridine derivatives. (a) **28a**, $Pd(PPh_3)_4$, CuI, TEA, THF, reflux, 68%; (b) TMSBr, acetonitrile, 0°C, 66%; (c) **30a**, $Pd(PPh_3)_4$, CuI, TEA, THF, rt, 31%; (d) TMSBr, acetonitrile, 0°C, 90%

Having two different fluorescent derivatives is beneficial simply for the fact that their behaviour in a biological system is unknown until cellular experiments are performed. It is unknown how the fluorophore will affect binding to GCase, permeability of the aziridine compound to enter into the cell, permeability into the lysosome and tendencies to become trapped in different compartments/organelles of the cell. From the fluorescence spectra in Figure 15 and Figure 16 it already appears that the Dichlorofluorescein derivative **31** will be less sensitive to low pH in terms of its fluorescence intensity and therefore in terms of its ability to ionize. Acridine and Dichlorofluorescein are different in the sense that Acridine possesses a nitrogen within its ring structure with a pKa of around 5.6 resulting in a significant percentage of the fluorophore becoming positively charged in the acidic environment of the lysosome thus affecting binding affinity to GCase. In addition, weakly basic amines are known to spontaneously accumulate in the acidic lysosome (a process called lysosomotropism) where they become protonated and are unable to passively diffuse by the lysosomal membrane. Such behavior of a fluorescent probe intended to image a lysosomal enzyme could potentially result in false positive signal due to the lysomotropism. On the other hand, Dichlorofluorescein has two ionisable phenols and a carboxylic acid moiety with a pKa of approximately 4.8 resulting in predominantly an anionic species

inside in a living cell. Besides having different chemical properties, the two fluorescent derivatives also fluoresce at different wavelengths which is useful to avoid overlap with other fluorescent compounds in an *in vitro* experiment such as DAPI (for revealing the nucleus of a cell) or LysoTracker® dye for staining lysosomes. Both of these dyes would be useful in future cell based imaging experiments to validate the fluorescent probes. The fluorescent probes synthesized in this section have the potential to monitor GCase trafficking inside living cells, a potential mechanism of PD progression.

Radioactive Derivatives

PET imaging can be used to non-invasively track GCase activity in a living biological organism like a mouse or human. In order to do this, a radioactive derivative of **7,** labeled with a PET isotope like ^{18}F**,** needs to be developed to be employed as a radiopharmaceutical imaging agent.

The first fluorinating strategy attempted was Sonogashira coupling using commercially available 4-fluoro-iodobenzene (FIB). Radiochemical ^{18}F fluorination using ^{18}F-FIB is a technique shown to be successful for other compounds, including highly polar compounds, similar to the deprotected conduritol aziridines.[75] The MOM protected aziridine **19** was alkylated using 6-iodo-alkyne to cleanly obtain alkyne **32** in 30% yield (Scheme 5). Subsequent Sonogashira coupling with FIB was shown to be efficient in refluxing acetonitrile, yielding aryl-fluorinated aziridine **33** nearly quantitatively after only 30 minutes reaction time. Then, fluorinated derivative **33** was deprotected using TMSBr deprotection to yield the free aziridine **34** in 49% yield. These were encouraging results, since high yields and rapid reactions are required for radiochemistry using the short-lived ^{18}F isotope. Interestingly, it was found that the MOM groups of **32** could be deprotected before Sonogashira coupling to give alkyne **35**, an extremely polar derivative. For Sonogashira coupling of **35** with FIB the solvent was switched to 1:1 acetonitrile: water to compensate for the increased polarity of the reactants and to ensure solubility. It was surprising that this Sonogashira coupling proceeded in the presence of water as Sonogashira couplings are often required to be anhydrous. The coupling of FIB with **35** was just as efficient as with **32** to also yield compound **34** quantitatively. The robustness of this coupling was comforting for performing future radiochemical reactions.

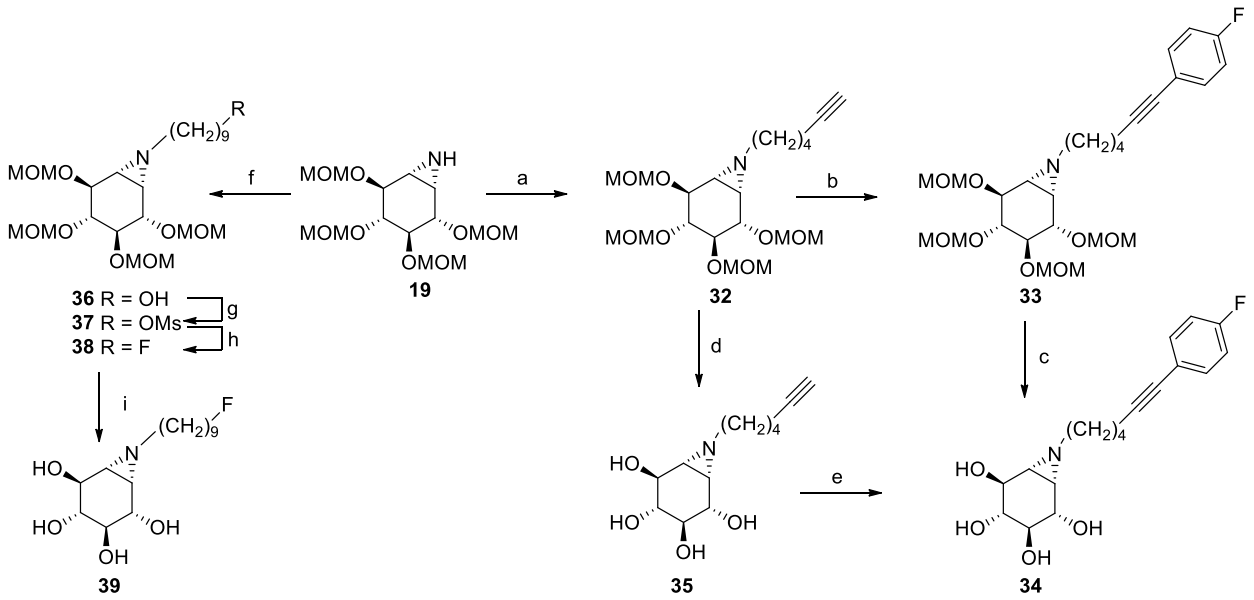

Scheme 5: Synthesis of fluorinated conduritol aziridine authentic standards for radiochemistry. (a) 6-iodo-1-hexyne, DIPEA, acetonitrile, reflux, 30%; (b) FIB, $Pd(PPh_3)_4$, CuI, TEA, acetonitrile, reflux, 15 min, 95%; (c) TMSBr, acetonitrile, 0°C, 30 min, 49%; (d) TMSBr, acetonitrile, 0°C, 30 min, 95%; (e) FIB, $Pd(PPh_3)_4$, CuI, TEA, acetonitrile: H_2O 1:1, reflux, 15 min, 95%; (f) 9-bromo-1-nonanol, DIPEA, NaI, acetonitrile, reflux 35%; (g) MsCl, TEA, CH_2Cl_2, 0° - rt, 90%; (h) TEAF, acetonitrile, reflux, 15 min 56%; (i) TMSBr, acetonitrile, 0°C, 30 min, 75%

After having promising results using Sonogashira coupling with FIB, efforts were made to utilize these conditions for radiolabelling alkyne **35**. To investigate this reaction ^{18}F-FIB must be synthesized and then conjugated to alkyne **35** using Sonogashira coupling. The synthesis of ^{18}F-FIB has been published by Wuest et al. and they have shown excellent results from using commercially available precursor (4-iodophenyl)diphenylsulfonium triflate **40** (Scheme 6).[76] Using a GE TRACERlab FX N PRO automated synthesis module, ^{18}F-FIB **41** was made by azeotropically drying a mixture of ^{18}F fluoride in K2.2.2/K_2CO_3, adding the diaryl sulfonium precursor **40** in acetonitrile and reacting this mixture for 15 minutes at 90°C. The reaction was diluted with water, loaded onto a Waters (Milford, MA, US) Sep-Pak® tC18 plus light cartridge, washed with water and crude ^{18}F-FIB **41** was eluted to a separate reactor using acetonitrile. This reactor contained alkyne **35** and all the reagents required for Sonogashira coupling. The reaction was heated to 90°C for 20 minutes, cooled, filtered using a 0.2 µm Nylon filter then analyzed using HPLC. Unexpectedly, **42** was not formed by this reaction, despite the successful reaction using non-radioactive ^{19}F-FIB. This was confusing considering the successful Sonogashira coupling used to make the non-radioactive fluorinated standards in the laboratory. To investigate this reaction further, fluorination of diphenylsulfonium triflate **40** into ^{18}F-FIB **41** was investigated using ^{19}F fluoride. It appeared, under the exact same conditions except stoichiometric amounts of fluoride instead of

radiochemical amounts of fluoride were used, FIB was not synthesized according to TLC and NMR using the same reaction conditions as reported earlier. Instead, a compound having a different but similar TLC Rf value to ^{19}F-FIB always appeared. After analyzing the NMR spectra of this side product (Appendix 1) it was confirmed that this species was not ^{19}F- FIB nor the starting material. The Wuest group was contacted for some insight but it seemed they have never tried this synthesis using ^{19}F fluoride because ^{19}F-FIB is commercially available and the radiochemical labeling reactions reliably worked as they could show the ^{18}F-FIB was being synthesized through co-injection experiments using HPLC. Furthermore, they used the purified ^{18}F-FIB to conduct successful Sonogashira couplings to prepare a variety of PET tracers.[75]

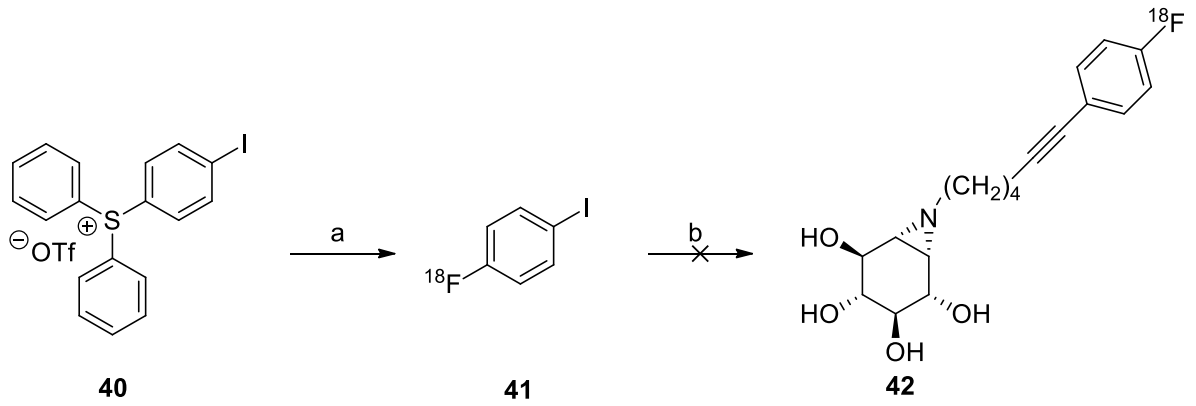

Scheme 6: Sonogashira radiolabelling of compound 35. (a) K[^{18}F]F K_{222}, K_2CO_3 , acetonitrile, 90°C, 15 min; (b) **35**, $Pd(PPh_3)_4$, CuI, TEA, acetonitrile: H_2O 1:1, 90°C, 20 min.

The part of the Wuest protocol that was changed for the formation of **42** was the absence of an HPLC purification step after formation of ^{18}F-FIB **41**. This step was omitted because it was assumed that upon washing **41** on a Waters tC_{18} Sep-Pak that the only compound being retained would be ^{18}F-FIB. Indeed, upon characterization of the contents in the reaction mixture after purification on a Waters tC_{18} Sep-Pak it was found that the starting material diphenylsulfonium triflate **40** was also retained despite its polarity and would contaminate the Sonogashira coupling step. Considering that the ^{18}F isotope is present at μg to ng levels in a radiochemical reaction, even having small amounts of contaminating **40,** a potent electrophile**,** could possibly interfere with the Sonogashira coupling of **41** with **35** thus preventing the preparation of the PET tracer.

Considering the automated synthesis modules were not setup to do an intermediary HPLC purification, attempts were made to try and purify the crude reaction mixture of the fluorination of **40** without having to do a HPLC purification in between reactions. Solvent conditions were optimized so that

a Waters silica gel Sep-Pak could be used to elute ^{18}F-FIB but trap the positively charged diaryl sulphonium triflate **40** before entering the second reaction. Different solvents were tested on the silica gel Sep-Pak to find that diethyl ether appeared to not elute **40** from the cartridge while completely eluting FIB. This was encouraging because instead of purifying ^{18}F-FIB **41** using HPLC, a silica gel cartridge may be used to remove **40** plus other polar impurities before the second reaction to takes place. Unfortunately, upon HPLC analysis of the ^{18}F-FIB **41** reaction mixture it appeared purity did not differ substantially between a mixture purified with a silica gel cartridge and without. The UV trace at 254 nm did not differ significantly between the crude mixture purified with and without the silica Sep Pak despite TLC analysis showing no traces of **40** (Figure 16). It was obvious that either some of **40** was still passing through or some other impurity existed that could not be removed without an HPLC purification. Since the cyclotron facility in Thunder Bay is not currently set up properly for doing HPLC purification in the middle of an automated synthesis, this strategy was set aside to be pursued in the future.

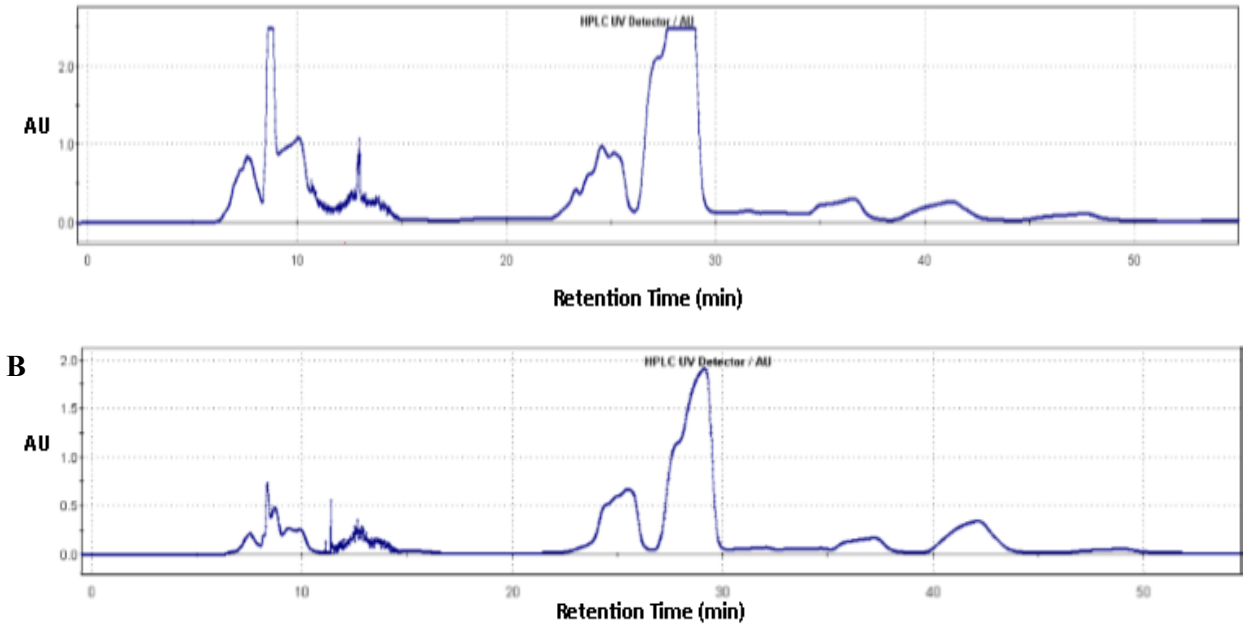

Figure 16: HPLC chromatogram of the reaction mixture of diaryl sulphonium triflate 40 with KF, K_2CO_3, K2.2.2 in acetonitrile at 90°C for 15 minutes after washing on a Waters tC18 Sep Pak. A) without additional Waters silica gel Sep Pak purification and B) with additional Waters silica gel Sep Pak purification. The mixture was co-injected with commercially available FIB which can be seen at around 28 minutes. HPLC separation was performed using a gradient elution as follows: (A: water; B: CH_3CN; 0 min 50% B, 8 min 50% B, 21 min 80% B). The flow rate of the system was 3 mL/min.

The most common fluorination strategy to prepare low levels of PET tracers for initial *in vivo* studies in animals is to perform manual synthesis using small amounts of ^{18}F fluoride for S_N2

displacement of a leaving group installed onto a precursor. Commonly used leaving groups for this type of chemistry are mesyl and tosyl groups. Alkylating the MOM protected aziridine **19** with 9-bromo-nonanol successfully yielded **36** and upon treatment with mesyl chloride **37** was obtained in excellent yield. The mesylated precursor **37** was treated with tetra ethyl ammonium fluoride (TEAF) in refluxing acetonitrile to get fluorinated **38** with a 56% yield in 15 minutes. MOM deprotection with TMSBr using previously optimized conditions afforded fluorinated *N*-alkylated conduritol aziridine **39** with a 75% yield in approximately 40 minutes (Scheme 5). Given the high yields and short reaction times, this synthetic method also shows promise for ^{18}F radiochemical labelling.

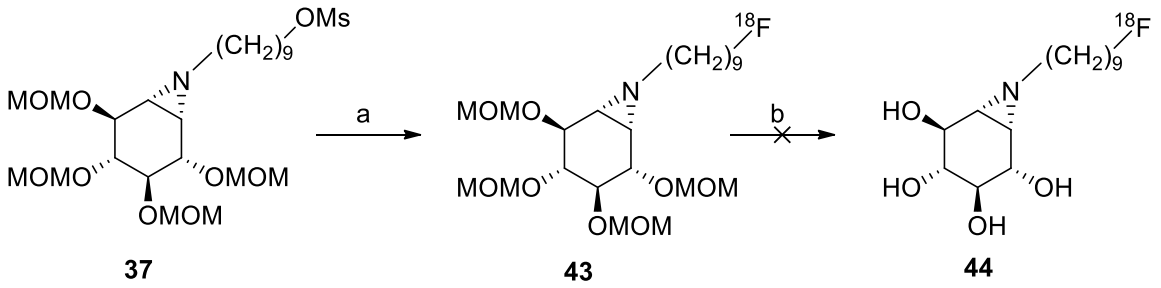

37 **43** **44**

Scheme 7: Radiolabelling of 37 using nucleophilic fluoride to perform a mesyl substitution. (a) [^{18}F]TEAF, acetonitrile, 90°C, 15 min; (b) 1) TMSBr, acetonitrile, rt, 20 minutes, 2) saturated $NaHCO_3$.

Considering the hardships presented by the automated synthesis modules, which are typically reserved for clinical translation of a PET tracer, this reaction was attempted using low levels of activity (≈ 300 MBq) for manual radiochemical synthesis. For this reaction the ^{18}F in $H_2{}^{18}O$ was first loaded onto a Waters (Milford, MA, US) Sep-Pak® light QMA anion-exchange cartridge (filled with quaternary ammonium chloride polymer) and the cartridge was washed with 5 mL of hexanes to remove all water according to a known procedure.[77] The cartridge was then eluted upside down (to improve ^{18}F elution yield) using tetra ethyl ammonium bicarbonate (TEAB) in pure acetonitrile. This allowed for elution of the ^{18}F without any azeotropic drying to remove contaminating water which would interfere with the nucleophilic substitution reaction. The ^{18}F-TEAF was mixed with **37** and heated on a thermomixer for 15 minutes at 90°C (Scheme 7). Radio-TLC suggests that the ^{18}F-fluorine was successfully incorporated into the aziridine compound (Figure 17). The deprotection was attempted by cooling the mixture to room temperature and adding TMSBr directly. The mixture was stirred at room temperature for 20 minutes then quenched with saturated $NaHCO_3$ The mixture was analyzed by radio-TLC but it appeared decomposition had occurred as the radioactive peaks were only detected at the baseline despite the authentic standard having an R_f above the baseline. Time permitting, it would be useful to try different deprotection conditions but access to ^{18}F limited the number of attempts had at this reaction.

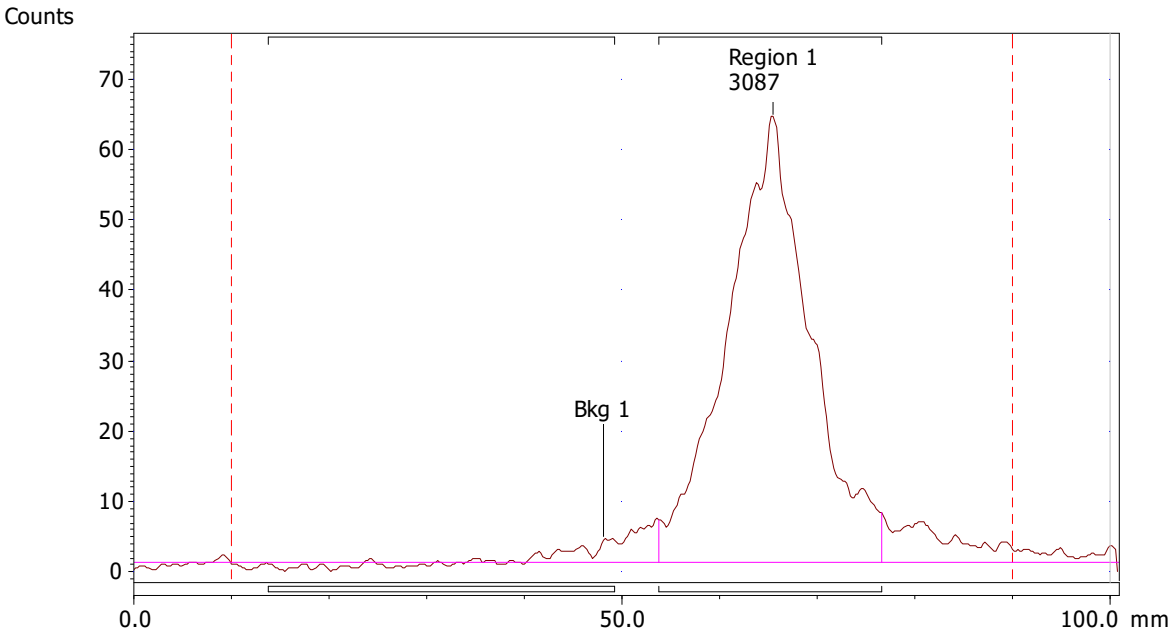

Figure 17: Radio-TLC chromatogram showing TLC after reaction of Mesylate 37 to get fluorinated 43. Compound **43** was shown to match the R_f of authentic standard **38** of 0.70 in 2:1 EtOAc: Hexanes. Radiochemical purity appears to be over 90%.

Enzyme Kinetics – Measuring Inactivation Rates of Novel Inhibitors

To compare the rate of GCase inactivation of fluorinated derivatives **34** and **39** to that of lead compound **7,** a range of eight concentrations of the inhibitor predicted to surround the K_i value were incubated with Cerezyme® (recombinant GCase), and the reaction mixtures were assayed for residual enzyme activity at different time intervals. Small aliquots of these reaction mixtures were withdrawn and diluted 20-fold in 96 well plates containing a final concentration of 4 mM of the substrate 2,4-DNP-β-D-Glc. Dilution of the reaction mixture effectively halts further inactivation by diluting the inhibitor and active site competition by excess substrate. Residual enzymatic activity at different time points and concentrations was monitored by quantifying the release of 2,4-DNP after 2,4- DNP-β-D-Glc cleavage by Cerezyme®.

In Figure 18, k_i is the rate constant for inhibitor inactivation of an enzyme and K_i (k_{-1}/k_1) is the dissociation constant for the inhibitor with the enzyme otherwise known as the binding affinity.[78] The ratio k_i/K_i is an indication of the efficiency of an inhibitor, taking into account both binding efficiency and inactivation rate.

$$E + I \underset{k_{-1}}{\overset{k_1}{\rightleftharpoons}} E \bullet I \xrightarrow{k_i} E\text{-}I$$

Figure 18: General depiction of an irreversible inhibitor binding to an enzyme. The rate constant of the of the inhibitor dissociating from the enzyme (k_{-1}) over the rate constant of the inhibitor binding to the enzyme (k_1) gives the dissociation constant K_i for the inhibitor to the enzyme. Smaller K_i values equate to higher binding affinities. Reaction of the enzyme with the inhibitor can occur after binding to form an irreversible enzyme-inhibitor complex. The rate of this reaction is k_i. The ratio of k_i/K_i is an overall measure of the efficiency of an irreversible inhibitor.

The velocity data obtained from this inactivation assay was fit, using the GraphPad Prism software, to **Equation 1** a one phase decay equation. From this equation it is possible to obtain an observed rate constant k_{obs} for the inactivation of Cerezyme® by the inhibitors tested. The observed rate constant would allow for the determination of enzyme kinetic parameters k_i and K_i.

Equation 1: $$Y = (Y_0 - Plateau)e^{(-k_{obs})x} + Plateau$$

Inactivation data would follow **Equation 2** if saturation of the enzyme's active site occurs at high inhibitor concentrations. This allows for separation of k_i and K_i values. The data will have an observable curve when this equation can be used effectively.

Equation 2: $$k_{obs} = \frac{k_i[I]}{K_i + [I]}$$

In cases where saturation cannot be observed due to rapid inactivation of the enzyme at high concentrations of inhibitor, the data will appear linear and **Equation 3** must be used which gives the second order rate constant as the ratio of k_i to K_i.

Equation 3: $$k_{obs} = \frac{k_i[I]}{K_i}$$

All of the inhibitors tested followed **Equation 3** demonstrating their highly efficient rate of inactivation. The kinetic analysis of the aziridine inhibitors can be seen in Figure 19**.** The rapid inactivation of Cerezyme® by the inhibitors tested in this work prevented the determination of individual K_i and k_i values. This is because at saturating concentrations of inhibitor, the enzyme is almost instantaneously inactivated. As a result, we could only determine the second order rate constant of inactivation k_i/K_i, a parameter still useful to compare the efficiency of fluorinated probes **34** and **39** to lead compound **7**. This was not surprising as Adams *et al.* demonstrated these *N*-alkylated conduritol aziridines to be very efficient inactivators of GCase. It was found that the k_i/K_i values for butyl, hexyl and octyl (**7**) conduritol aziridines to be 3.8 ± 0.1 $mM^{-1}min^{-1}$, 640 ± 30 $mM^{-1}min^{-1}$, and 3670 ± 70 $mM^{-1}min^{-1}$

respectively.[46] It is clear from this data that as carbons are added to the alkyl chain binding affinity increases dramatically.

From examining the k_i/K_i values obtained from the inactivation experiments it is clear that the binding affinities **34** and **39** are not much different than that of lead compound **7** (Figure 19). The k_i/K_i values for **7**, **34**, and **39** were found to be 6600 ± 500 $mM^{-1}min^{-1}$, 5100 ± 100 $mM^{-1}min^{-1}$, and 7700 ± 400 $mM^{-1}min^{-1}$ respectively. This demonstrates how potency was conserved upon installation of the fluorine or fluorinating handle. With a k_i/K_i of $77\% \pm 2\%$ that of lead compound **7** the Sonogashira coupled derivative **34** appears to be slightly less efficient at binding to Cerezyme® than **7** possibly due to the rigidity imposed by the aromatic/alkyne structure reducing interaction with the hydrophobic binding site in GCase. Alternatively, with a k_i/K_i of $116\% \pm 5\%$ that of lead compound **7, 39** appears to be slightly more efficient at inactivating Cerezyme®, possibly due to the increased length of alkyl chain where Adams *et al.* has previously shown to significantly impact the binding affinities of these alkylated conduritol aziridines.[46] This does give rationale to synthesize conduritol aziridines with longer alkyl chains in the future to try and discover the upper limits of this trend. Regardless, this kinetic information shows that fluorinated derivatives **34** and **39** do not suffer from decreased binding affinity to GCase and radioactive derivatives have promise as PET imaging probes for imaging GCase in living organisms. In fact, [^{11}C]-deprenyl is an irreversible inhibitor used to PET image monoamine oxidase B in the human brain. Since [^{11}C]-deprenyl was measured to inactivate monoamine oxidase B with a k_i/K_i of 6400 $mM^{-1}min^{-1}$,[79] we are confident that the fluorinated PET tracer candidates prepared in this thesis have sufficient inactivation rates to be used as PET tracers for imaging GCase in the brain of animals or humans assuming permeability of the BBB.

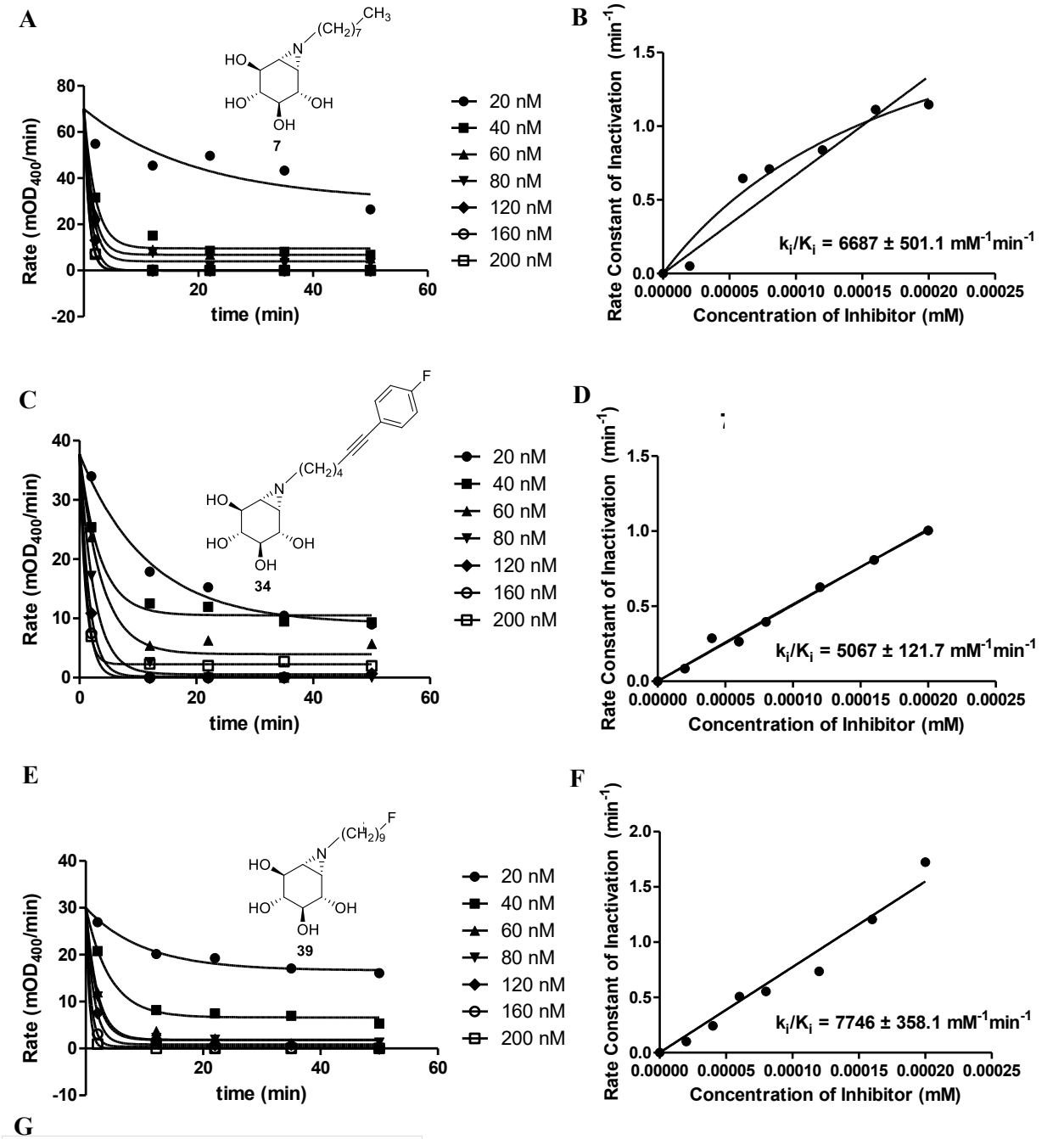

Figure 18: Inactivation of GCase experiment. Plot of remaining enzyme activity over time at the indicated inhibitor concentrations fitted to a one phase decay equation for A) **7**, C) **34**, E) **39**. Plots of the observed rate constants of inactivation versus the concentration of inhibitor for B) **7**, D) **34**, F) **39**. G) k_i/K_i calculated for **7, 34** and **39** normalized to **7.**

Future Work

Fluorescent Derivatives

Having access to two fluorescent derivatives, it is now possible to begin characterizing these compounds *in vitro*. The first experiment would be to measure the inactivation rate constants of each fluorescent derivative **29** and **31** towards GCase. Enzyme inactivation rates of Cerezyme® would be done to estimate the binding affinity of **29** and **31** towards recombinant human GCase. Enzyme kinetic studies will also be done with GBA2 and GBA3 to evaluate enzyme selectivity of **29** and **31.** Next the ability of the probes to get into a cell with healthy GCase activity would be measured. In a healthy cell, GCase should be concentrated in the lysosomes so overlaying a fluorescent image of probes **29** or **31** with an image of cells incubated with LysoTracker® should show fluorescence of both in the same location. Lastly the probes should be incubated with high concentrations of a competitive GCase inhibitor to compete with **29** and **31** for the GCase binding site. By showing that **29** and **31** do not accumulate in the lysosome when GCase is not available it can be assumed that the probes are bound to GCase and not just freely floating in the cell or being trapped inside the lysosome by accumulated charge.

After these experiments conclude that **29** and **31** have high affinity and specificity towards GCase, *in vitro* studies will be done to assess if these probes are able to cross the blood brain barrier (BBB) or if they are substrates of p-glycoprotein or a multidrug resistance transporter.[57] In addition, experiments performed by Dr. Shusheng Wang in the Phenix lab has indicated the conduritol aziridines are transported by *myo*-inositol transport proteins. These transport proteins are highly expressed in the cells that form the BBB and could transport the aziridine compounds into the brain. Experiments would first incubate cells with the probes **29** and **31** in the presence of *myo*-inositol as a competition assay. If the aziridines are substrates of these transporters, high concentration of *myo*-inositol would prevent their cellular uptake. Another test using a trans-well assay with a mono-layer of canine kidney cells can be used to measure the probes ability to escape the protein pumps that often make small lipophilic compounds impermeable to the BBB.[81]

After validation of **29** and **31** as effective molecular probes is complete, these fluorescent compounds may act as molecular tools for studying GCase in cell models and animal tissue samples to elucidate its role in the progression of PD. If the compounds are shown to suffer from poor binding affinity, binding efficiency, GCase selectivity or cell permeability then new derivatives will be developed using structure activity relationship information to overcome these issues.

Radioactive Derivatives

Although the fluorescent derivatives would act as activity based probes designed for imaging GCase in cells, it would be beneficial to know that the fluorinated derivatives also have the ability to permeate cells and label GCase *in cellulo*. This would provide a more accurate indication on how they would behave *in vivo* compared to fluorescent derivatives which contain bulky fluorophores that can affect enzyme binding and membrane permeability. Studies can be done to measure inactivation rates of GCase in cells by incubating cells with different concentrations of fluorinated derivatives **34** and **39**, preparing cell lysates from these cells and then measuring residual enzyme activity after incubation. In this way it is possible to obtain information on the selectivity of our compounds to GCase over GBA2 and GBA3, to obtain information on enzyme inactivation in a more natural setting and to determine how the compounds accumulate in a cellular environment.

Once a radioactive derivative has been made, fully characterized and tested for quality control, animal experiments can commence to study **34** and **39**'s biodistribution in a living organism and their BBB permeability. If **34** or **39** can permeate the BBB successfully then comparative studies can commence to demonstrate the difference in GCase levels in a healthy animal and GCase levels in animal with PD. If an image difference can be shown it could validate both GCase as a target in the study of PD and the ability of **34** or **39** to detect GCase activity in an *in vivo* model. These PET probes would be valuable molecular tools for elucidating the involvement of GCase in PD, aid in drug design that seek to increase GCase levels in PD and Gaucher disease and help unravel the molecular mechanisms of disease progression involving GCase.

Reversible Inhibitors

Although there are many examples of irreversible PET imaging agents[82] it is possible that an irreversible PET tracer that is very potent may suffer from biodistribution issues. Considering there is GCase in several tissues in the body besides the brain it is possible that a potent irreversible inhibitor may interact and become trapped by GCase outside the brain. Although modifying an irreversible inhibitor to improve its biodistribution is possible it may be beneficial to design a reversible inhibitor derivative of our compounds. This inhibitor can be designed so that it binds strongly to the enzyme but never becomes covalently bound to it. Reversible active site inhibitors of GCase have already been synthesized in the literature. They have been shown as well to also possess molecular chaperone abilities, promoting the trafficking of mutant and misfolded GCase to the lysosome as a potential therapy of Gaucher disease. Once trafficked to the lysosome, a reversible inhibitor may dissociate from the enzyme, allowing the

enzyme to act upon its natural substrate glucosylceramide. In this way a reversible inhibitor may act as a suitable PET imaging agent but also act as a potential drug for both Gaucher Disease and potentially PD.

Conclusions

N-octyl conduritol aziridine **7** has been shown to be an extremely potent and selective inhibitor of GCase in the literature.[46] Recent evidence strongly suggests GCase is involved in the progression of PD and could possibly be a therapeutic target. The objective of this thesis work was to develop synthetic routes to prepare *N*-alkylated conduritol aziridine derivatives as potential activity-based probes for studying GCase in biological systems. The synthesis of **7** was optimized using MOM protecting groups to set in place a synthesis pathway that is efficient, tolerant of the addition of new functional groups and finishes with a rapid deprotection step to yield the final compounds. This synthesis pathway was implemented to produce two fluorescent derivatives **29** and **31** for the detection of GCase in cell based systems. Two fluorinated derivatives **34** and **39** were also produced with the intention of using this methodology to prepare radioactive derivatives **42** and **44** for detection of GCase in animal based models using PET imaging. In future work, these activity based probes will be tested for cell permeability, BBB permeability, GCase specificity and the ability to detect GCase in biological systems. If successful with detecting GCase, whether it be through fluorescent microscopy or PET imaging, these activity based probes will be invaluable molecular tools for elucidating GCase's involvement in the progression of PD, for evaluating therapeutic potential of new drugs and for the accurate and early diagnosis of PD.

Experimental

All buffers and reagents were obtained from Fisher Scientific or Sigma-Aldrich and used without further purification. Synthetic reactions were monitored by TLC using precoated silica gel plates (Silicycle 60F254, 0.25mm thickness). Compounds were detected by ultraviolet light ($\lambda = 254$nm) followed by visualization with ammonium molybdate (10% w/v in 2M H_2SO_4), permanganate (1% w/v in water), or ninhydrin (1.5% w/v solution in butanol), with heating. Flash chromatography was performed using Silicyle silica gel (230-400 mesh). NMR spectra were obtained using a Varian Unity Inova 500 MHz spectrometer dissolving samples in the appropriate deuterated solvents ($CDCl_3$, or CD_3OD). Chemical shifts were reported in ppm downfield from tetramethylsilane. Low resolution ESI mass spectrometry was performed on a Advion Expression CMS Mass Spectrometer. HPLC was done using a VP 250/10 Nucleosil 100-5 C18 Nautilus semi-preparative column (100Å, 250 × 10mm, 5 µm). [^{18}F] Fluoride (n.c.a.) was produced on a TR-24 cyclotron (Advanced Cyclotron Systems Inc., Richmond, Canada) via the $^{18}O(p,n)^{18}F$ nuclear reaction. Depending on the activity required the target was irradiated at 18 MeV and the F-18 containing O^{18} enriched water was transferred and used directly for use in synthesis, or the previously emptied target was washed with deionized water followed by transfer to the reaction set up.

Synthesis

(±)-(((3aR,4S,5R,6R,7S,7aS)-2,2-dimethylhexahydrobenzo[d][1,3]dioxole-4,5,6,7-tetrayl)tetrakis(oxy))tetrakis(tert-butyldimethylsilane) (8)

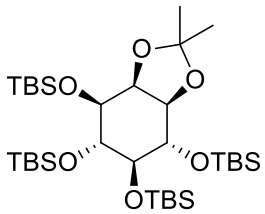

1 (2.08 g, 9.46 mmol) was dissolved in 125 mL of DMF. Imidazole (3.86 g, 56.76 mmol) and TBSCl (8.56 g, 56.76 mmol) were added and the reaction mixture was heated to 80°C and stirred overnight. The next day TBSOTf (5 g, 18.92 mmol) and 2,6-lutidine (2.2 mL, 18.92 mmol) were added and the reaction was reacted another 24 hours. The reaction was cooled to room temperature and the solvent was removed under vacuum. The crude residue was dissolved in 150 mL of EtOAc and washed with 150 mL of H_2O. The aqueous layer was extracted 2 x with 100 mL of EtOAc and the organic layers were combined, washed with brine, dried with Na_2SO_4 and filtered. The solvents were removed under vacuum and resulting residues was purified using silica gel column chromatography (2% Ethyl ether: Hexanes) to get

8 (3.5 g, 55%) as a colourless oil. ^{1}H NMR (500 MHz, $CDCl_3$) δ 4.38 – 4.30 (m, 2H), 4.04 – 3.96 (m, 2H), 3.84 (d, *J* = 4.3 Hz, 1H), 3.55 (d, *J* = 7.7 Hz, 1H), 1.46 (s, 3H), 1.29 (s, 3H), 0.92 – 0.90 (m, 18H), 0.90 – 0.86 (m, 18H), 0.14 – 0.05 (m, 24H). ^{13}C NMR (126 MHz, $CDCl_3$) δ 113.03, 86.20, 84.37, 82.62, 82.03, 81.77, 81.72, 81.52, 78.50, 75.02, 49.76, 31.34, 30.98, 30.72, 30.68, 28.56, 23.36, 22.77, 22.76, 22.71, 4.77, 1.57, 1.50, 1.31, 1.05, 1.00, 0.15, 0.02, -0.00. LRMS (APCI): m/z Calcd for $[C_{33}H_{72}O_6Si_4 + Na]^+$: 699.4298; found: 699.8.

(±)-(1R,2S,3S,4R,5R,6S)-3,4,5,6-tetrakis((tert-butyldimethylsilyl)oxy)cyclohexane-1,2-diol (9)

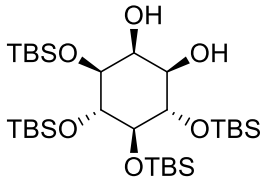

8 (48 mg, 0.07 mmol) was mixed in 1.75 mL of CH_2Cl_2 and cooled to 0°C. Freshly made 4:4:1 TFA: CH_2Cl_2: H_2O (0.175 mL) was added to this mixture and the reaction was stirred vigorously at 0°C for 1 hour. The reaction was then quenched with saturated $NaHCO_3$ at the same temperature and partitioned between 10 mL of EtOAc and 10 mL of H_2O. The aqueous layer was extracted 2 x with 10 mL of EtOAc and the organic layers were combined, washed with brine, dried with Na_2SO_4 and filtered. The solvents were removed under vacuum and resulting residues was purified using silica gel column chromatography (2%→5% EtOAc: Hexanes) to get **9** (28 mg, 63%) as a colourless oil. ^{1}H NMR (500 MHz, $CDCl_3$) δ 4.02 (dd, *J* = 7.4, 5.8 Hz, 2H), 3.81-3.70 (m, 2H), 3.26 (dd, *J* = 12.1, 3.5 Hz, 1H), 2.71 (dd, *J* = 11.4, 3.2 Hz, 1H), 0.96 – 0.90 (m, 18H), 0.90-0.84 (m, 18H), 0.27 – 0.04 (m, 24H). LRMS (ESI -ve): m/z Calcd for $[C_{30}H_{68}O_6Si_4 - H]^-$: 635.4020; found: 635.6.

(±)-(3aR,4S,5R,6R,7S,7aS)-2,2-dimethylhexahydrobenzo[d][1,3]dioxole-4,5,6,7-tetrayl tetrabenzoate (11)

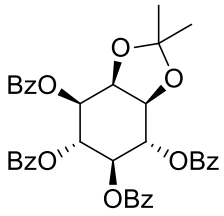

1 (1 g, 4.54 mmol) was added to 26 mL of dry pyridine with DMAP (55 mg, 0.454 mmol). BzCl (4.22 mL, 36.32 mmol) was added to the mixture and the reaction occurred for 24 hours at room temperature. The mixture was diluted with 100 mL of EtOAc and washed with 100 mL of a 5% $CuSO_4$ aqueous solution. The aqueous layer was extracted 2 x with 50mL of EtOAc and the organic layers were

combined, washed with brine, dried with Na_2SO_4 and filtered. The solvents were removed under vacuum and the product was purified by silica gel column chromatography (8:1 Hexanes: EtOAc) to get **11** (2.74 g, 95 %) as a white powder. NMR consistent with that published in the literature.[83]

(±)-(1S,2R,3R,4S,5R,6S)-5,6-dihydroxycyclohexane-1,2,3,4-tetrayl tetrabenzoate (12)

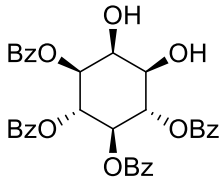

11 (13 g, 20.42 mmol) was dissolved in 80% $AcOH_{(aq)}$ and refluxed for 4 hours. Solvent was removed under vacuum. The product was purified by silica gel column chromatography (1:2 → 1:1 EtOAc: Hexanes) to get **12** (11.56 g, 95 %) as a white powder. ^{1}H NMR (500 MHz, $CDCl_3$) δ 8.00 (d, *J* = 7.9 Hz, 2H), 7.94 (d, *J* = 7.9 Hz, 2H), 7.88 – 7.79 (m, 2H), 7.53 – 7.46 (m, 2H), 7.37 – 7.30 (m, 4H), 7.31 – 7.22 (m, 4H), 6.34 (dd, *J* = 10.9, 9.2 Hz, 1H), 5.97 – 5.83 (m, 2H), 5.47 (dd, *J* = 10.4, 2.3 Hz, 1H), 4.62 (d, *J* = 2.3 Hz, 1H), 4.14 (dd, *J* = 8.8, 1.0 Hz, 1H), 3.43 (br s, 1H). ^{13}C NMR (126 MHz, $CDCl_3$) δ 167.17, 165.89, 165.85, 165.81, 133.56, 133.48, 133.29, 133.26, 130.03, 129.84, 129.78, 129.14, 129.10, 129.05, 128.94, 128.56, 128.46, 128.40, 73.85, 72.44, 71.16, 71.05, 70.70, 70.17. LRMS (ESI): m/z Calcd for $[C_{34}H_{28}O_{10} + Na]^+$: 619.1575; found: 619.7.

(±)-(1R,2S,3R,4S,5S,6R)-5-azido-6-((methylsulfonyl)oxy)cyclohexane-1,2,3,4-tetrayl tetrabenzoate (13)

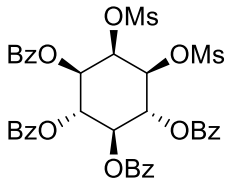

13a

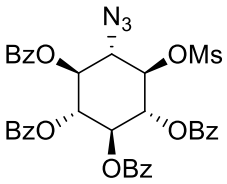

13

12 (5 g, 8.39 mmol) was dissolved in 24 mL of pyridine and cooled to 0°C. MsCl (3.25 mL, 41.94 mmol) was added dropwise and the reaction was allowed to warm to room temperature overnight. The mixture was diluted with 100 mL of EtOAc and washed with 100 mL of an 5% $CuSO_4$ aqueous solution. The aqueous layer was extracted 2 x with 50mL of EtOAc and the organic layers were combined, washed with brine, dried with Na_2SO_4 and filtered. The solvents were removed under vacuum and the crude was filtered through a pad of silica gel using 1:1 EtOAc: Hexanes to quantitatively get 6 grams of essentially pure dimesylate **13a** ^{1}H NMR (500 MHz, $CDCl_3$) δ 7.99 (dd, *J* = 17.4, 7.3 Hz, 4H), 7.83 (d, *J* = 8.0 Hz, 4H), 7.56 – 7.48 (m, 2H), 7.47 – 7.34 (m, 6H), 7.34 – 7.27 (m, 4H), 6.22 (dd, *J* = 11.6, 8.7 Hz, 1H), 6.12

(dd, J = 11.5, 8.7 Hz, 1H), 5.95 (dd, J = 11.5, 8.5 Hz, 1H), 5.74 – 5.59 (m, J = 5.4, 2.6 Hz, 2H), 5.32 (ddd, J = 11.2, 7.0, 2.9 Hz, 1H), 3.24 (s, 3H), 2.99 (s, 3H). ^{13}C NMR (126 MHz, $CDCl_3$) δ 165.53, 165.48, 165.39, 165.25, 133.94, 133.86, 133.62, 133.55, 130.14, 129.99, 129.93, 129.84, 128.72, 128.62, 128.50, 128.42, 128.38, 77.25, 74.34, 70.49, 69.41, 69.28, 69.13, 39.42, 38.99. The crude dimesylate (1 g, 1.328 mmol) was dissolved in 7 mL of DMF and NaN_3 (432 mg, 6.64 mmol) was added. The reaction was heated to 75°C and reacted for 48 hours. The mixture was cooled to room temperature and diluted with 100 mL of EtOAc and 100 mL of H_2O. The aqueous layer was extracted 2 times with 50 mL of EtOAc and the organic layers were combined, washed with brine, dried with Na_2SO_4 and filtered. The solvents were removed under vacuum and the crude was not shown to contain **13**.

(±)-1,2-*O*-benzylidene-*myo*-inositol (15)

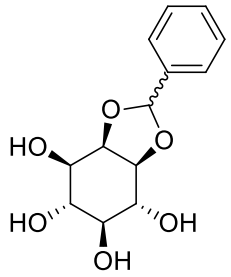

Myo-inositol (15 g, 83.33 mmol) and p-toluene sulfonic acid (700 mg, 3.68 mmol) were dissolved in 160 mL of DMF. In a second flask dimethoxy toluene (20 mL, 133.25 mmol) was dissolved in 48 mL of DMF. This solution was added to the reaction vessel with stirring and the mixture was heated to 120°C for 1 h. Anhydrous sodium carbonate (1170 mg, 11.14 mmol) was then added to the reaction mixture and the solvent was removed under vacuum. The resulting residue was purified using silica gel column chromatography (1:0 → 2:1, CH_2Cl_2:MeOH) to get **15** (15.57 g, 70%) as a white powder. NMR consistent with that published in the literature.[74]

(±)-(3aR,4R,5S,6S,7R,7aS)-4,5,6,7-tetrakis(methoxymethoxy)-2-phenylhexahydrobenzo[d][1,3]dioxole (16)

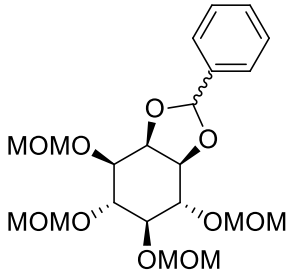

15 (15 g, 55.9 mmol) was dissolved in 45 mL of DMF and 66.2 mL of DIPEA. MOMCl (21 mL, 276.5 mmol) was added slowly at room temperature and the mixture was heated to 65°C overnight. The reaction was allowed to cool to room temperature and was quenched with 200 mL of water. The aqueous layer was extracted with 3 times 200 mL of EtOAc. The organic portions were collected and washed with 0.1 M HCl until neutralized and washed with brine. The organic layer was dried with sodium sulphate, filtered and concentrated under vacuum. The residue was purified with silica gel column chromatography (1:1, EtOAc: Hexanes) to get **16** as a diastereotopic mixture (*dr*, 50:50), (24 g, 95%) in the form of a colourless oil. ^{1}H NMR (500 MHz, $CDCl_3$) δ 7.61 – 7.55 (m, 2H), 7.51 – 7.43 (m, 2H), 7.41 – 7.33 (m, 6H), 6.23 (s, 1H), 5.86 (s, 1H), 4.90 – 4.75 (m, 16H), 4.57 – 4.46 (m, 2H), 4.38 – 4.23 (m, 2H), 4.17 – 4.07 (m, 2H), 4.07 – 3.91 (m, 4H), 3.72 – 3.57 (m, 2H), 3.50 – 3.39 (m, 18H), 3.38 – 3.35 (m, 6H). ^{13}C NMR (126 MHz, $CDCl_3$) δ 129.55, 129.13, 128.37, 127.23, 126.25, 104.61, 103.59, 97.51, 97.15, 96.59, 79.47, 78.90, 78.71, 78.33, 77.92, 77.51, 76.45, 75.79, 75.53, 74.82, 56.19, 55.83. LRMS (ESI): m/z Calcd for $[C_{21}H_{32}O_{10} + Na]^+$: 467.1888; found: 467.6.

(±)-(1R,2S,3S,4R,5R,6S)-3,4,5,6-tetrakis(methoxymethoxy)cyclohexane-1,2-diol (17)

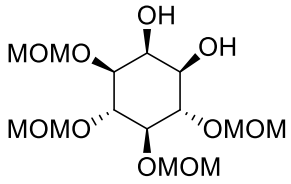

16 (23 g, 33.75 mmol) was dissolved in 50 mL of EtOAc. 3 grams of 10 wt % Pd/C was added and the reaction was stirred under hydrogen atmosphere (1 atm) overnight. The mixture was filtered through a small portion of celite followed by silica gel to provide essentially pure **17** (11.4 g, 95%) after concentration under vacuum as a colourless oil. ^{1}H NMR (500 MHz, $CDCl_3$) δ 4.93 – 4.68 (m, 8H), 4.41 – 4.37 (m, 1H), 4.26 – 4.19 (m, 1H), 3.98 (dd, *J* = 14.9, 9.7 Hz, 1H), 3.67 (dd, *J* = 14.6, 9.3 Hz, 1H), 3.55 – 3.49 (m, 1H), 3.48 – 3.40 (m, 12H), 2.88 – 2.80 (m, 1H). ^{13}C NMR (126 MHz, $CDCl_3$) δ 98.96, 98.51,

98.33, 96.68, 84.52, 78.90, 77.34, 70.81, 70.38, 56.31, 56.06, 55.78. LRMS (ESI): m/z Calcd for $[C_{14}H_{28}O_{10} + Na]^+$: 379.1575; found: 379.0.

(±)-(1R,2S,3R,4S,5S,6R)-3,4,5,6-tetrakis(methoxymethoxy)cyclohexane-1,2-diyl dimethanesulfonate (18)

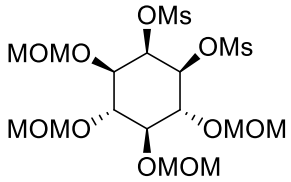

17 (600 mg, 1.68 mmol) was dissolved in 4 mL of pyridine and cooled to 0°C. Mesyl chloride (0.65 mL, 8.42 mmol) was added dropwise and the reaction was allowed to warm to room temperature and react overnight. The mixture was separated between 50 mL 5% $CuSO_4$ solution and 50 mL of EtOAc. The aqueous layer was extracted 2 times with 50 mL of EtOAc and the organic layers were washed once with water and once with brine. The organic layer was dried with sodium sulfate, filtered and concentrated under vacuum to get **18** (815 mg, 95%) as a yellow oil. ^{1}H NMR (500 MHz, $CDCl_3$) δ 5.30 – 5.21 (m, 1H), 4.94 – 4.69 (m, 8H), 4.55 (dt, *J* = 10.1, 2.7 Hz, 1H), 3.93 (dd, *J* = 10.9, 8.6 Hz, 1H), 3.86 (dd, *J* = 11.1, 8.7 Hz, 1H), 3.69 (dd, *J* = 6.5, 3.5 Hz, 1H), 3.51 (dd, *J* = 10.9, 8.2 Hz, 1H), 3.48 – 3.37 (m, 12H), 3.22 – 3.17 (m, 6H). ^{13}C NMR (126 MHz, $CDCl_3$) δ 98.85, 98.75, 98.65, 98.56, 96.42, 79.25, 78.89, 76.42 , 75.72, 73.35,56.65 , 56.63, 56.41, 39.45, 39.19. LRMS (ESI): m/z Calcd for $[C_{16}H_{32}O_{14}S_2 + Na]^+$: 535.1126; found: 535.0.

(±)-(1R,2S,3R,4R,5S,6S)-2,3,4,5-tetrakis(methoxymethoxy)-7-azabicyclo[4.1.0]heptane (19)

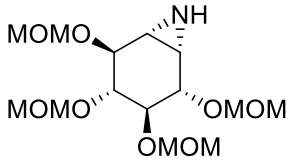

18 (11 g, 21.48 mmol) and NaN_3 (1.54 g, 23.63 mmol) was dissolved in 185 mL of DMF and heated at 75°C for 2 days. The mixture was cooled to room temperature and partitioned between 400 mL of water and 400 mL of EtOAc. After extracting 3 times with 400 mL EtOAc the organic layers were combined and washed with brine then dried with sodium sulphate. The solvent was filtered and concentrated under vacuum to get the monoazide compound in a crude mixture as a colourless oil. To this was added triethylamine (6.3 mL, 45.11 mmol) and Ph_3P (8.45 g, 32.22 mmol) which were then dissolved in 130 mL of THF and allowed to react for 30 minutes at room temperature. 13 mL of water was added and the reaction mixture was heated to reflux overnight. The reaction was quenched with 400 mL of water and

extracted 3 times with 400 mL of EtOAc. The organic layers were combined and washed with brine, dried with sodium sulphate, filtered and concentrated under vacuum. The crude residue was purified using silica gel column chromatography (100% EtOAc) to get **19** (4.14 g, 58% over 2 steps) as a light yellow oil. ^{1}H NMR (500 MHz, $CDCl_3$) δ 4.89 – 4.70 (m, 8H), 3.89 – 3.73 (m, 2H), 3.56 (dd, J = 9.4 Hz, J = 9.4 Hz 1H), 3.42 (s, 6H), 3.38 (s, 6H), 3.37 – 3.31 (m, 1H), 2.70 – 2.57 (m, 1H), 2.48 – 2.34 (m, 1H), 0.79 (br s, 1H). ^{13}C NMR (126 MHz, $CDCl_3$) δ 98.38, 97.95, 97.67, 97.16, 80.26, 79.90, 78.78, 75.87, 56.25, 56.13, 55.99, 55.61, 34.94, 33.72. LRMS (ESI): m/z Calcd for $[C_{14}H_{27}NO_8 + Na]^+$: 360.162888; found: 360.3. HRMS (TOF ESI); found: 360.1634.

(±)-(1R,2S,3R,4R,5S,6S)-2,3,4,5-tetrakis(methoxymethoxy)-7-octyl-7-azabicyclo[4.1.0]heptane (20)

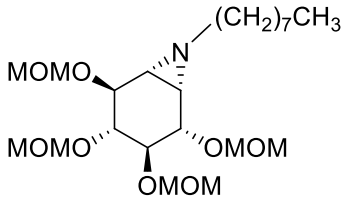

19 (200 mg, 0.593 mmol) was dissolved in 6.2 mL of acetonitrile. DIPEA (0.31 mL, 1.778 mmol), and iodo octane (0.32 mL, 1.778 mmol) were added and the reaction was refluxed for 2 days. The mixture was diluted with 100 mL of EtOAc and 100 mL H_2O. The aqueous layer was extracted with 75 mL of EtOAc 2 times and the organic layers were combined, washed with brine, dried with Na_2SO_4 and filtered. The solvents were removed under vacuum and the crude was purified using silica gel chromatography (1:2 → 1:1 EtOAc: Hexanes) to get **20** (146 mg, 55%) as a colourless oil. ^{1}H NMR (500 MHz, $CDCl_3$) δ 4.91 – 4.68 (m, 8H), 3.81 – 3.74 (m, 2H), 3.54 (dd, J = 6.8, 3.6 Hz, 1H), 3.48 – 3.39 (m, 12H), 3.39 – 3.31 (m, 2H), 2.70 – 2.61 (m, 1H), 1.96 (dd, J = 5.7, 3.4 Hz, 1H), 1.91 – 1.81 (m, 1H), 1.66 (t, J = 5.5 Hz, 1H), 1.63 – 1.48 (m, 2H), 1.36 – 1.21 (m, 9H), 0.88 (dd, J = 9.4, 4.0 Hz, 3H). ^{13}C NMR (126 MHz, $CDCl_3$) δ 98.50, 98.09, 97.64, 97.18, 80.34, 79.75, 79.00, 61.35, 56.23, 55.93, 55.58, 43.44, 42.28, 31.98, 29.73, 29.68, 29.37, 27.45, 22.81, 14.25. LRMS (ESI): m/z Calcd for $[C_{22}H_{43}NO_8 + Na]^+$: 472.2881; found: 472.4.

(±)-(1R,2S,3R,4R,5S,6S)-7-octyl-7-azabicyclo[4.1.0]heptane-2,3,4,5-tetraol (7)

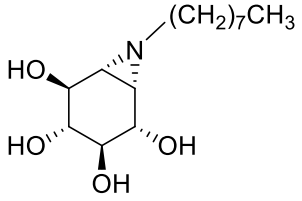

20 (40 mg, 0.089 mmol) was dissolved in 0.65 mL of acetonitrile and cooled to 0°C. TMSBr (233 µg, 1.78 mmol) was added slowly to the mixture and this was stirred for 40 minutes at 0°C. The reaction was quenched with 2 mL of saturated sodium bicarbonate while stirring vigorously and allowed to warm to room temperature. The volatiles were removed under vacuum. The resulting solids were dissolved in 1:1 MeOH:$CHCl_3$, filtered and the solvents were again removed under vacuum. This crude mixture was purified using silica gel column chromatography (1:6, MeOH:$CHCl_3$) and lyophilized to get **7** (15 mg, 62%). ^{1}H NMR (500 MHz, CD_3OD) δ 3.66 (dd, *J* = 8.4, 3.6 Hz, 1H), 3.59 (d, *J* = 8.1 Hz, 1H), 3.23 – 3.15 (m, 1H), 3.02 (dd, *J* = 10.3, 8.2 Hz, 1H), 2.38 – 2.29 (m, 1H), 2.17 – 2.07 (m, 1H), 1.94 – 1.86 (m, 1H), 1.59 (d, *J* = 6.8 Hz, 1H), 1.58 – 1.49 (m, 2H), 1.36 – 1.20 (m, 10H), 0.86 (t, *J* = 6.8 Hz, 3H). ^{13}C NMR (126 MHz, CD_3OD) δ 77.84, 74.06, 73.42, 73.12, 62.08, 49.85, 45.84, 45.42, 33.04, 30.73, 30.40, 28.42, 23.74, 14.45. LRMS (ESI): m/z Calcd for $[C_{14}H_{27}NO_4 + H]^+$: 274.201285; found: 274.5. HRMS (TOF ESI); found: 274.2023.

(±)-5,5-difluoro-1,3,7,9-tetramethyl-10-(5-((1R,2S,3R,4R,5S,6S)-2,3,4,5-tetrakis(methoxymethoxy)-7-azabicyclo[4.1.0]heptan-7-yl)pentyl)-5H-dipyrrolo[1,2-c:2',1'-f][1,3,2]diazaborinin-4-ium-5-uide (21)

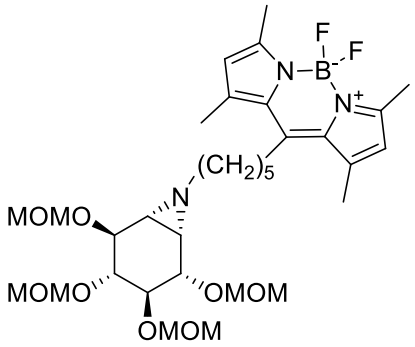

19 (250 mg, 0.741 mmol) was dissolved in 7.5 mL of acetonitrile. DIPEA (0.38 mL, 2.222 mmol), NaI (333 mg, 2.222 mmol) and **21a** (441 mg, 1.111 mmol) were added and the reaction was refluxed for 2 days. The mixture was diluted with 100 mL of EtOAc and 100 mL H_2O. The aqueous layer was extracted with 75 mL of EtOAc 2 times and the organic layers were combined, washed with brine, dried with

Na_2SO_4 and filtered. The solvents were removed under vacuum and the crude was purified using silica gel chromatography (1:1 → 2:1 EtOAc: Hexanes) to get **21** (244 mg, 55%) as a red solid. ^{1}H NMR (500 MHz, $CDCl_3$) δ 6.05 (s, 2H), 4.87 – 4.72 (m, 8H), 3.77 (dd, *J* = 8.7, 3.4 Hz, 1H), 3.73 (d, *J* = 8.3 Hz, 1H), 3.57 – 3.47 (m, 1H), 3.46 – 3.37 (m, 12H), 3.37 – 3.32 (m, 1H), 3.00 – 2.89 (m, 2H), 2.74 – 2.59 (m, 1H), 2.51 (s, 6H), 2.41 (s, 6H), 1.99 – 1.85 (m, 2H), 1.68 – 1.58 (m, 7H). ^{13}C NMR (126 MHz, $CDCl_3$) δ 153.87, 146.60, 140.46, 131.54, 121.70, 98.40, 98.08, 97.71, 97.19, 80.20, 79.80, 78.91, 76.69, 60.58, 56.28, 56.18, 55.95, 55.59, 43.46, 42.21, 31.97, 29.45, 28.50, 28.13, 16.49, 14.59. LRMS (ESI): m/z Calcd for $[C_{32}H_{50}BF_2N_3O_8 + Na]^+$: 676.3551; found: 676.9.

(±)-9-(6-((1R,2S,3R,4R,5S,6S)-2,3,4,5-tetrakis(methoxymethoxy)-7-azabicyclo[4.1.0]heptan-7-yl)hex-1-yn-1-yl)acridine (28)

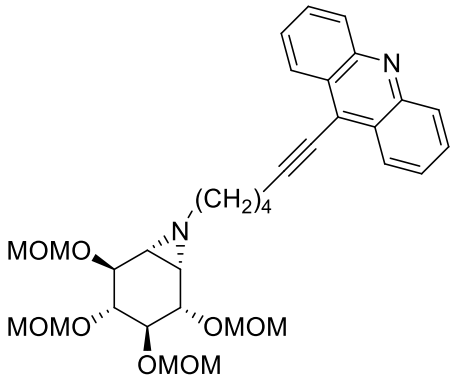

9-chloroacridine (150 mg, 0.702 mmol) and potassium iodide (1165 mg, 7.020 mmol) was dissolved in 15 mL of acetone and refluxed overnight in the dark. The resulting slurry was dissolved in 100 mL of EtOAc and 100 mL of water. The organic layer was collected and the aqueous layer was extracted 2 more times with 100 mL of EtOAc. The organic layers were combined, washed with brine, dried with sodium sulphate and concentrated under vacuum. The resulting solid **28a** was used directly in the next step. Some of the isolated **28a** (109 mg, 0.358 mmol) and compound **32** (62 mg, 0.149 mmol) was dissolved in a degassed solution of 1:1 THF:triethylamine (2 mL). To this solution was added tetrakis (3.5 mg, 0.003 mmol) and CuI (5.7 mg, 0.03 mmol). The solution was refluxed for 1.5 hours and then cooled to room temperature. The mixture was separated between 20 mL of EtOAc and 20 mL of water. The aqueous layer was extracted 3 times with 20 mL EtOAc. The organic layers were combined, washed with brine, dried with sodium sulphate, filtered and concentrated under vacuum. The resulting residue was purified using silica gel chromatography (2:1 to 5:1 EtOAc:Hexanes) to get **28** (60 mg, 68%) as an orange solid. ^{1}H NMR (500 MHz, $CDCl_3$) δ 8.46 (d, *J* = 8.5 Hz, 2H), 8.21 (d, *J* = 8.7 Hz, 2H), 7.78 (dd, *J* = 7.5, 7.5 Hz, 2H), 7.59 (dd, *J* = 7.4, 7.4 Hz, 2H), 4.86 – 4.63 (m, 8H), 3.81 – 3.75 (m, 2H), 3.60 – 3.52 (m, 1H), 3.44 – 3.30 (m, 12H), 2.89 – 2.70 (m, 3H), 2.14 – 1.98 (m, 2H), 1.98 – 1.91 (m, 2H), 1.91 – 1.80 (m, 2H), 1.71

(d, J = 6.0 Hz, 1H). 1.29 - 1.21 (m, 1H). ^{13}C NMR (126 MHz, $CDCl_3$) δ 148.55, 130.22, 129.78, 126.81, 126.23, 98.31, 97.93, 97.57, 97.10, 80.16, 79.70, 78.76, 76.64, 60.31, 56.16, 56.02, 55.78, 55.43, 43.53, 42.12, 29.06, 26.60, 20.30. LRMS (ESI): m/z Calcd for $[C_{33}H_{42}N_2O_8 + H]^+$: 595.3014; found: 595.0.

(±)-(1R,2S,3R,4R,5S,6S)-7-(6-(acridin-9-yl)hex-5-yn-1-yl)-7-azabicyclo[4.1.0]heptane-2,3,4,5-tetraol (29)

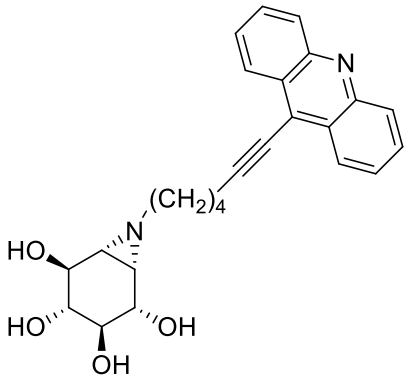

28 (50 mg, 0.084 mmol) was dissolved in 0.65 mL of acetonitrile and cooled to 0°C. TMSBr (220 µL, 1.68) mmol) was added slowly to the mixture and this was stirred for 40 minutes at 0°C. The reaction was quenched with 2 mL of saturated sodium bicarbonate while stirring vigorously and allowed to warm to room temperature. The volatiles were removed under vacuum. The resulting solids were dissolved in 1:1 MeOH: $CHCl_3$, filtered and the solvents were again removed under vacuum. This crude mixture was purified using silica gel column chromatography (1:6 → 1:5 MeOH: EtOAc) and lyophilized to get **29** (15 mg, 62%). ^{1}H NMR (500 MHz, CD_3OD) δ 8.44 (d, J = 8.2 Hz, 2H), 8.12 (d, J = 8.3 Hz, 2H), 7.86 (dd, J = 7.5, 7.5 Hz, 2H), 7.67 (dd, J = 7.2, 7.2 Hz, 2H), 3.79 (dd, J = 8.4, 3.1 Hz, 1H), 3.72 (d, J = 8.0 Hz, 1H), 3.16 (dd, J = 9.3, 9.3 Hz, 1H), 2.97 – 2.75 (m, 2H), 2.52 (dd, J = 12.9, 6.3 Hz, 1H), 2.38 (dd, J = 10.3, 5.8 Hz, 1H), 2.12 – 1.98 (m, 1H), 1.98 – 1.84 (m, 4H), 1.78 (d, J = 6.2 Hz, 1H). ^{13}C NMR (126 MHz, CD_3OD) δ 149.05, 132.15, 129.35, 127.81, 127.76, 109.93, 77.55, 77.53, 77.48, 76.15, 74.10, 73.30, 72.90, 61.18, 45.83, 45.43, 30.03, 27.53, 20.81. LRMS (ESI): m/z Calcd for $[C_{25}H_{26}N_2O_4 + H]^+$: 419.197083; found: 419.7. HRMS (TOF ESI); found: 419.1980.

(±)-2',7'-dichloro-3',6'-diacetate-5(6)-(6-((1R,2S,3R,4R,5S,6S)-2,3,4,5-tetrakis(methoxymethoxy)-7-azabicyclo[4.1.0]heptan-7-yl)hex-1-yn-1-yl)-fluorescein (30)

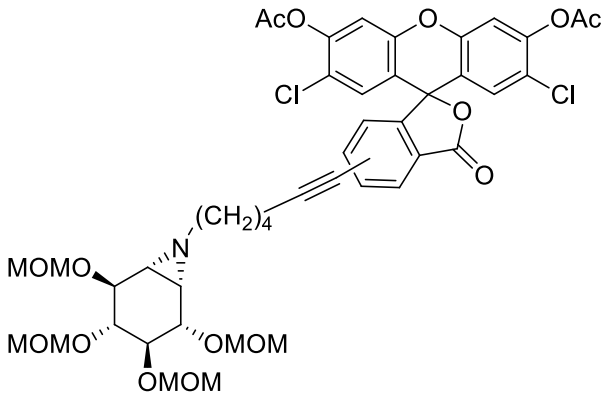

32 (54 mg, 0.130 mmol) and **30a** (95 mg, 0.155 mmol) were added to 4 mL of THF spiked with 0.1 mL of TEA. To this mixture was added $Pd(PPh_3)_4$ (3 mg, 0.0026 mmol) and CuI (5 mg, 0.026 mmol). This mixture was reacted for 2 days at room temperature. The mixture was filtered and the mixture was diluted with 50 mL of EtOAc and 50 mL H_2O. The aqueous layer was extracted with 25 mL of EtOAc 2 times and the organic layers were combined, washed with brine, dried with Na_2SO_4 and filtered. The solvents were removed under vacuum and the crude was purified using silica gel chromatography (1:2 EtOAc: Hexanes) to get **30** (36 mg, 31%) as a clear slightly orange oil. ^{1}H NMR (500 MHz, $CDCl_3$) δ 8.10 – 7.94 (m, 1H), 7.84 – 7.56 (m, 1H), 7.49 (dd, *J* = 24.5, 7.8 Hz, 1H), 7.14 (s, 2H), 6.87 (d, *J* = 14.0 Hz, 1H), 4.92 – 4.67 (m, 8H), 3.92 – 3.87 (m, 1H), 3.74 (dd, *J* = 29.4, 8.2 Hz, 2H), 3.53 (dd, *J* = 19.9, 11.1 Hz, 1H), 3.48 – 3.38 (m, 12H), 3.37 – 3.32 (m, 1H), 2.81 – 2.60 (m, 1H), 2.58 – 2.40 (m, 2H), 2.37 (s, 4H), 2.02 – 1.87 (m, 2H), 1.85 – 1.52 (m, 6H). ^{13}C NMR (126 MHz, $CDCl_3$) δ 167.95, 167.83, 150.15, 149.73, 149.61, 148.54, 138.83, 128.95, 128.38, 127.24, 126.05, 123.88, 122.76, 117.39, 112.78, 98.35, 97.97, 97.62, 97.13, 93.82, 80.47, 80.18, 79.73, 78.99, 78.85, 76.66, 60.36, 56.19, 56.06, 55.84, 55.72, 55.49, 55.45, 43.47, 42.17, 29.72, 28.83, 26.28, 20.64, 19.47. LRMS (ESI): m/z Calcd for $[C_{44}H_{47}Cl_2NO_{15} + H]^+$: 900.2396; found: 901.3.

(±)-2',7'-dichloro-5(6)-(6-((1R,2S,3R,4R,5S,6S)-2,3,4,5-tetrahydroxy-7-azabicyclo[4.1.0]heptan-7-yl)hex-1-yn-1-yl)-fluorescein (31)

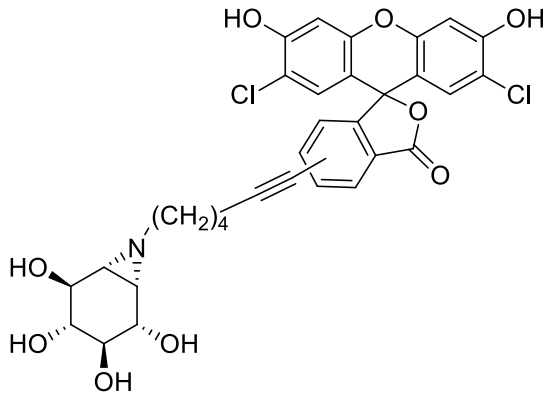

30 (36 mg, 0.04 mmol) was dissolved in 0.5 mL of acetonitrile and cooled to 0°C. TMSBr (105 µL, 0.80 mmol) was added slowly to the mixture and this was stirred for 40 minutes at 0°C. The reaction was quenched with 1 mL of saturated sodium bicarbonate while stirring vigorously and allowed to warm to room temperature. The volatiles were removed under vacuum. 1 mL of MeOH and 15 mg of K_2CO_3 were added and the slurry was stirred for 1 hour at room temperature. The resulting solution was dissolved in 1:1 MeOH: $CHCl_3$, filtered and the solvents were again removed under vacuum. This crude mixture was purified using silica gel column chromatography (10% → 15% MeOH: $CHCl_3$) and lyophilized to get **29** (23 mg, 90%) as an orange solid. ^{1}H NMR (500 MHz, CD_3OD) δ 8.19 – 7.98 (m, 1H), 7.67 – 7.55 (m, 1H), 7.27 – 7.13 (m, 1H), 7.11 (d, *J* = 4.3 Hz, 2H), 6.58 (s, 2H), 3.72 (dd, *J* = 8.4, 2.9 Hz, 1H), 3.66 (dd, *J* = 31.7, 7.9 Hz, 1H), 3.07 (dd, *J* = 18.2, 8.3 Hz, 1H), 2.53 (t, *J* = 6.4 Hz, 1H), 2.50 – 2.41 (m, 1H), 2.35 – 2.10 (m, 1H), 2.06 – 1.96 (m, 1H), 1.88 – 1.62 (m, 7H). ^{13}C NMR (126 MHz, CD_3OD) δ 180.48, 176.14, 158.78, 155.18, 133.21, 130.83, 129.67, 129.59, 129.17, 129.13, 126.91, 126.77, 112.75, 106.37, 104.78, 93.79, 80.77, 77.73, 77.64, 74.15, 74.06, 73.40, 72.97, 61.43, 61.35, 45.93, 45.48, 29.82, 27.52, 27.42, 24.21, 20.05. LRMS (ESI -ve): m/z Calcd for $[C_{32}H_{27}Cl_2NO_9 - H]^-$: 638.0990; found: 637.7.

(±)-(1R,2S,3R,4R,5S,6S)-7-(hex-5-yn-1-yl)-2,3,4,5-tetrakis(methoxymethoxy)-7-azabicyclo[4.1.0]heptane (32)

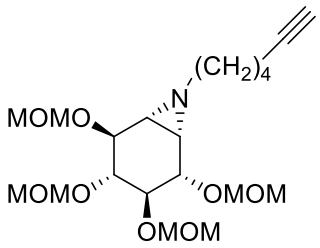

19 (700 mg, 2.075 mmol), 6-iodo-1-hexyne (0.82 mL, 6.224 mmol) and DIPEA (1.08 mL, 6.224 mmol) were dissolved in 22 mL of acetonitrile and heated to reflux for 2 days. The reaction was allowed to cool to room temperature and the solvent was removed under vacuum. The crude reaction mixture was partitioned between 200 mL of EtOAc and 200 mL of water. The aqueous layer was extracted 2 more times with 100 mL of EtOAc. The organic layers were combined and washed with brine, dried with sodium sulphate, filtered and concentrated under vacuum. The mixture was then purified using silica gel chromatography (1:1 EtOAc:Hexanes) to get **32** (228 mg, 30%) as a colourless oil. ^{1}H NMR (500 MHz, $CDCl_3$) δ 4.87 – 4.70 (m, 8H), 3.75 (dd, *J* = 14.0, 5.6 Hz, 2H), 3.51 (dd, *J* = 9.5, 9.4 Hz, 1H), 3.42 (s, 6H), 3.39 (s, 6H), 3.36 – 3.28 (m, 1H), 2.69 – 2.57 (m, 1H), 2.25 – 2.15 (m, 2H), 1.99 – 1.84 (m, 3H), 1.73 – 1.50 (m, 5H). ^{13}C NMR (126 MHz, $CDCl_3$) δ 98.46, 98.06, 97.70 , 97.19 , 84.50, 80.32 , 79.76 , 78.89 , 76.81, 68.52, 60.44, 56.29, 56.15 , 55.94, 55.60 , 43.53, 42.21, 28.67, 26.25, 18.49. LRMS (ESI): m/z Calcd for $[C_{20}H_{35}NO_8 + Na]^+$: 440.2255; found: 440.5.

(±)-(1R,2S,3R,4R,5S,6S)-7-(6-(4-fluorophenyl)hex-5-yn-1-yl)-2,3,4,5-tetrakis(methoxymethoxy)-7-azabicyclo[4.1.0]heptane (33)

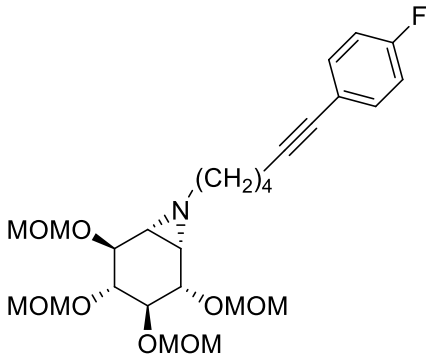

32 (75.06 mg, 0.18 mmol), triethylamine (0.1 mL, 0.72 mmol), CuI (8 mg, 0.04 mmol) and tetrakis (4 mg, 0.034 mmol) were dissolved in 3 mL of acetonitrile. To this was added 4-fluoroiodobenzene (22 µL, 0.198 mmol) and the reaction was refluxed for 20 minutes. The reaction was cooled and partitioned between 20 mL of water and 20 mL of EtOAc. The aqueous phase was extracted 2 times with 20 mL of EtOAc and the organic layers were combined. The organic portion was washed with brine, dried with sodium sulphate, filtered and concentrated under vacuum. After silica gel column chromatography (1:2 EtOAc:Hexanes) **33** (90 mg, 95%) was isolated as a colourless oil. ^{1}H NMR (500 MHz, $CDCl_3$) δ 7.35 (dd, J = 5.6, 8.4 Hz, 2H), 6.96 (dd, J = 8.7, 8.7 Hz, 2H), 4.86 – 4.72 (m, 8H), 3.77 (dd, J = 5.3, 10.1 Hz, 2H), 3.53 (dd, J = 9.5, 9.5 Hz, 1H), 3.46 – 3.38 (m, J = 7.4, 2.8 Hz, 12H), 3.38 – 3.31 (m, 1H), 2.69 (dd, J = 11.4, 6.5 Hz, 1H), 2.41 (t, J = 6.0 Hz, 2H), 2.02 – 1.89 (m, 2H), 1.83 – 1.64 (m, 5H). ^{13}C NMR (126 MHz, $CDCl_3$) δ 163.09, 161.10, 133.42, 133.35, 120.11, 115.52, 115.35, 98.42, 98.03, 97.65, 97.17, 89.75, 80.27, 79.73, 78.89, 76.77, 60.54, 56.25, 56.12, 55.88, 55.54, 43.51, 42.23, 28.89, 26.53, 19.42. LRMS (ESI): m/z Calcd for $[C_{26}H_{38}FNO_8 + H]^+$: 512.2654; found: 512.2.

(±)-(1R,2S,3R,4R,5S,6S)-7-(6-(4-fluorophenyl)hex-5-yn-1-yl)-7-azabicyclo[4.1.0]heptane-2,3,4,5-tetraol (34)

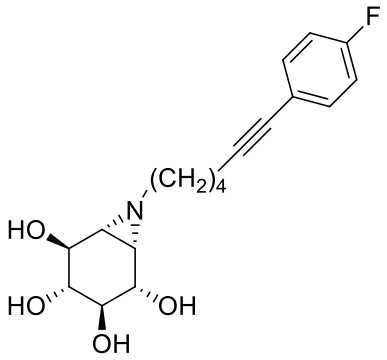

33 (50 mg, 0.098 mmol) was dissolved in 1 mL of acetonitrile and cooled to 0°C. TMSBr (256 µL, 1.960 mmol) was added slowly to the mixture and this was stirred for 40 minutes at 0°C. The reaction was quenched with 2 mL of saturated sodium bicarbonate while stirring vigorously at 0°C and allowed to warm to room temperature. The solvent was removed under vacuum. The resulting solids were dissolved in 1:1 MeOH: $CHCl_3$, filtered and the solvents were again removed under vacuum. This crude mixture was purified using silica gel column chromatography (1:6, MeOH: $CHCl_3$) and lyophilized to get **34** (16 mg, 49%) as an off white solid. ^{1}H NMR (500 MHz, CD_3OD) δ 7.38 (dd, *J* = 5.5, 8.6 Hz, 2H), 7.03 (dd, *J* = 8.8, 8.8 Hz, 2H), 3.70 (dd, *J* = 8.4, 3.5 Hz, 1H), 3.65 (d, *J* = 8.1 Hz, 1H), 3.24 (dd, *J* = 8.7, 10.1 Hz, 1H), 3.06 (dd, *J* = 8.2, 10.3 Hz, 1H), 2.49 – 2.36 (m, 3H), 2.30 – 2.19 (m, 1H), 1.96 (dd, *J* = 6.0, 3.7 Hz, 1H), 1.81 – 1.70 (m, 2H), 1.71 – 1.61 (m, 3H). ^{13}C NMR (126 MHz, CD_3OD) δ 134.49, 134.42, 116.40, 116.23, 90.45, 80.65, 77.88, 74.08, 73.43, 73.13, 61.39, 45.89, 45.41, 29.79, 27.59, 19.86. LRMS (ESI): m/z Calcd for $[C_{18}H_{22}FNO_4 + H]^+$: 336.160563; found: 336.6. HRMS (TOF ESI); found: 336.1615.

Or

35 (21.7 mg, 0.09 mmol), triethylamine (50 µg, 0.36 mmol), CuI (4 mg, 0.02 mmol) and tetrakis (2 mg, 0.0017 mmol) were dissolved in 1.5 mL of an acetonitrile water mixture (1:1). To this was added 4-fluoroiodobenzene (11 µL, 0.099 mmol) and the reaction was heated at 90°C for 20 minutes. The reaction was cooled and partitioned between 10 mL of water and 10 mL of EtOAc. The aqueous phase was extracted 2 times with 10 mL of EtOAc and the organic layers were combined. The organic portion was washed with brine, dried with sodium sulphate, filtered and concentrated under vacuum. After silica gel column chromatography (1:6, MeOH:$CHCl_3$) **34** (27 mg, 90%) was isolated as a white solid and matched the TLC, mass and NMR from the compound made through the alternate pathway.

(±)-(1R,2S,3R,4R,5S,6S)-7-(hex-5-yn-1-yl)-7-azabicyclo[4.1.0]heptane-2,3,4,5-tetraol (35)

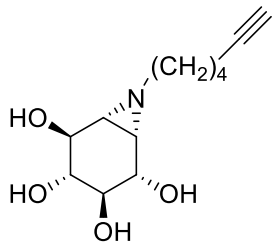

32 (200 mg, 0.480 mmol) was dissolved in 5 mL of acetonitrile and cooled to 0°C. TMSBr (1.26 mL, 9.592 mmol) was added slowly to the mixture and this was stirred for 40 minutes at 0°C. The reaction was quenched with 10 mL of saturated sodium bicarbonate while stirring vigorously at 0°C and allowed to warm to room temperature. The solvent was removed under vacuum. The resulting solids were dissolved in 1:1 MeOH:$CHCl_3$, filtered and the solvents were again removed under vacuum. This crude mixture was purified using silica gel column chromatography (6:1 to 5:1, EtOAc: MeOH) and lyophilized to get **35** (110 mg, 95%) as an white solid. ^{1}H NMR (500 MHz, CD_3OD) δ 3.75 (dd, *J* = 8.3, 3.1 Hz, 1H), 3.65 (d, *J* = 8.1 Hz, 1H), 3.29 – 3.22 (m, 1H), 3.11 (dd, *J* = 8.7, 9.9 Hz, 1H), 2.40 (dd, *J* = 11.7, 7.0 Hz, 1H), 2.29 – 2.13 (m, 4H), 2.03 – 1.93 (m, 1H), 1.75 – 1.64 (m, 3H), 1.64 – 1.54 (m, 2H). ^{13}C NMR (126 MHz, CD_3OD) δ 84.82, 77.52, 74.03, 73.29, 72.89, 69.65, 61.21, 45.77, 45.37, 29.55, 27.38, 18.95. LRMS (ESI): m/z Calcd for $[C_{12}H_{19}NO_4 + Na]^+$: 264.1206; found: 264.5.

(±)-9-((1R,2S,3R,4R,5S,6S)-2,3,4,5-tetrakis(methoxymethoxy)-7-azabicyclo[4.1.0]heptan-7-yl)nonan-1-ol (36)

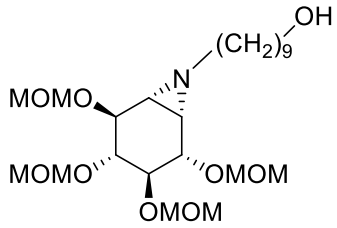

19 (700 mg, 2.075 mmol), 9-bromo-1-nonanol (1.39 g, 6.225 mmol), NaI (933 mg, 6.225 mmol) and DIPEA (1.08 mL, 6.225 mmol) were dissolved in 21 mL of acetonitrile and refluxed for 2 days. The reaction was allowed to cool to room temperature and the solvent was removed under vacuum. The crude reaction mixture was partitioned between 200 mL of EtOAc and 200 mL of water and extracted 2 more times with 200 mL of EtOAc. The organic layers were combined and washed with brine, dried with sodium sulphate, filtered and concentrated under vacuum. The mixture was then purified using silica gel chromatography (2:1 to 5:1 EtOAc: Hexanes) to get **36** (350 mg, 35%) as a colourless oil. ^{1}H NMR (500 MHz, $CDCl_3$) δ 4.92 – 4.72 (m, 8H), 3.77 (dd, *J* = 14.6, 5.7 Hz, 2H), 3.62 (dd, *J* = 6.6, 6.6 Hz, 2H), 3.53

(dd, J = 9.5, 9.5 Hz, 1H), 3.48 – 3.38 (m, 12H), 3.39 – 3.31 (m, 1H), 2.65 (dd, J = 7.6, 16.7 Hz, 1H), 2.00 – 1.91 (m, 1H), 1.92 – 1.82 (m, 1H), 1.66 (d, J = 6.0 Hz, 1H), 1.63 – 1.50 (m, 4H), 1.42 – 1.20 (m, 11H). ^{13}C NMR (126 MHz, $CDCl_3$) δ 98.36, 97.98, 97.52,97.06, 80.21, 79.62, 78.88, 76.76, 62.91, 61.18, 56.19, 56.07, 55.84, 55.49, 43.35,42.18, 32.81, 29.54, 29.49, 29.37, 27.28, 25.76. LRMS (ESI): m/z Calcd for $[C_{23}H_{45}NO_9 + Na]^+$: 502.2987; found: 502.9.

(±)-9-((1R,2S,3R,4R,5S,6S)-2,3,4,5-tetrakis(methoxymethoxy)-7-azabicyclo[4.1.0]heptan-7-yl)nonyl methanesulfonate (37)

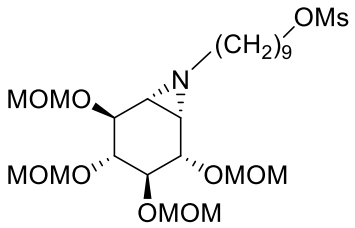

36 (130 mg, 0.27 mmol) was dissolved with triethylamine (57 µL, 0.41 mmol) in dichloromethane. The reaction mixture was cooled to 0°C and mesyl chloride (31 µL, 0.41 mmol) was added dropwise while vigorously stirring. The mixture was stirred on ice for 45 minutes before it was quenched with 3 mL of saturated NH_4Cl. The mixture was extracted 3 times with 5 mL of dichloromethane. The organic portions were washed with brine, dried with sodium sulphate, filtered and concentrated under vacuum. The resulting residue was purified on silica gel chromatography (1:1 to 2:1 EtOAc: Hexanes) to get **37** (105 mg, 70%) as a yellow oil. ^{1}H NMR (500 MHz, $CDCl_3$) δ 4.88 – 4.68 (m, 8H), 4.20 (dd, J = 6.6, 6.6 Hz, 2H), 3.78 – 3.69 (m, 2H), 3.53 – 3.48 (m, 1H), 3.46 – 3.35 (m, 12H), 3.36 – 3.29 (m, 1H), 2.99 (s, 3H), 2.68 – 2.57 (m, 1H), 1.97 – 1.91 (m, 1H), 1.89 – 1.78 (m, 1H), 1.76 – 1.67 (m, 2H), 1.63 (d, J = 6.1 Hz, 1H), 1.61 – 1.46 (m, 2H), 1.41 – 1.21 (m, 10H). ^{13}C NMR (126 MHz, $CDCl_3$) δ 98.43, 98.06, 97.58, 97.14, 80.27, 79.69, 78.94, 76.82, 70.29, 61.20, 56.25, 56.14, 55.90, 55.55, 43.41, 42.23, 37.45, 29.61, 29.58, 29.40, 29.20, 29.06, 27.33, 25.50. LRMS (ESI): m/z Calcd for $[C_{24}H_{47}NO_{11}S + Na]^+$: 580.2762; found: 581.0.

(±)-(1R,2S,3R,4R,5S,6S)-7-(9-fluorononyl)-2,3,4,5-tetrakis(methoxymethoxy)-7-azabicyclo[4.1.0]heptane (38)

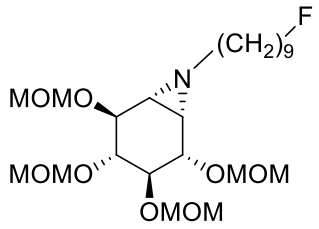

37 (45 mg, 0.081 mmol) was dissolved in 1 mL of acetonitrile. To this solution was added TEAF (24 mg, 0.162 mmol) and the mixture was refluxed in a preheated bath for 30 minutes. The reaction was cooled and separated between 30 mL of EtOAc and 30 mL of water. The water phase was extracted 2 more times with 15 mL of EtOAc and the organic layers were combined. The organic layers were washed with brine, dried with sodium sulphate, filtered and concentrated under vacuum. The resulting residue was purified using silica gel chromatography (2:1 to 1:1 EtOAc: Hexanes) to get **38** (22 mg, 56%) as a colourless oil. ^{1}H NMR (500 MHz, $CDCl_3$) δ 4.87 – 4.72 (m, 8H), 4.47 (t, *J* = 6.2, 6.2 Hz, 1H), 4.38 (t, *J* = 6.2, 6.2 Hz, 1H), 3.76 (dd, *J* = 13.8, 5.8 Hz, 2H), 3.52 (dd, *J* = 10.2, 8.9 Hz, 1H), 3.44 – 3.41 (m, 6H), 3.40 – 3.38 (m, 6H), 3.37 – 3.30 (m, 1H), 2.70 – 2.60 (m, 1H), 1.95 (dd, *J* = 6.0, 3.5 Hz, 1H), 1.91 – 1.80 (m, 1H), 1.74 – 1.61 (m, 3H), 1.61 – 1.47 (m, 2H), 1.42 – 1.22 (m, 10H). ^{13}C NMR (126 MHz, $CDCl_3$) δ 98.49, 98.09, 97.63, 97.18, 85.02, 83.72, 80.32, 79.74, 78.99, 61.29, 56.30, 56.17, 55.94, 55.59, 43.45, 42.27, 30.60, 30.45, 29.65, 29.54, 29.31, 27.40, 25.29. LRMS (ESI): m/z Calcd for $[C_{23}H_{44}FNO_8 + Na]^+$: 504.2943; found: 504.9.

(±)-(1R,2S,3R,4R,5S,6S)-7-(9-fluorononyl)-7-azabicyclo[4.1.0]heptane-2,3,4,5-tetraol (39)

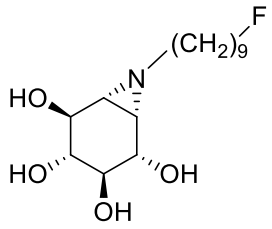

38 (40 mg, 0.083 mmol) was dissolved in 1 mL of acetonitrile and cooled to 0°C. TMSBr (218 µL, 1.663 mmol) was added slowly to the mixture and this was stirred for 40 minutes at 0°C. The reaction was quenched with 2 mL of saturated sodium bicarbonate while stirring vigorously at 0°C and allowed to warm to room temperature. The solvent was removed under vacuum. The resulting solids were dissolved in 1:1 MeOH:$CHCl_3$, filtered and the solvents were again removed under vacuum. This crude mixture was purified using silica gel column chromatography (14% to 19%, MeOH: $CHCl_3$) and lyophilized to get

39 (19 mg, 75%) as an white solid. ^{1}H NMR (500 MHz, CD_3OD) δ 4.46 (dd, *J* = 5.0, 10.9 Hz, 1H), 4.37 (dd, *J* = 5.0, 10.9 Hz, 1H), 3.76 – 3.67 (m, 1H), 3.66 – 3.58 (m, 1H), 3.24 (dd, *J* = 18.7, 9.9 Hz, 1H), 3.06 (dd, *J* = 10.1, 10.2 Hz, 1H), 2.45 – 2.29 (m, 1H), 2.24 – 2.10 (m, 1H), 1.99 – 1.90 (m, 1H), 1.77 – 1.51 (m, 5H), 1.51 – 1.24 (m, 10H). ^{13}C NMR (126 MHz, CD_3OD) δ 84.20, 77.85, 74.07, 73.43, 73.12, 62.05, 45.83, 45.42, 31.66, 30.65, 30.59, 30.55, 30.35, 28.37, 26.32. LRMS (ESI): m/z Calcd for $[C_{15}H_{28}FNO_4 + H]^+$: 306.207513; found: 306.5. HRMS (TOF ESI); found: 306.2082.

Radiochemistry

(±)-(1R,2S,3R,4R,5S,6S)-7-(6-(4-[^{18}F]-fluorophenyl)hex-5-yn-1-yl)-7-azabicyclo[4.1.0]heptane-2,3,4,5-tetraol (42)

The n.c.a. [^{18}F]fluoride was produced via the ^{18}O(p,n)^{18}F nuclear reaction from [^{18}O]H_2O on a TR-24 Cyclotron (Advanced Cyclotron Systems Inc., Richmond, Canada). Cyclotron-produced [^{18}F]fluoride was then trapped on a Waters Sep-Pak® light QMA anion-exchange cartridge conditioned with 5 mL of 1M K_2CO_3 followed by 10 mL of H_2O. The [^{18}F]fluoride was eluted with 86% K(2.2.2.)/K_2CO_3 (1.5 mL) into reactor 1 of the GE TRACERlab™ FX automated synthesis module. This solution was then dried azeotropically with additional acetonitrile (2 x 1 mL) under vacuum under a steady stream of nitrogen at 70°C and 120°C. Once fully dried, (4-iodophenyl)diphenylsulfonium triflate (10mg, 0.0186 mmol) in acetonitrile (1mL) was added and reacted for 15 min at 90 °C. Once the reaction was completed, the mixture was diluted with water (12mL) and passed through a Waters Sep-Pak® tC18 plus light cartridge. The cartridge was washed with additional water (10mL), and [^{18}F]FIB was eluted off in acetonitrile (1 mL) into reactor 2 which already contained **35** (3.15 mg, 0.0131 mmol), 0.5 mg of $Pd(PPh_3)_4$, 0.5 mg of CuI and 100 µL of TEA in 1 mL of H_2O. This reactor was heated to 90°C for 20 minutes. The mixture was cooled, filtered through a Nylon 0.2 µm filter then purified using HPLC and analyzed using radio-TLC.

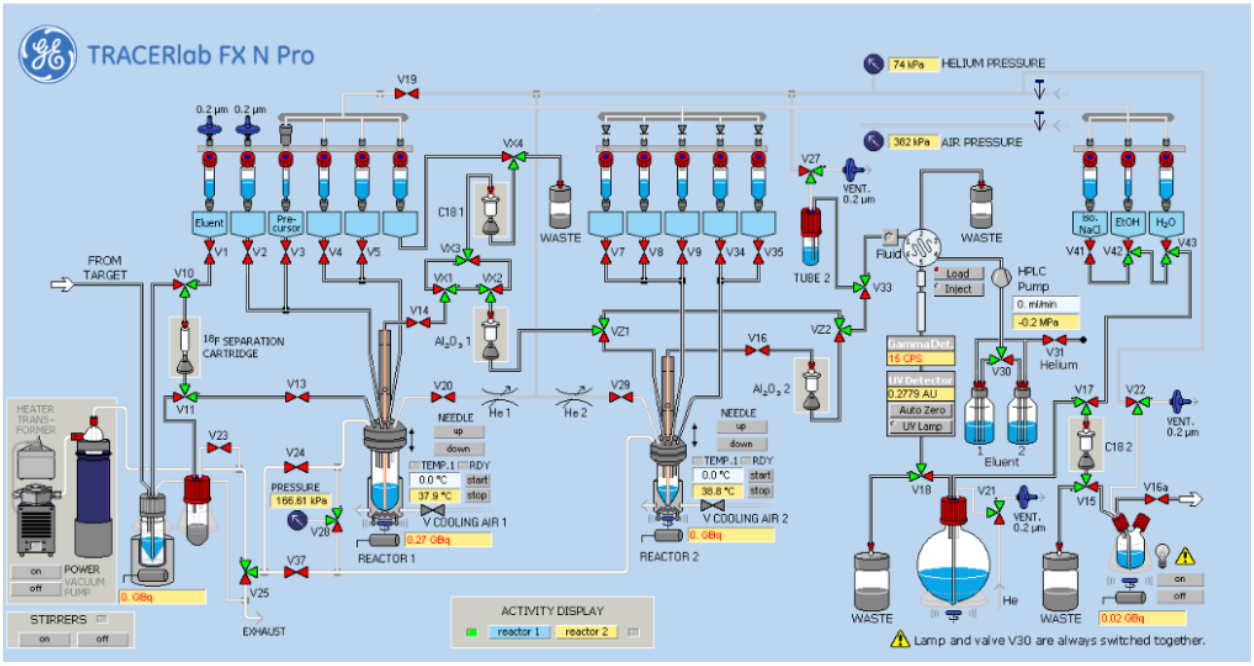

Figure 19: Scheme of one of the automated synthesis units to synthesize compound 42.

(±)- (1R,2S,3R,4R,5S,6S)-7-(9-[F^{18}-fluorononyl)-7-azabicyclo[4.1.0]heptane-2,3,4,5-tetraol (43)

The n.c.a. [^{18}F]fluoride was produced via the $^{18}O(p,n)^{18}F$ nuclear reaction from [^{18}O]H_2O on a TR-24 Cyclotron (Advanced Cyclotron Systems Inc., Richmond, Canada). Cyclotron-produced [^{18}F]fluoride was then trapped on a Waters Sep-Pak® light QMA anion-exchange cartridge conditioned with 5 mL of 1M K_2CO_3 followed by 10 mL of H_2O. The cartridge was rinsed with 5 mL of hexanes to remove the excess water then elute backwards using 15 mg of TEAB in 1 mL of pure acetonitrile into a 2 mL Eppendorf tube containing **37** (8 mg, 0.014 mmol) in 0.25 mL of acetonitrile. This solution was heated at 90°C on a thermomixer for 15 minutes then cooled to room temperature. Once the mixture was cooled 0.25 mL of a 1.15 M solution of TMSBr was added and the reaction was mixed for an additional 20 minutes. At this time 0.5 mL of saturate $NaHCO_3$ was added to quench the reaction. Radio-TLC showed the first reaction was successful but the second was not.

Enzyme Kinetic Experiments

Inactivation solutions contained a final concentration of 16.55 nM of Cerezyme® (Recombinant GCase) in 200 µL of Reaction Buffer (50 mM acetate, 0.2 % v/v Triton X-100, 0.3 % w/v sodium taurocholate, pH 5.5). The Cerezyme® was collected from left over patient vials and shown by Adams *et al.* to be approximately 8275 nM in the vial. These enzyme Reaction Buffers were brought to 37°C and spiked with a corresponding inhibitor to make the final inhibitor concentration either 20 nM, 40 nM, 60 nM, 80 nM, 120 nM, 160 nM and 200 nM. Once the inhibitor was added this was considered time = 0 minutes. Meanwhile a 96 well plate inside a Biotek Synergy 4 hybrid multi-mode reader at 37°C is being incubated. In the wells of the plate are waiting a high concentration of 2,4-DNP-β-Glc substrate what concentration? in 180 µL of Reaction Buffer. As the inhibitor inactivation is occurring, 20 µL aliquots are taken from the inactivation solutions and diluted on the plate containing the substrate bringing the final concentration of the substrate to 4 mM. Once all the aliquots are added the wells measured for absorbance at 400 nm for 8 minutes. At this time the measurements are paused and the next set of aliquots are taken to see how residual enzyme activity changes over time. Inactivation rates for varying inhibitor concentrations are calculated using GraphPad Prism software and Equation **1**. These observed rate constants are then used to calculate k_i/K_I using Equation **3**.

NMRs

^{1}H NMR of Compound **7** in CD_3OD

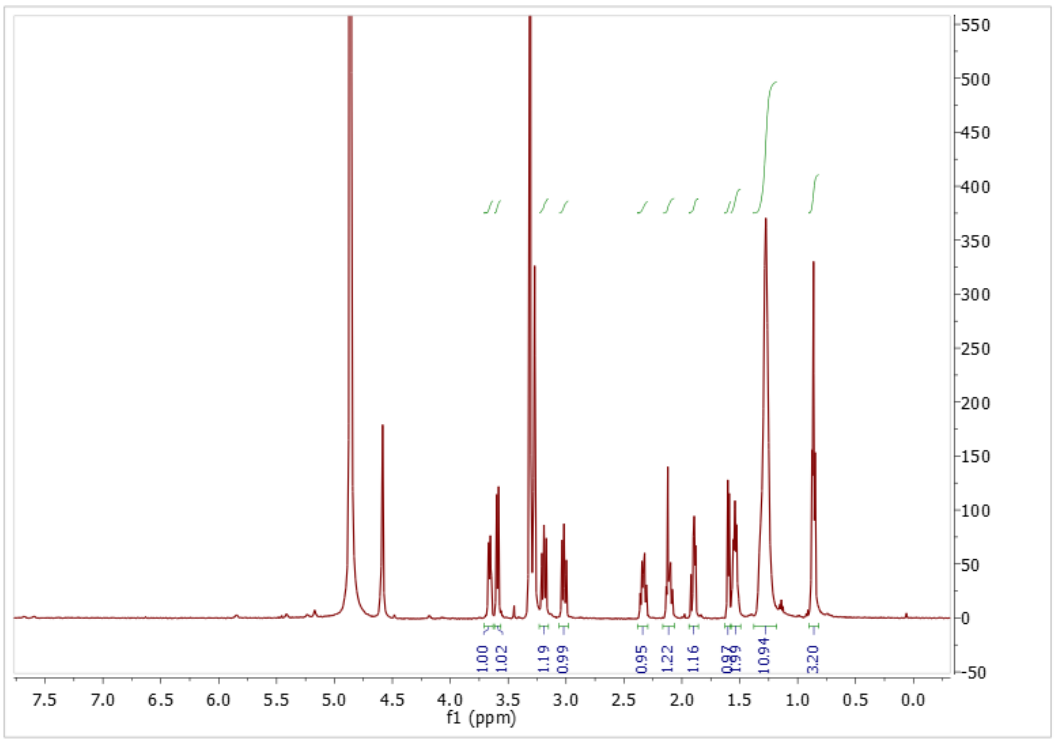

^{13}C NMR of Compound **7** in CD_3OD

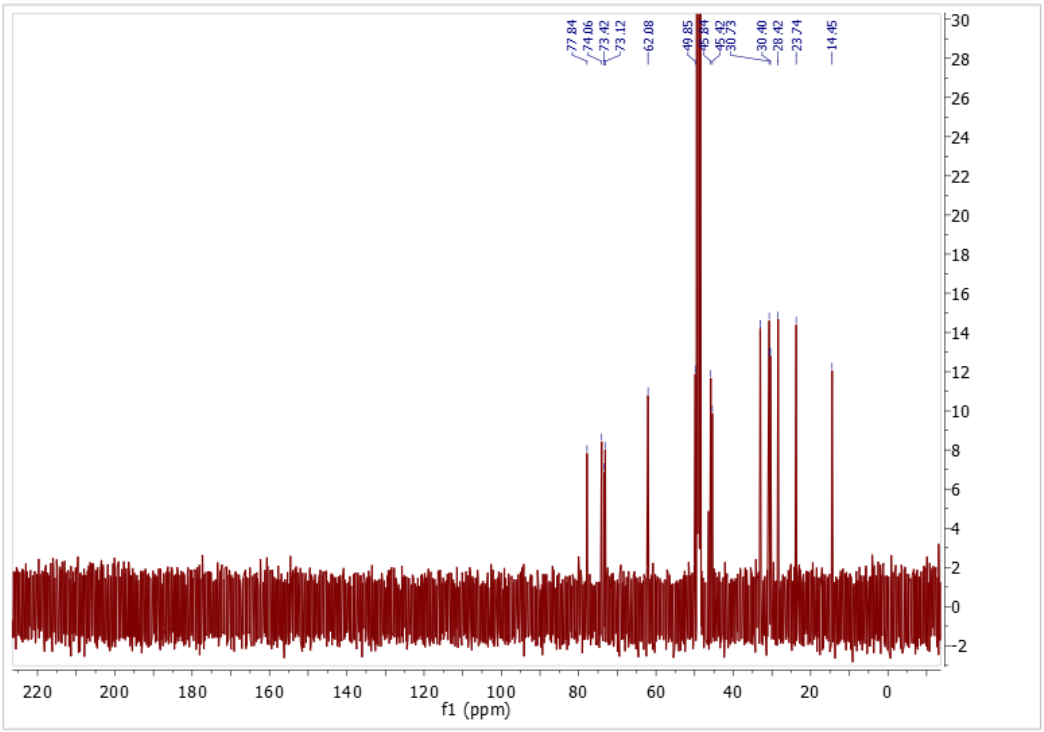

^{1}H NMR of Compound **8** in $CDCl_3$

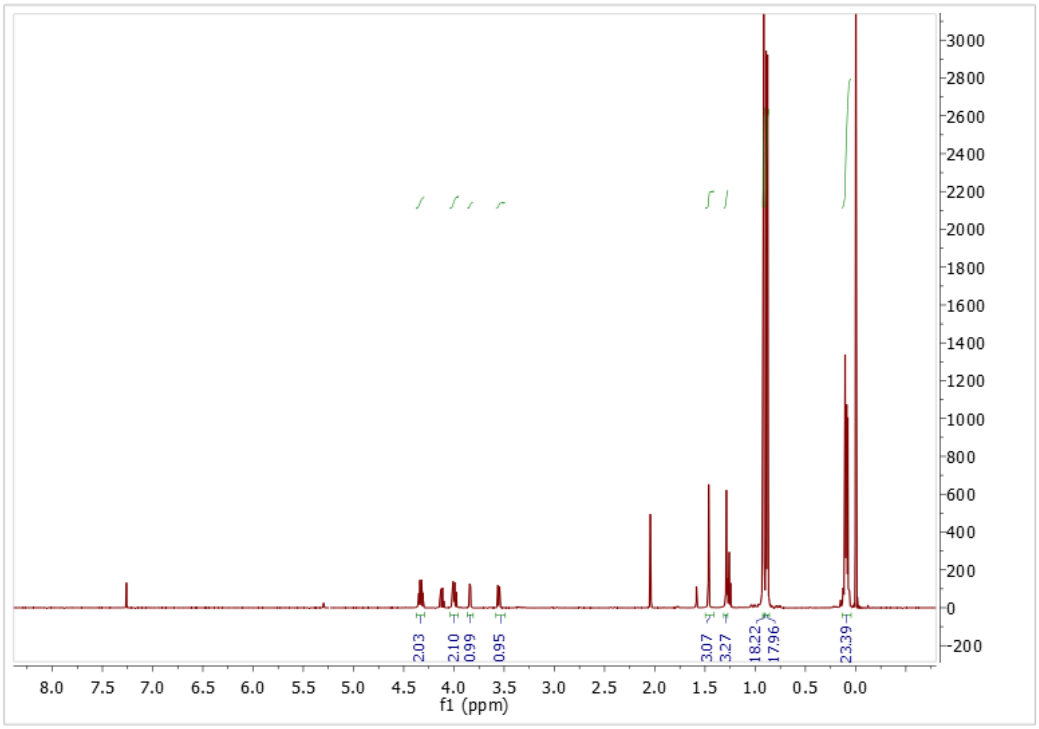

^{13}C NMR of Compound **8** in $CDCl_3$

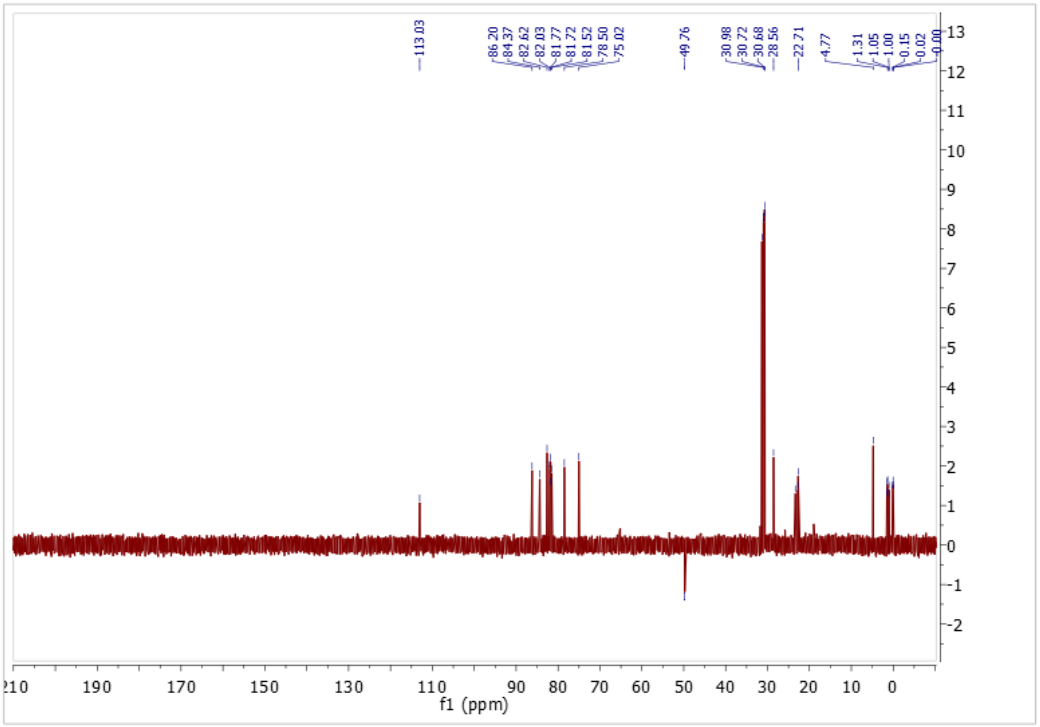

^{1}H NMR of Compound **9** in $CDCl_3$

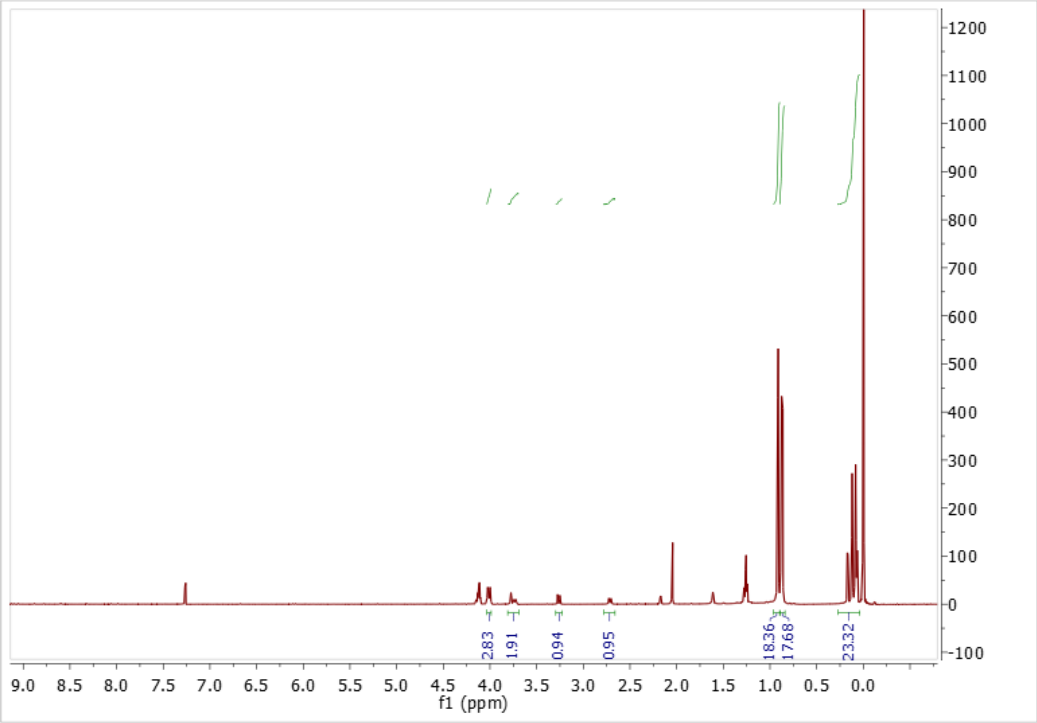

^{1}H NMR of Compound **12** in $CDCl_3$

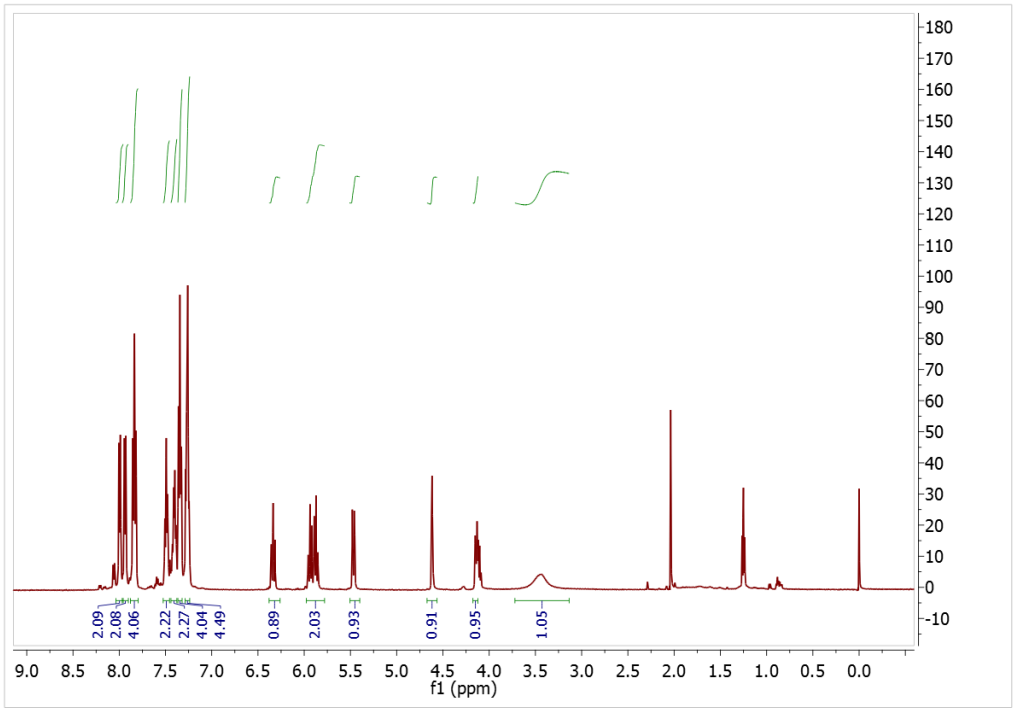

^{13}C NMR of Compound **12** in $CDCl_3$

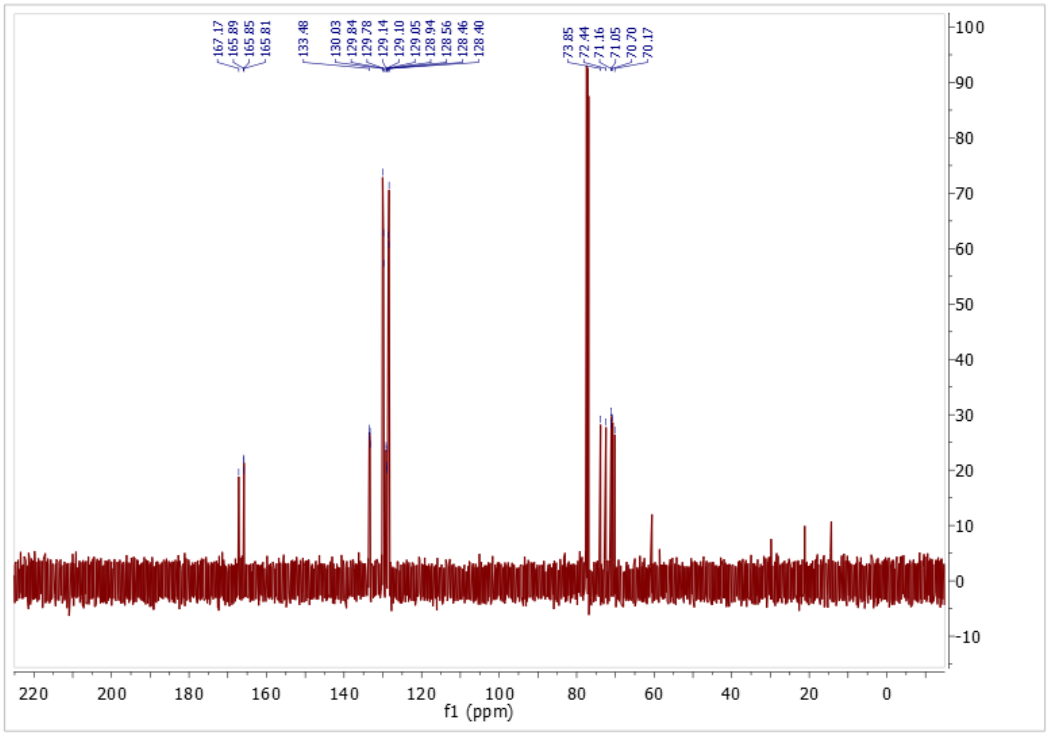

^{1}H NMR of Compound **13a** in $CDCl_3$

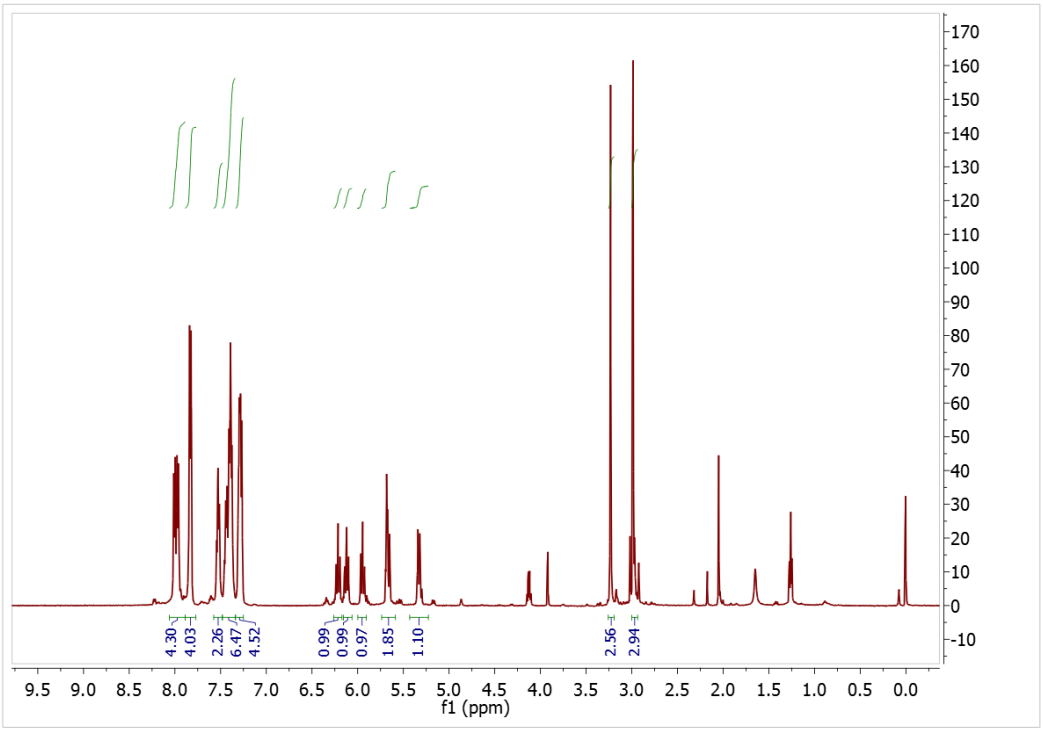

^{13}C NMR of Compound **13a** in $CDCl_3$

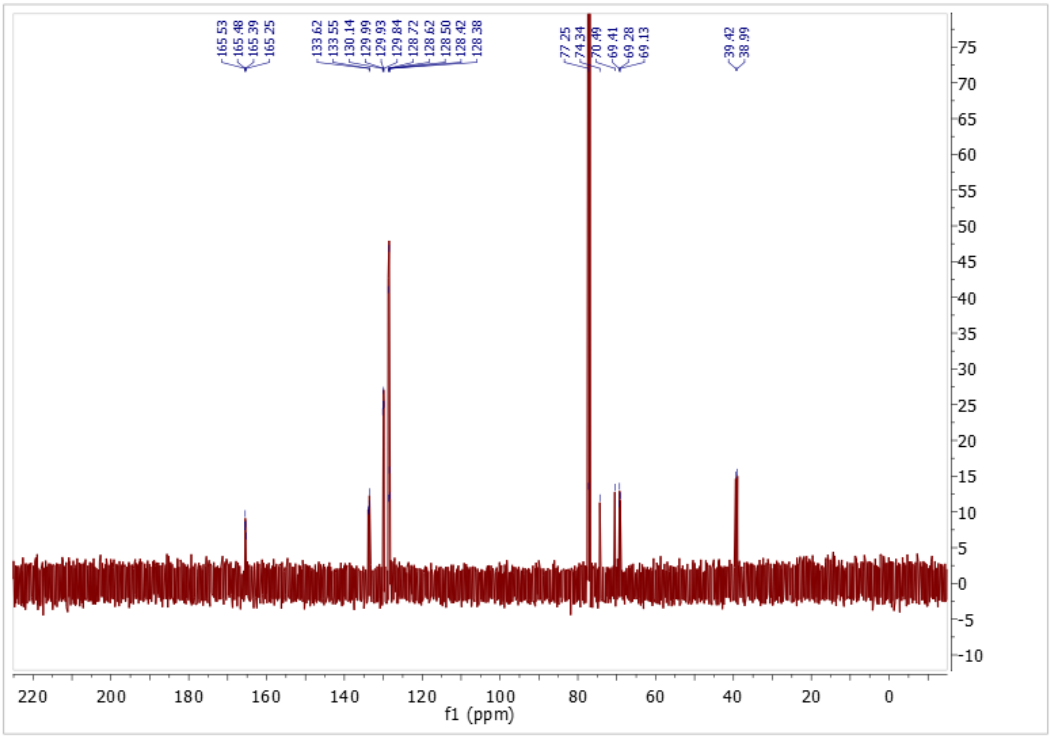

^{1}H NMR of Compound **16** in $CDCl_3$

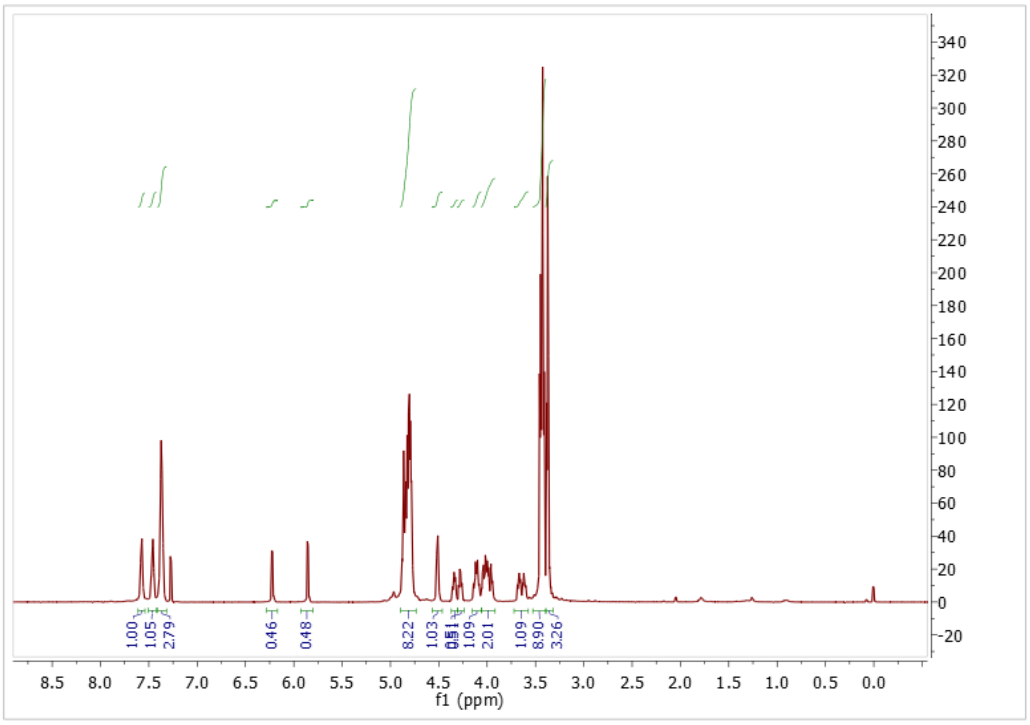

^{13}C NMR of Compound **16** in $CDCl_3$

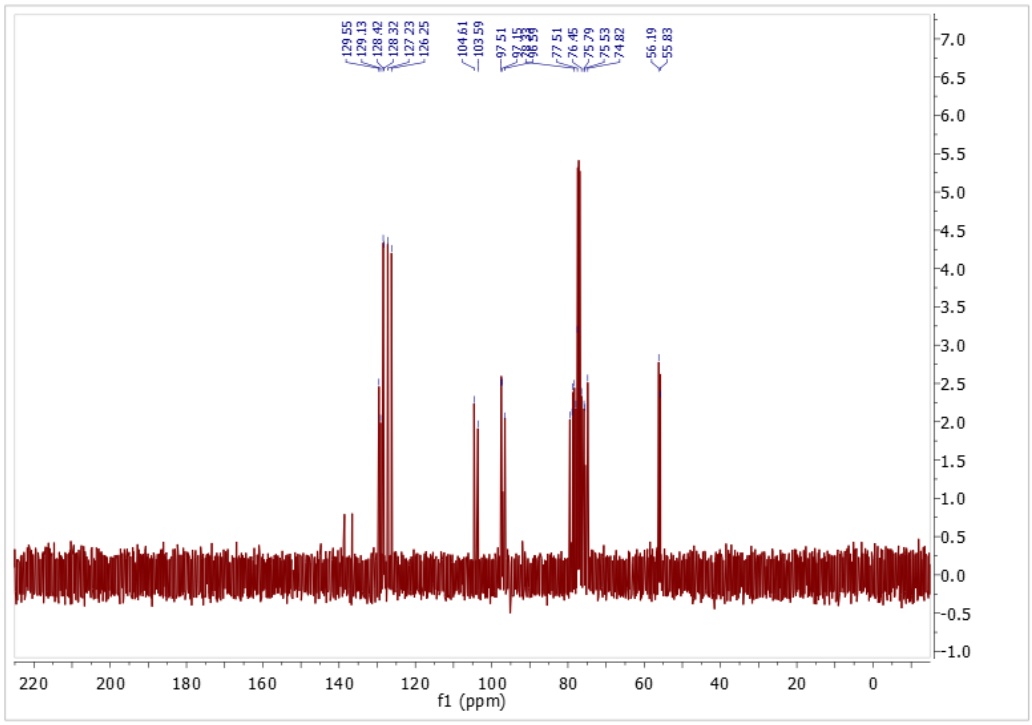

^{1}H NMR of Compound **17** in $CDCl_3$

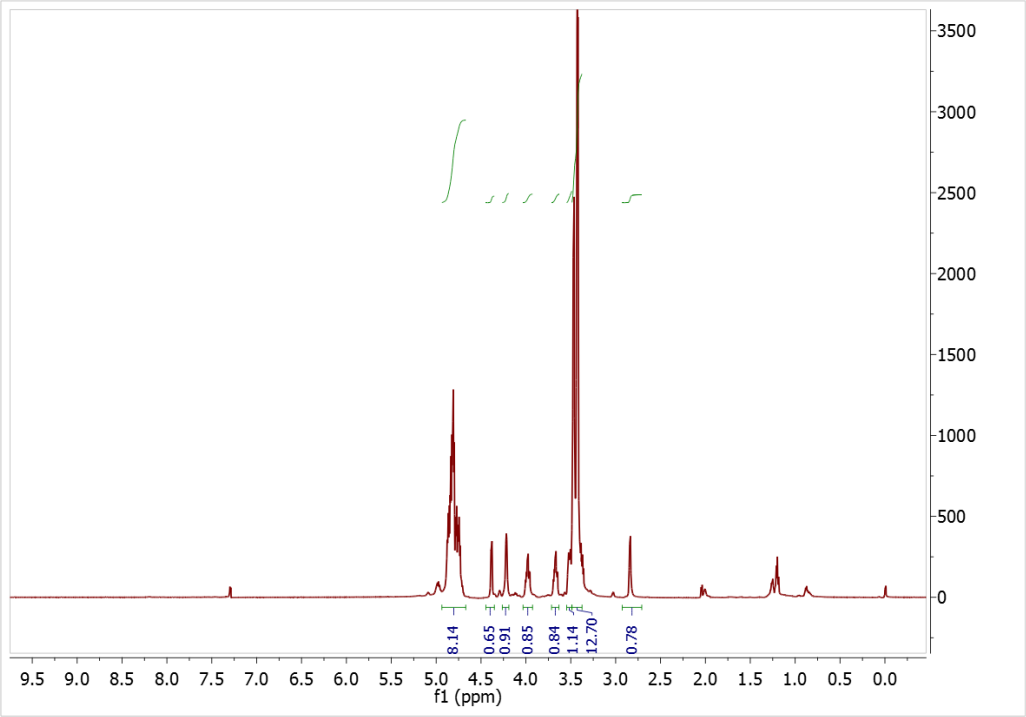

^{13}C NMR of Compound **17** in $CDCl_3$

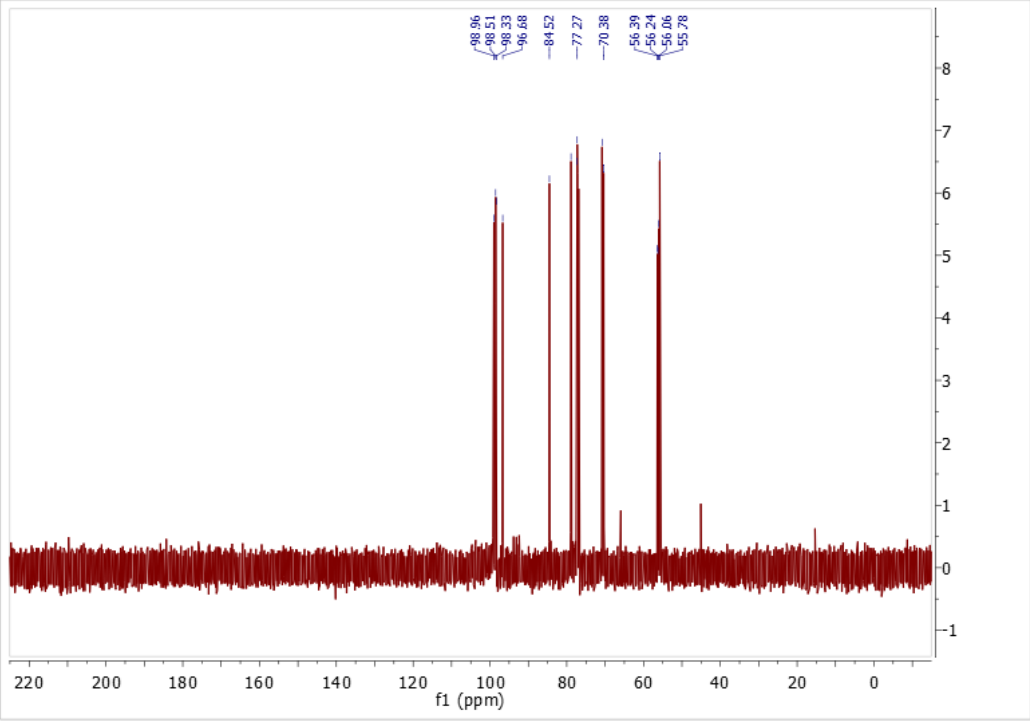

^{1}H NMR of Compound **18** in $CDCl_3$

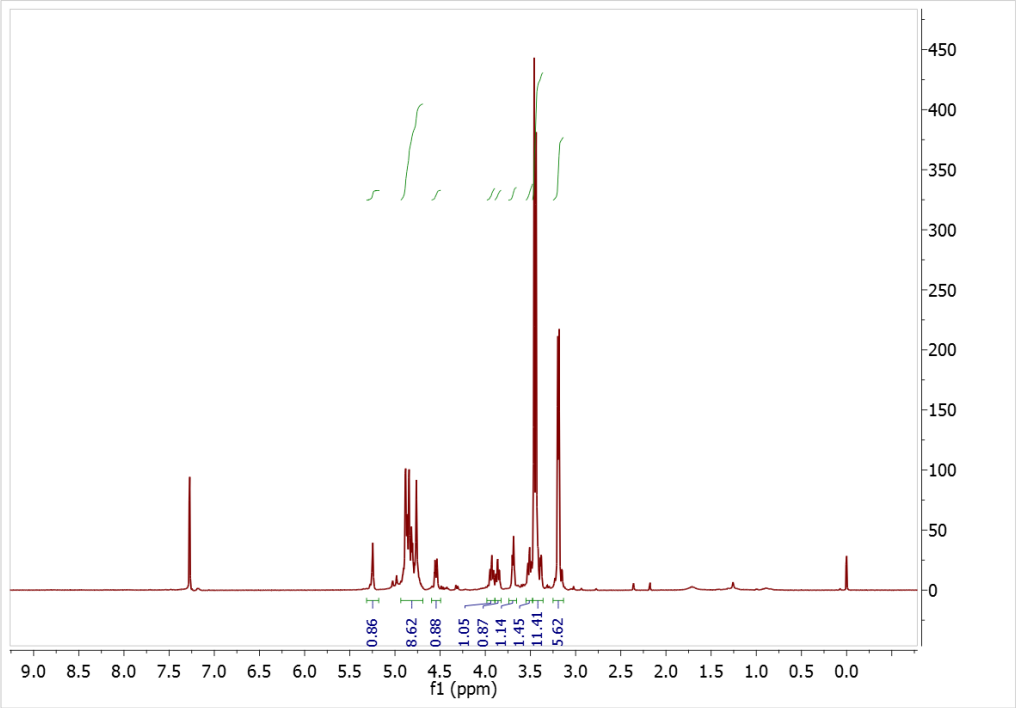

^{13}C NMR of Compound **18** in $CDCl_3$

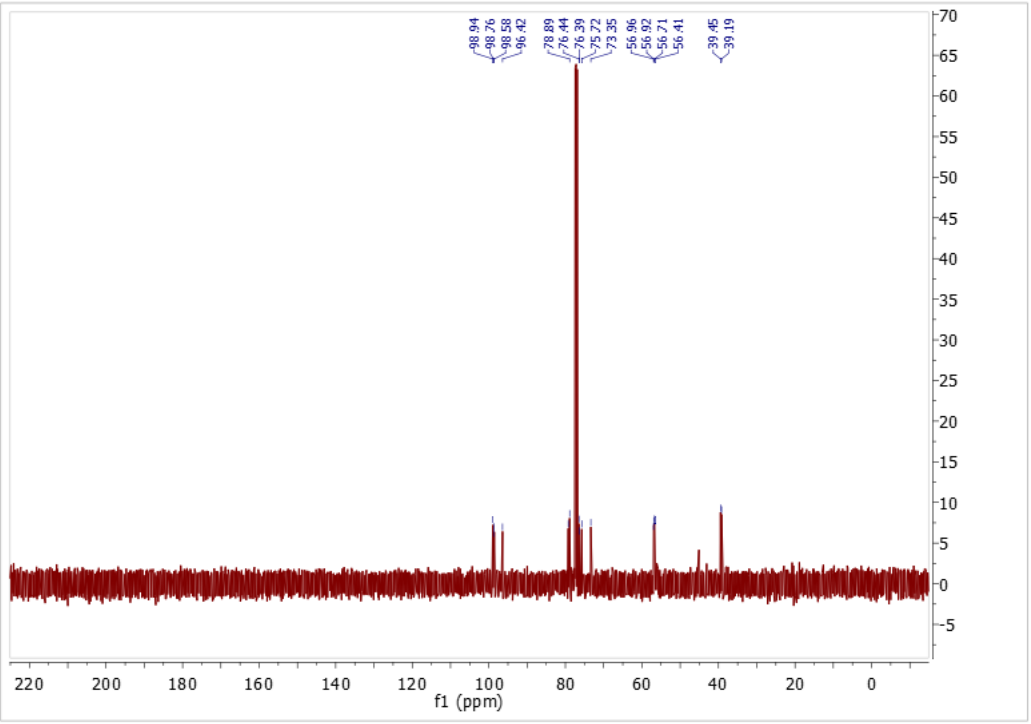

^{1}H NMR of Compound **19** in $CDCl_3$

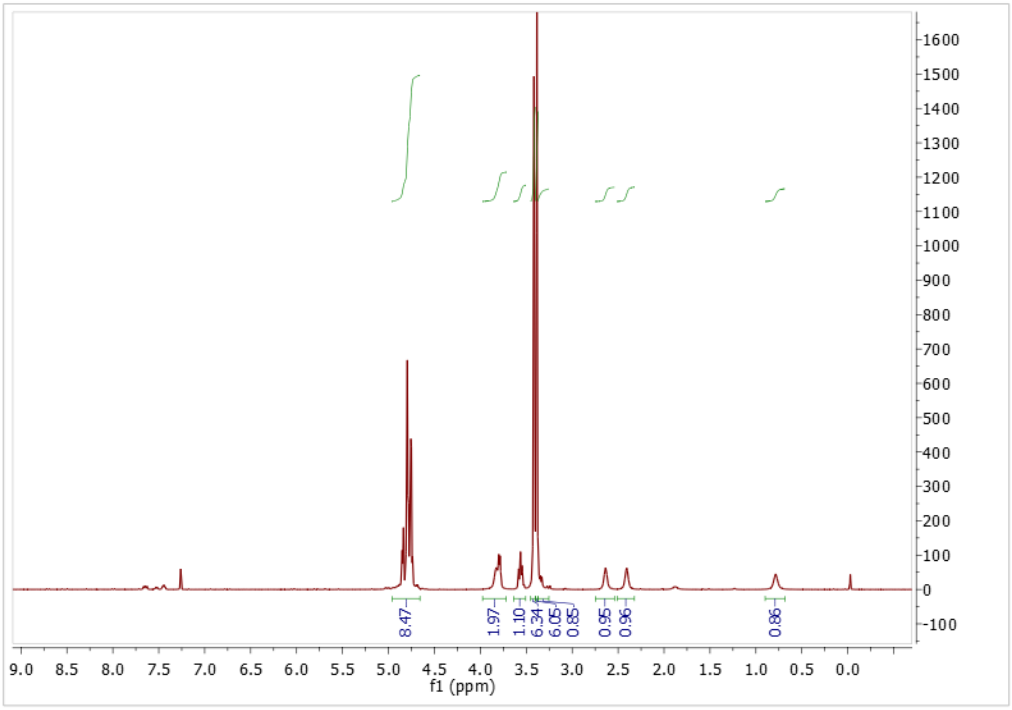

^{13}C NMR of Compound **19** in $CDCl_3$

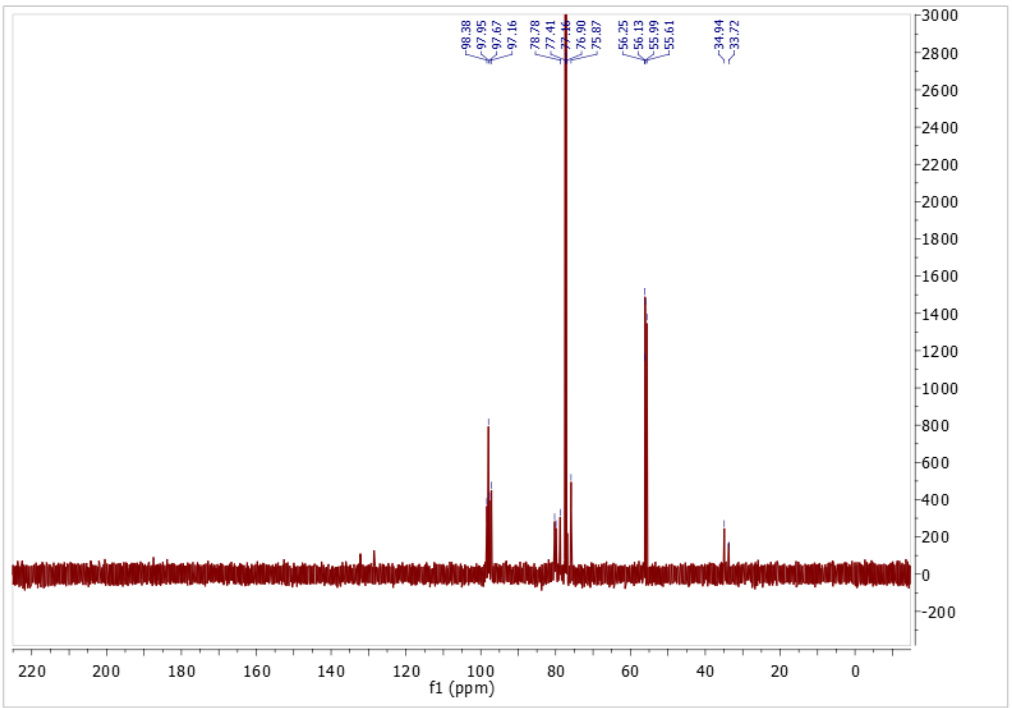

^{1}H NMR of Compound **20** in $CDCl_3$

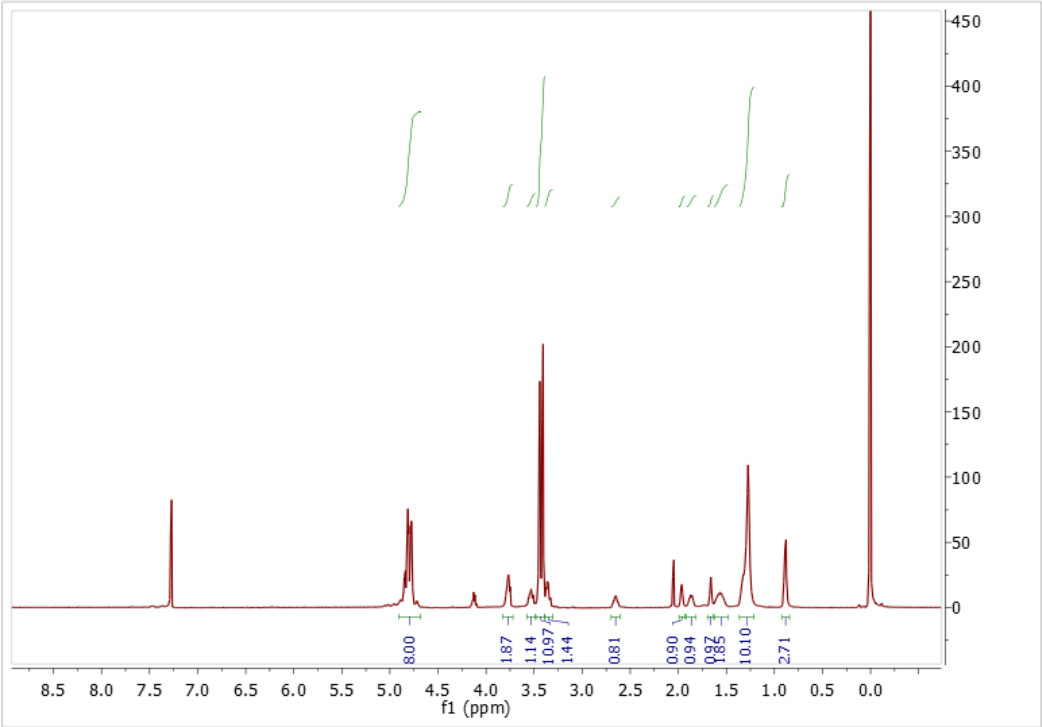

^{13}C NMR of Compound **20** in $CDCl_3$

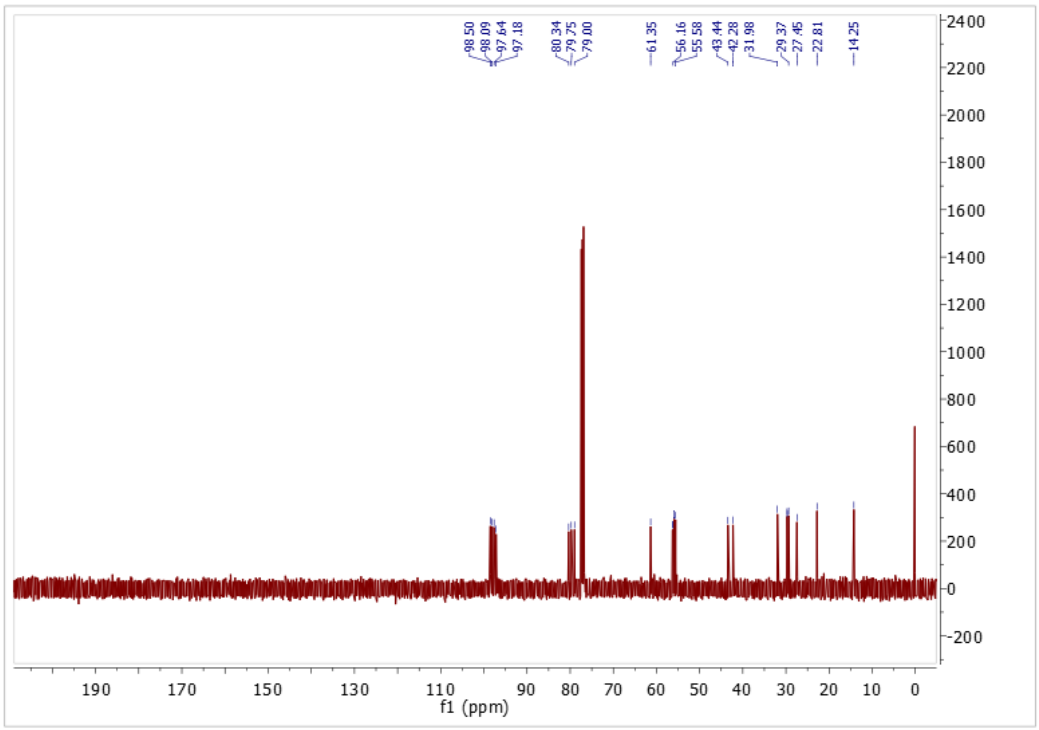

^{1}H NMR of Compound **21** in $CDCl_3$

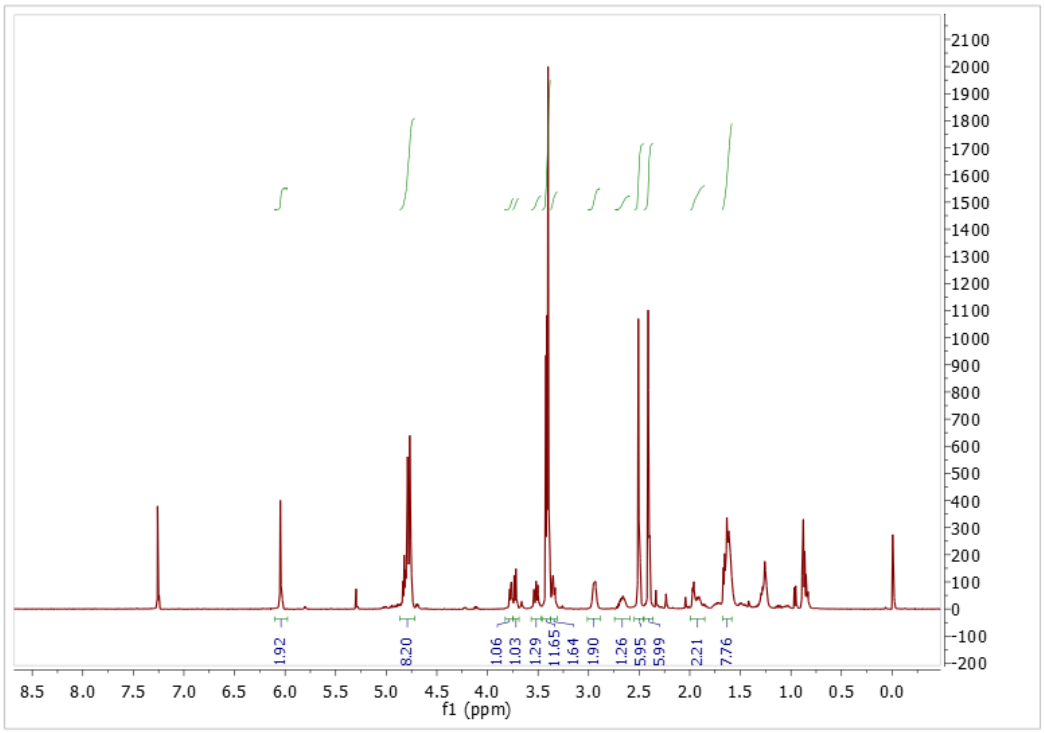

^{13}C NMR of Compound **21** in $CDCl_3$

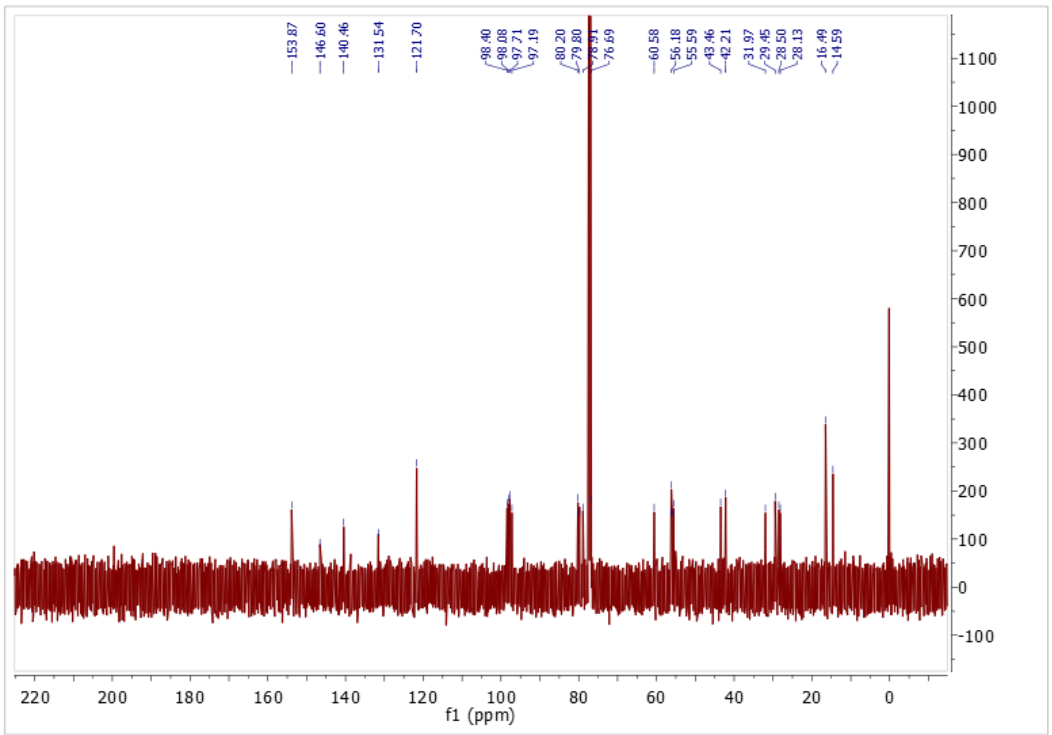

^{1}H NMR of Compound **28** in $CDCl_3$

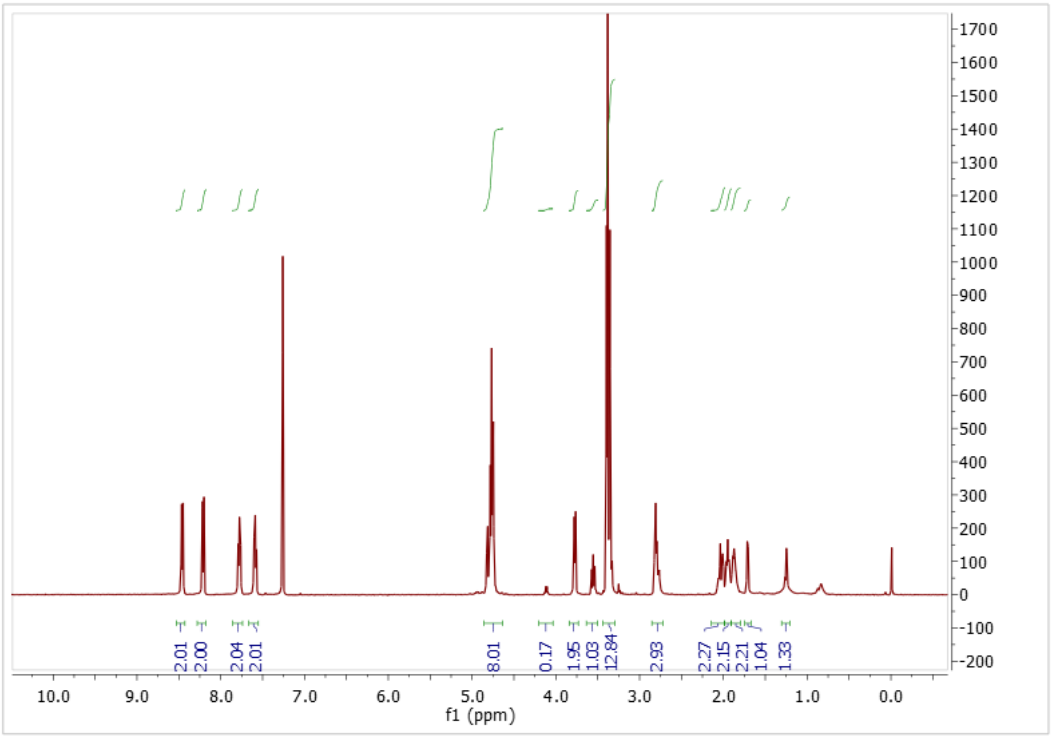

^{13}C NMR of Compound **28** in $CDCl_3$

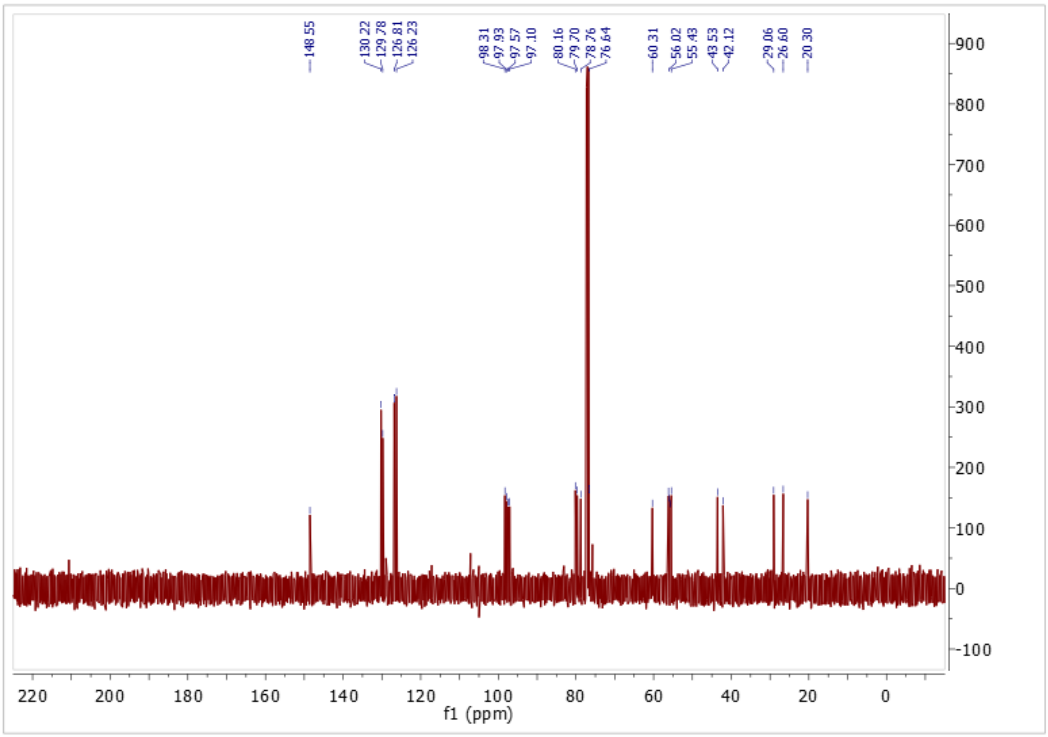

^{1}H NMR of Compound **29** in CD_3OD

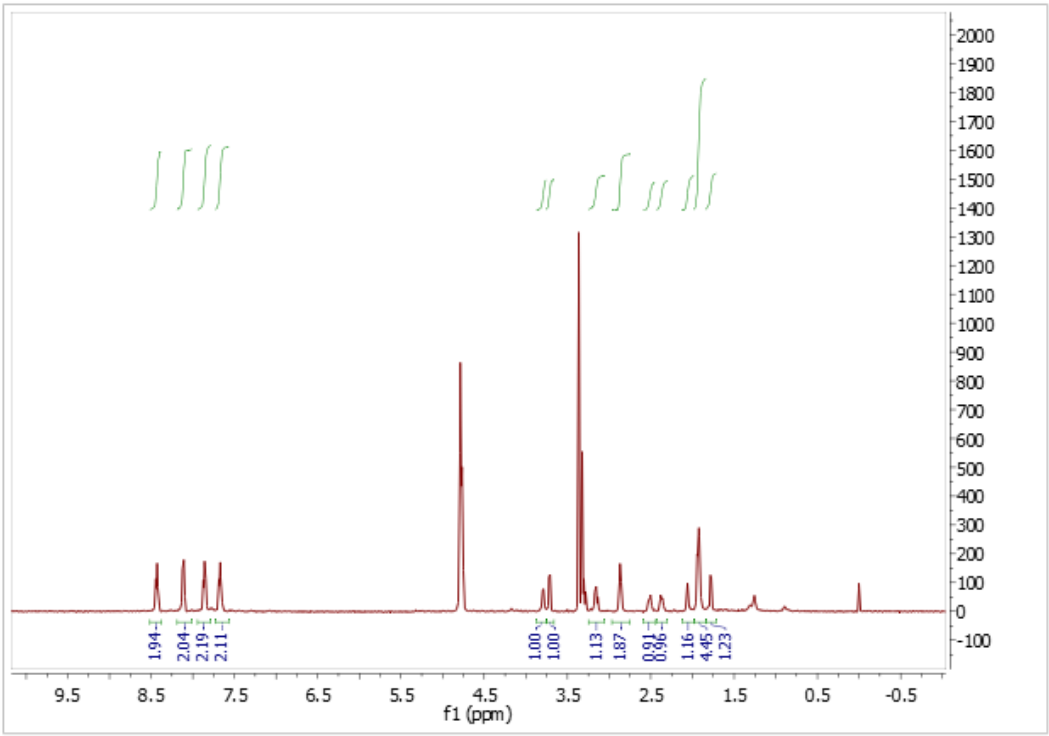

^{13}C NMR of Compound **29** in CD_3OD

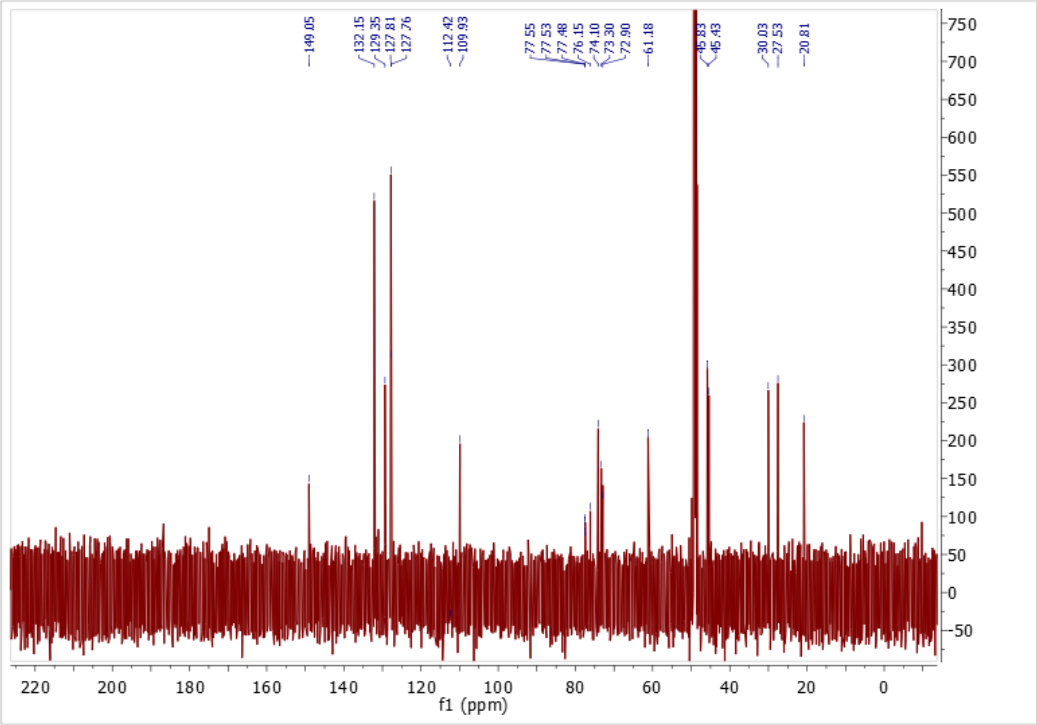

^{1}H NMR of Compound **30** in $CDCl_3$

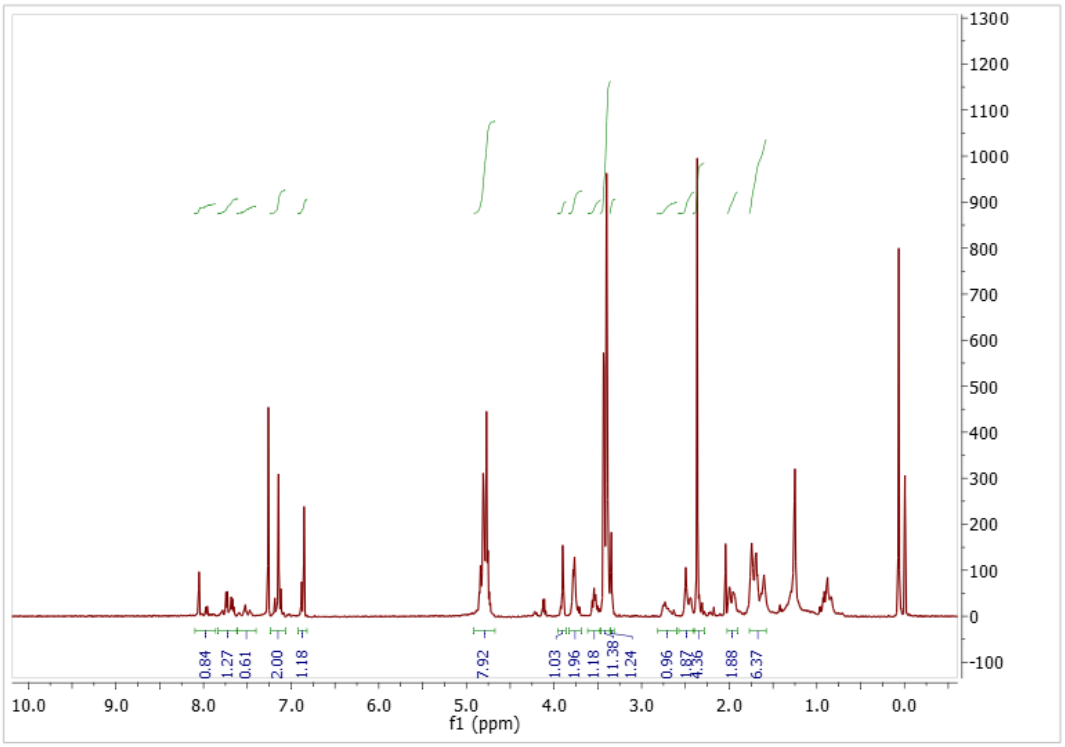

^{13}C NMR of Compound **30** in $CDCl_3$

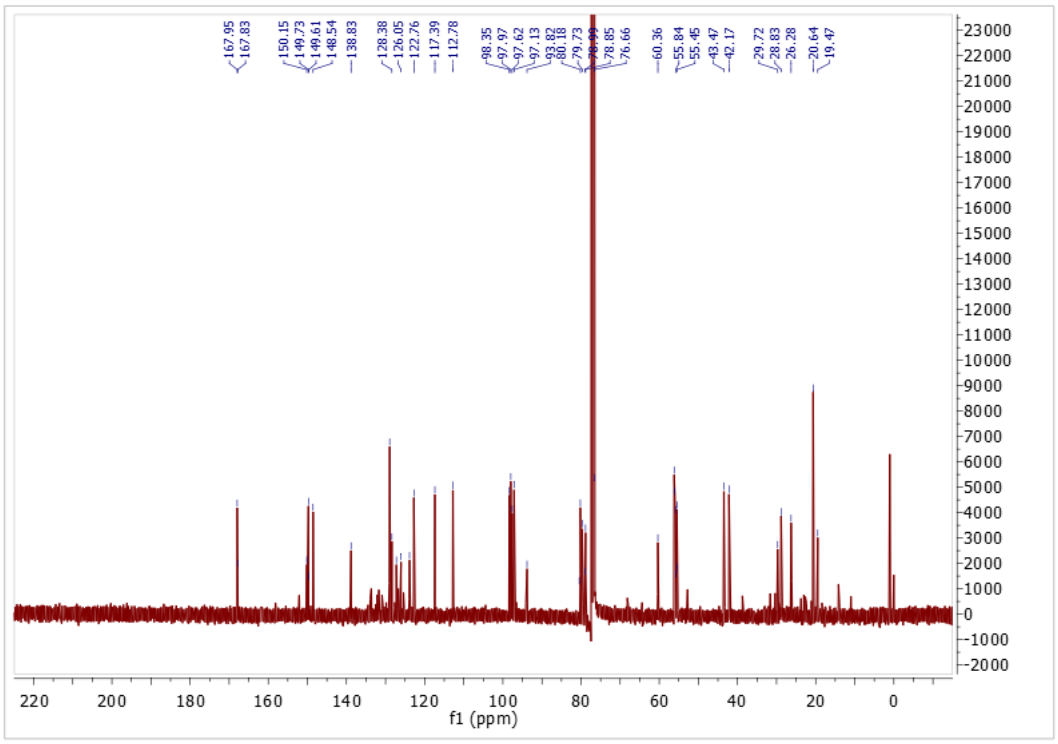

^{1}H NMR of Compound **31** in CD_3OD

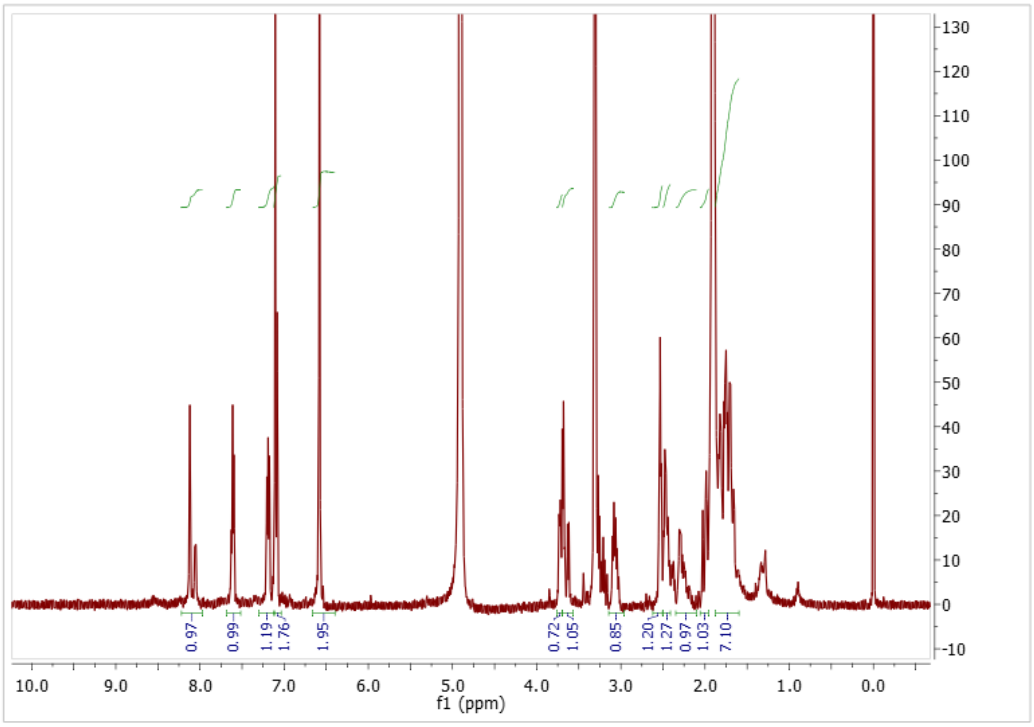

^{13}C NMR of Compound **31** in CD_3OD

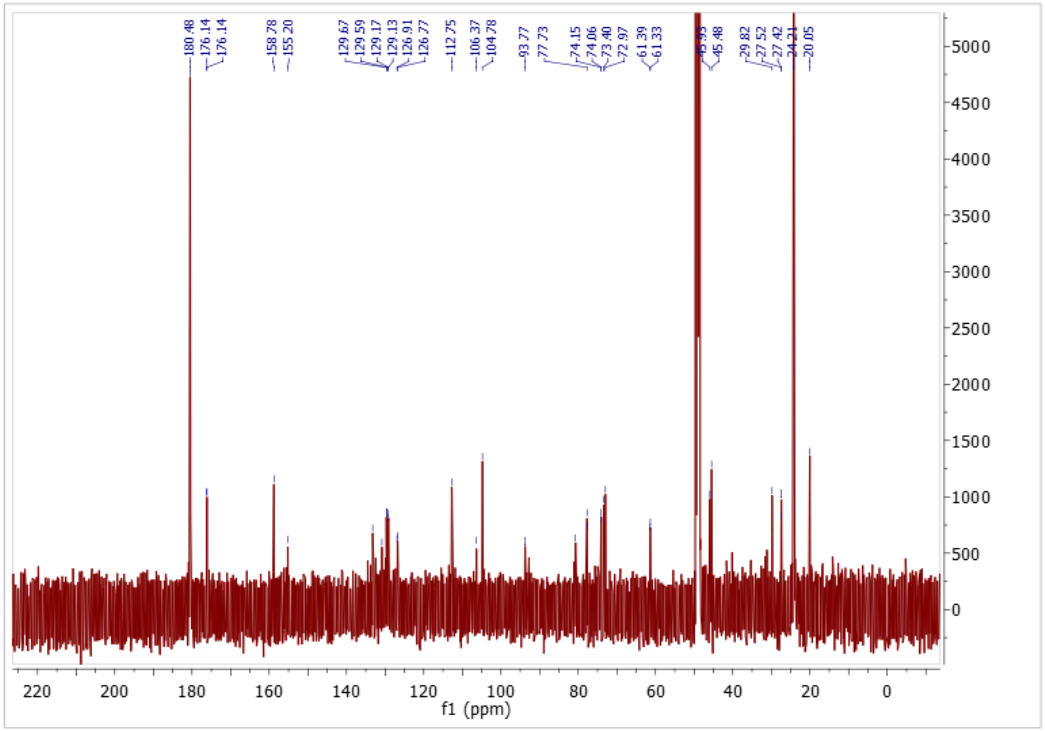

^{1}H NMR of Compound **32** in $CDCl_3$

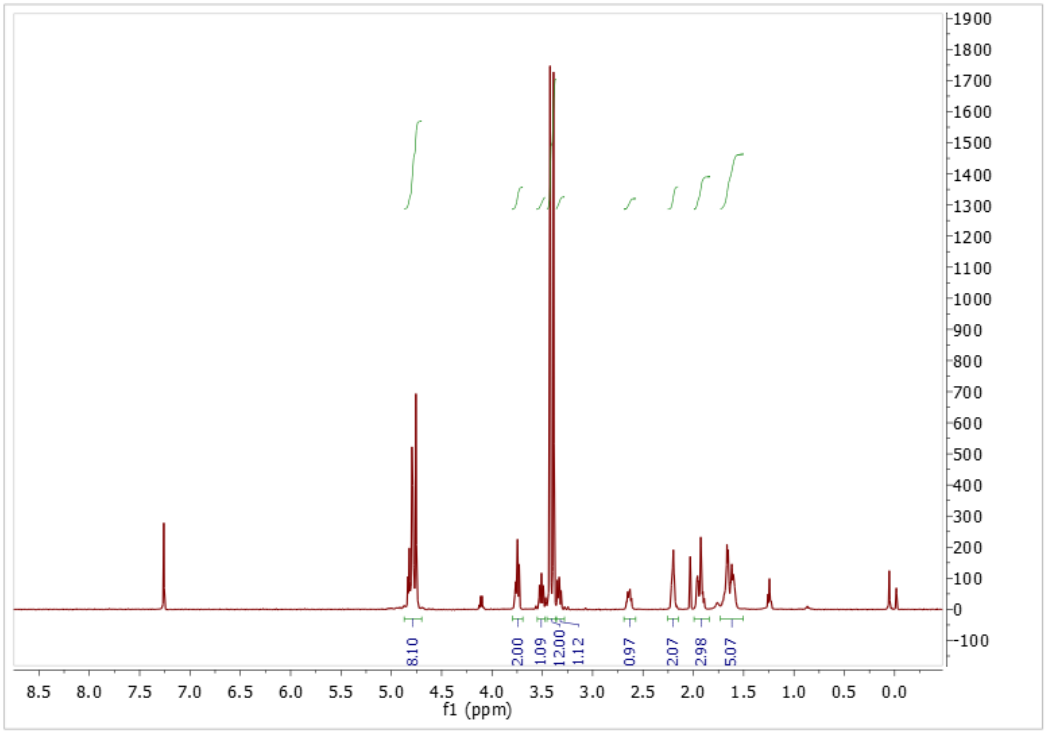

^{13}C NMR of Compound **32** in $CDCl_3$

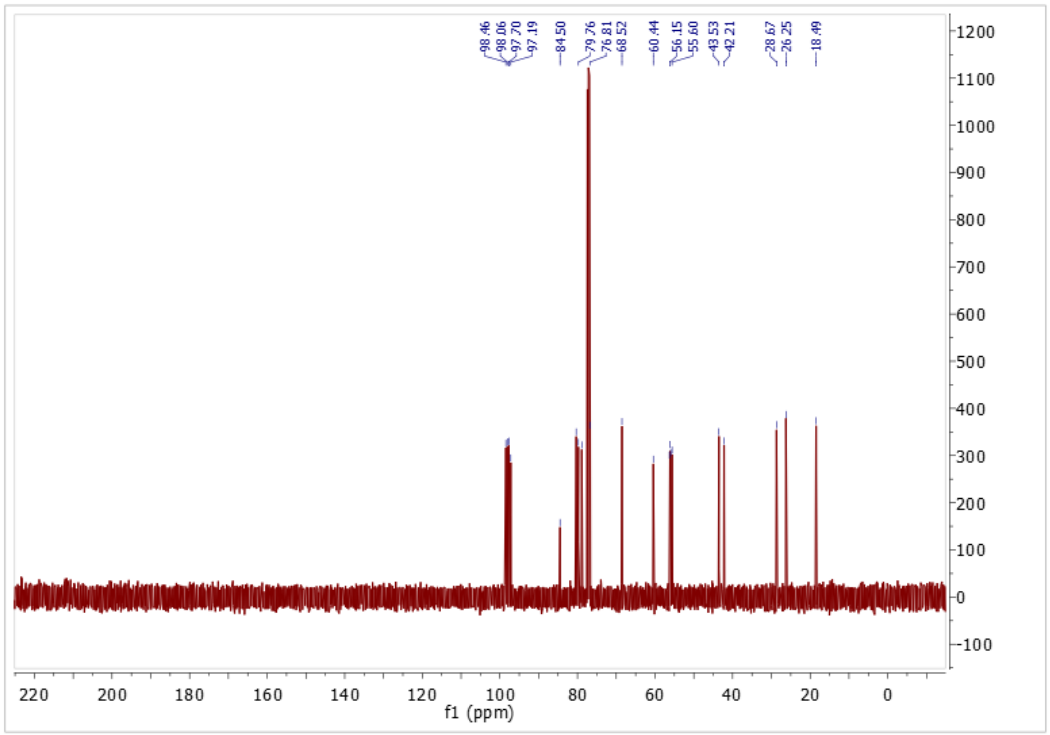

^{1}H NMR of Compound **33** in $CDCl_3$

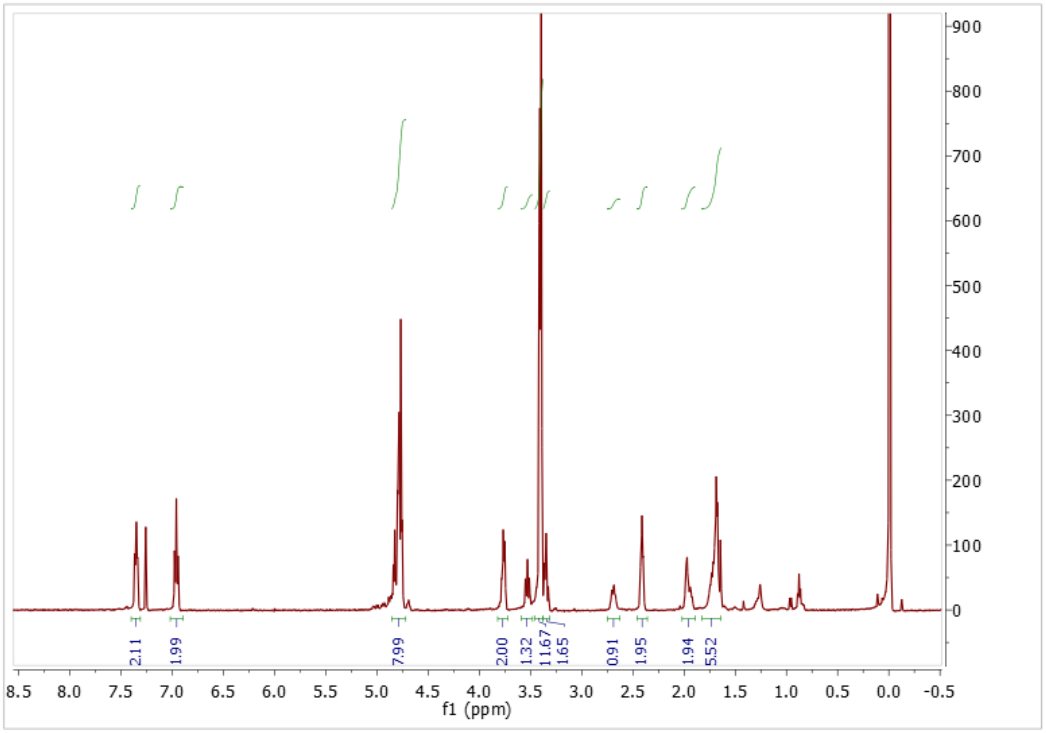

^{13}C NMR of Compound **33** in $CDCl_3$

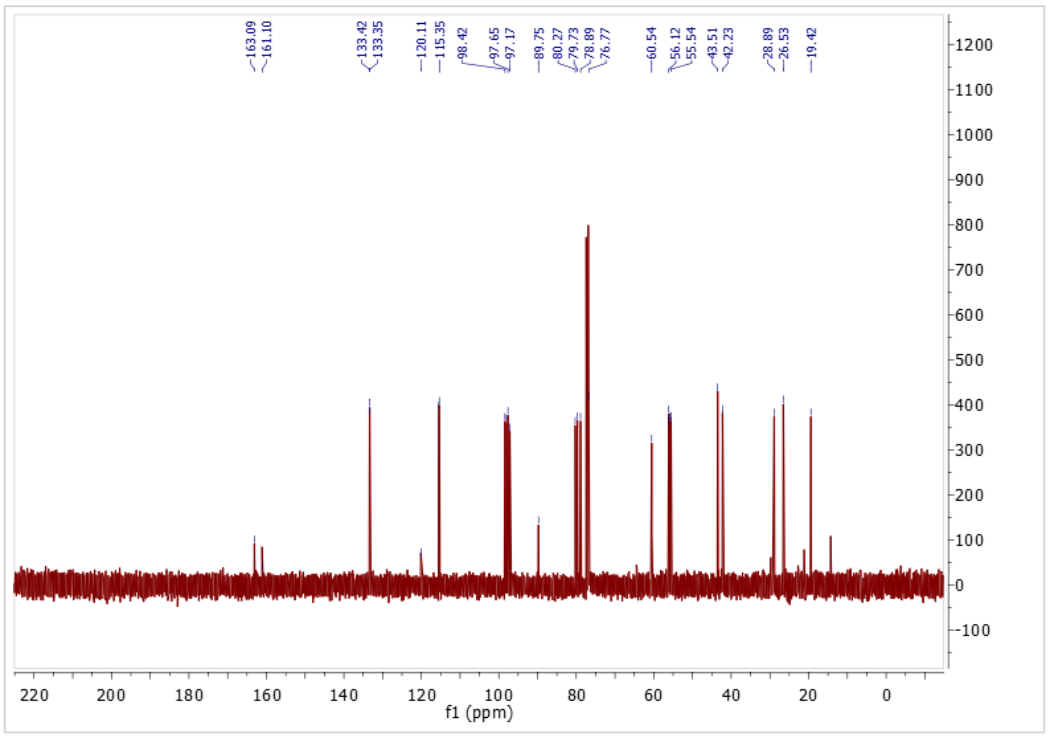

^{1}H NMR of Compound **34** in CD_3OD

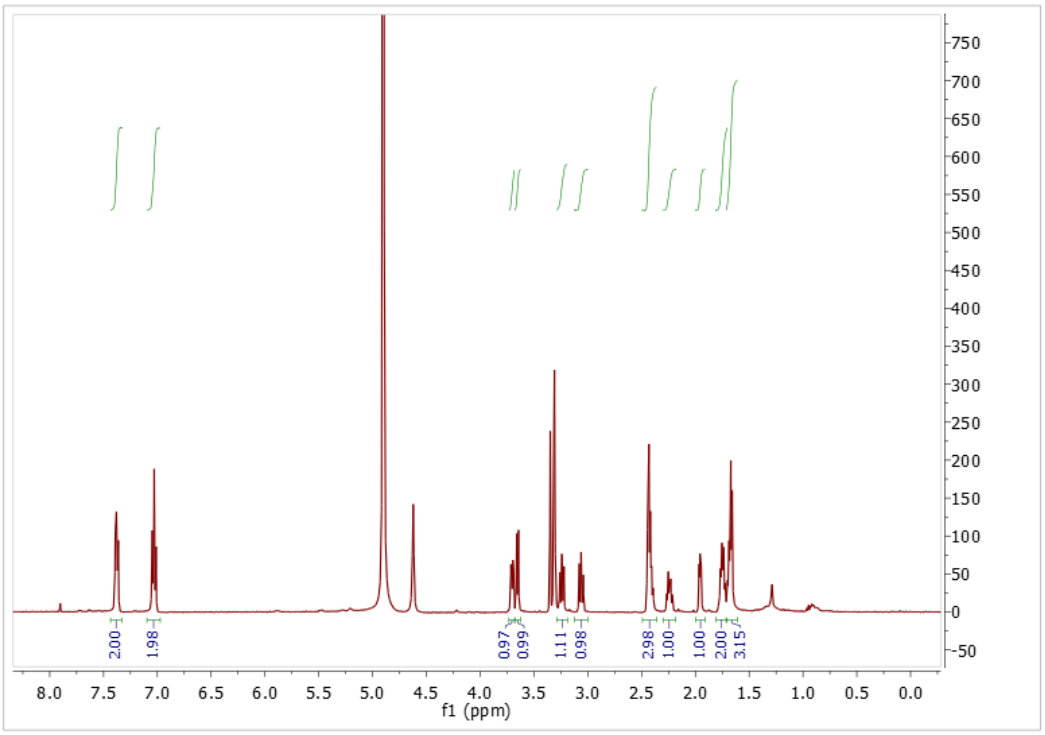

^{13}C NMR of Compound **34** in CD_3OD

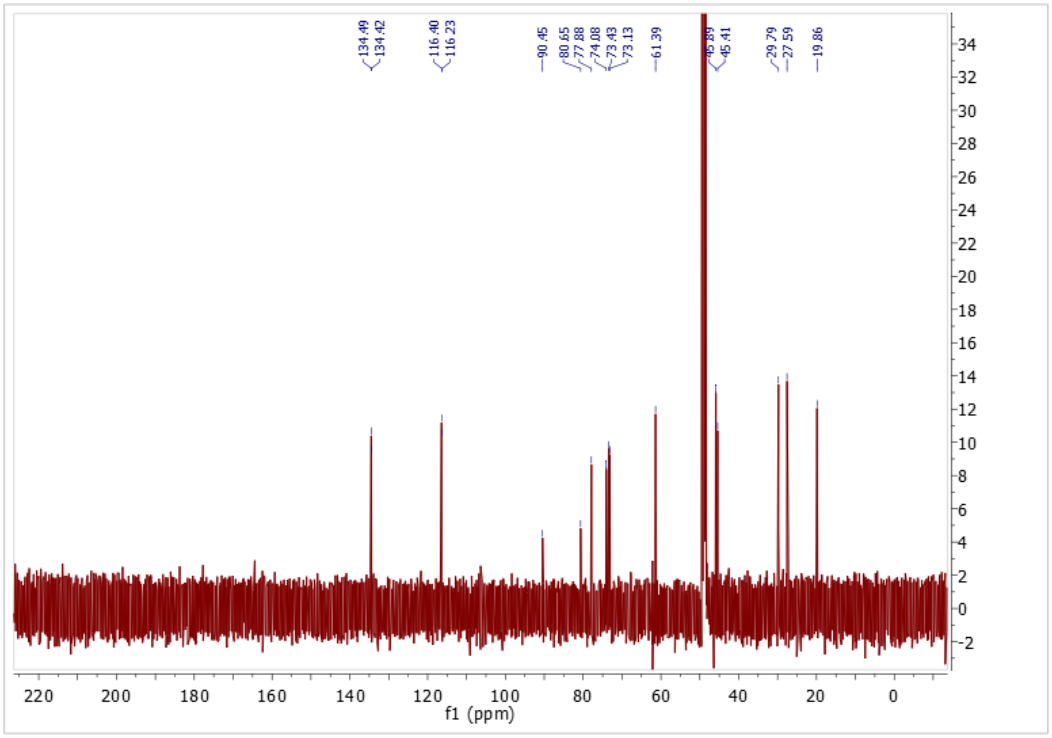

^{1}H NMR of Compound **35** in CD_3OD

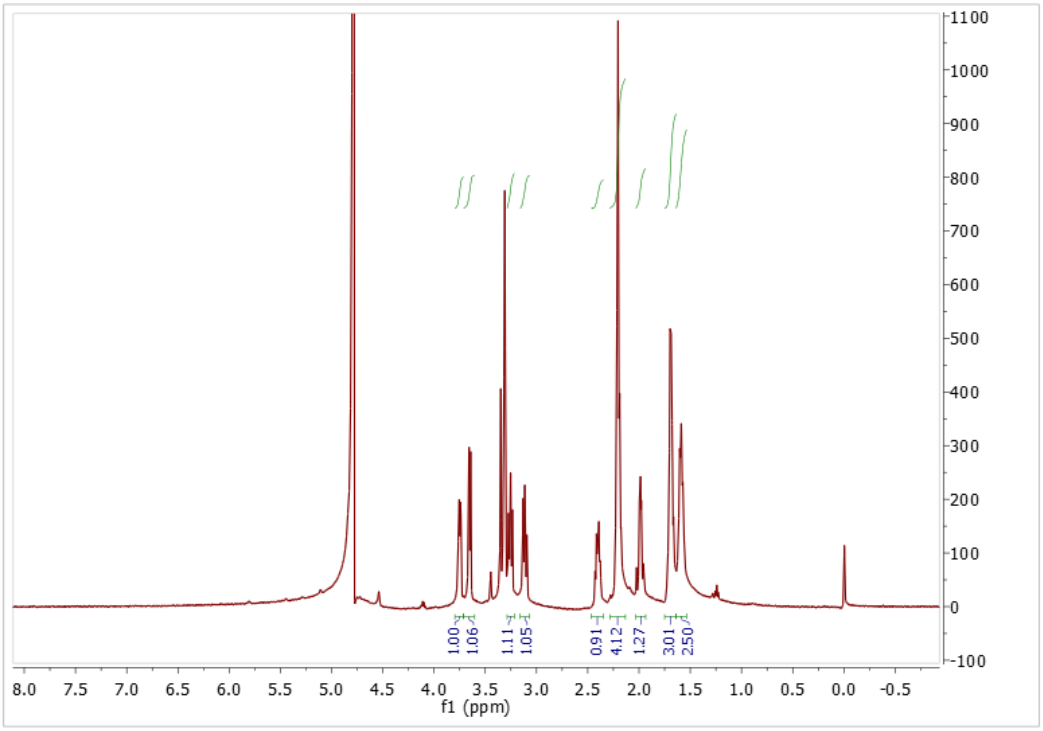

^{13}C NMR of Compound **35** in CD_3OD

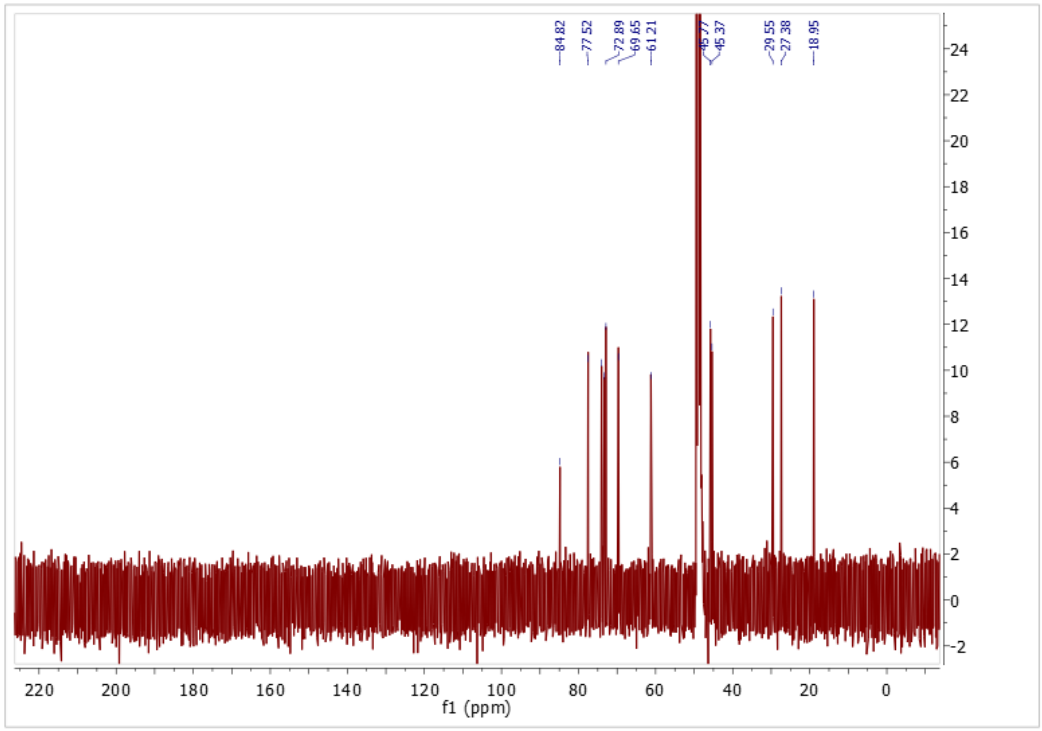

^{1}H NMR of Compound **36** in $CDCl_3$

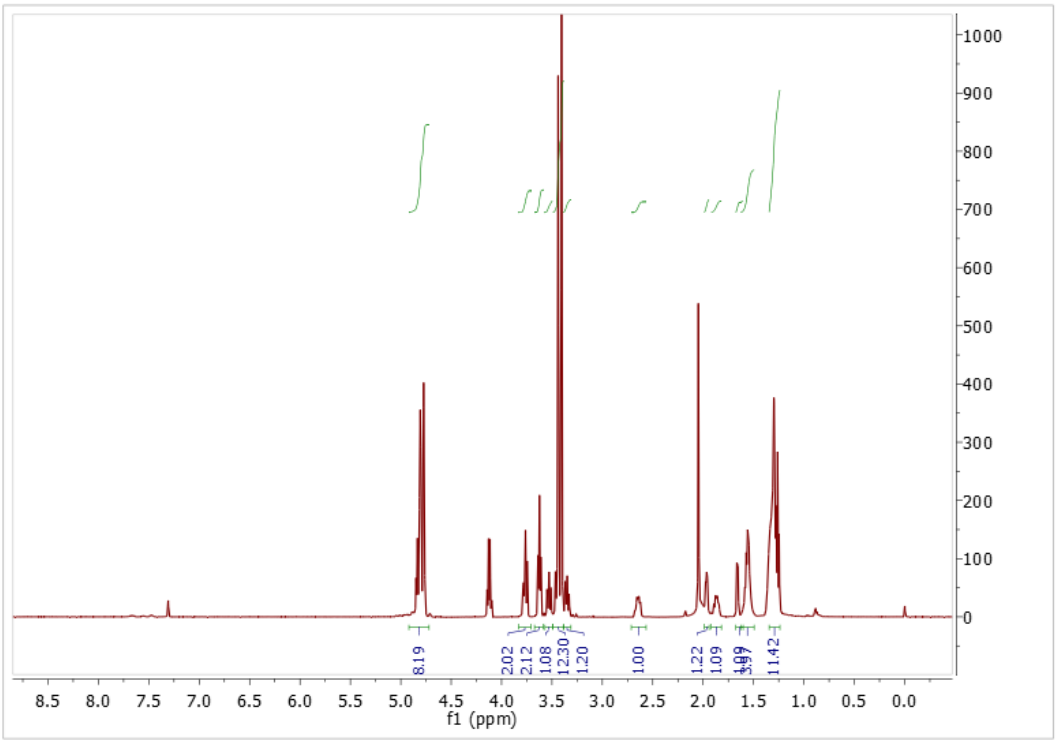

^{13}C NMR of Compound **36** in $CDCl_3$

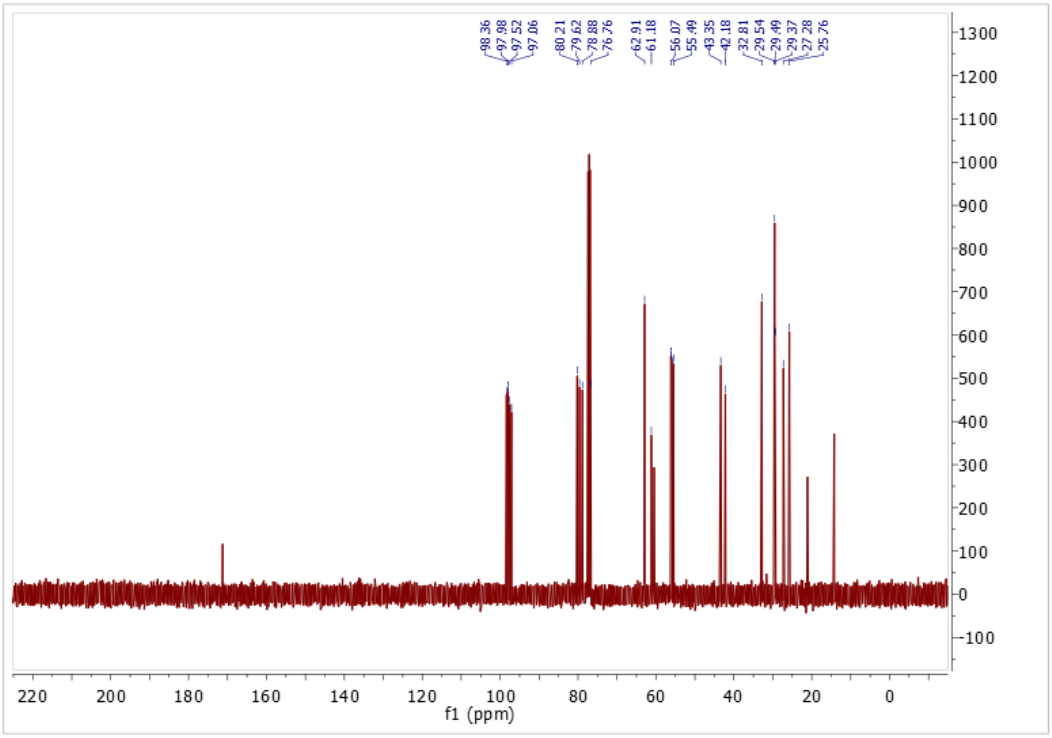

^{1}H NMR of Compound **37** in $CDCl_3$

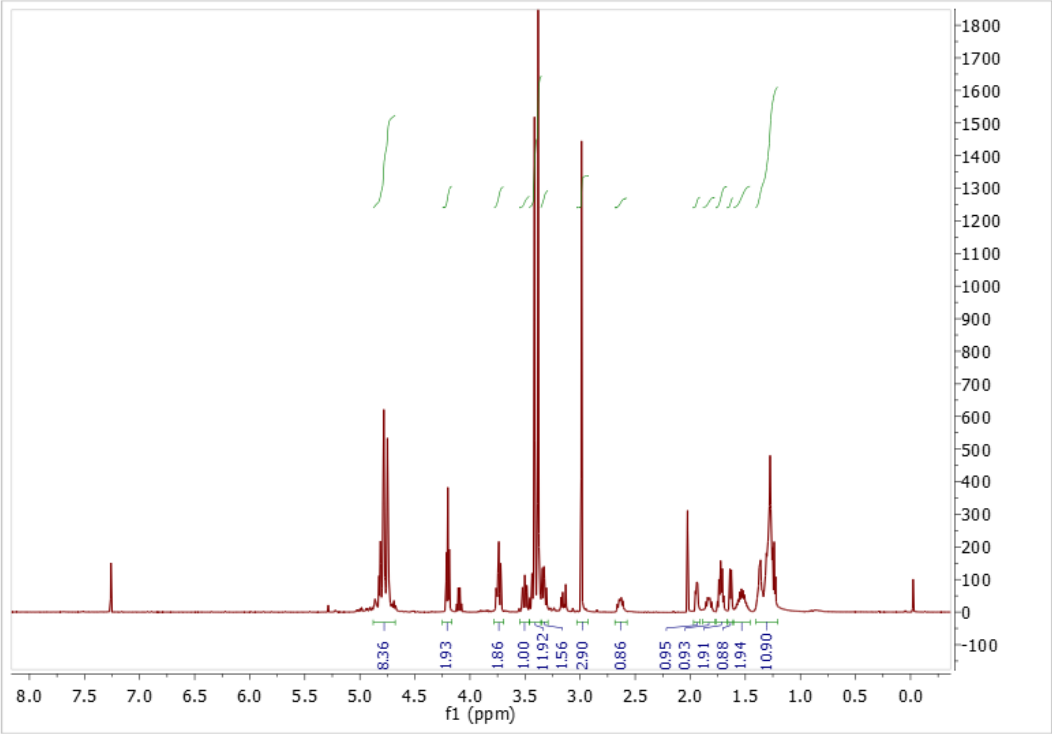

^{13}C NMR of Compound **37** in $CDCl_3$

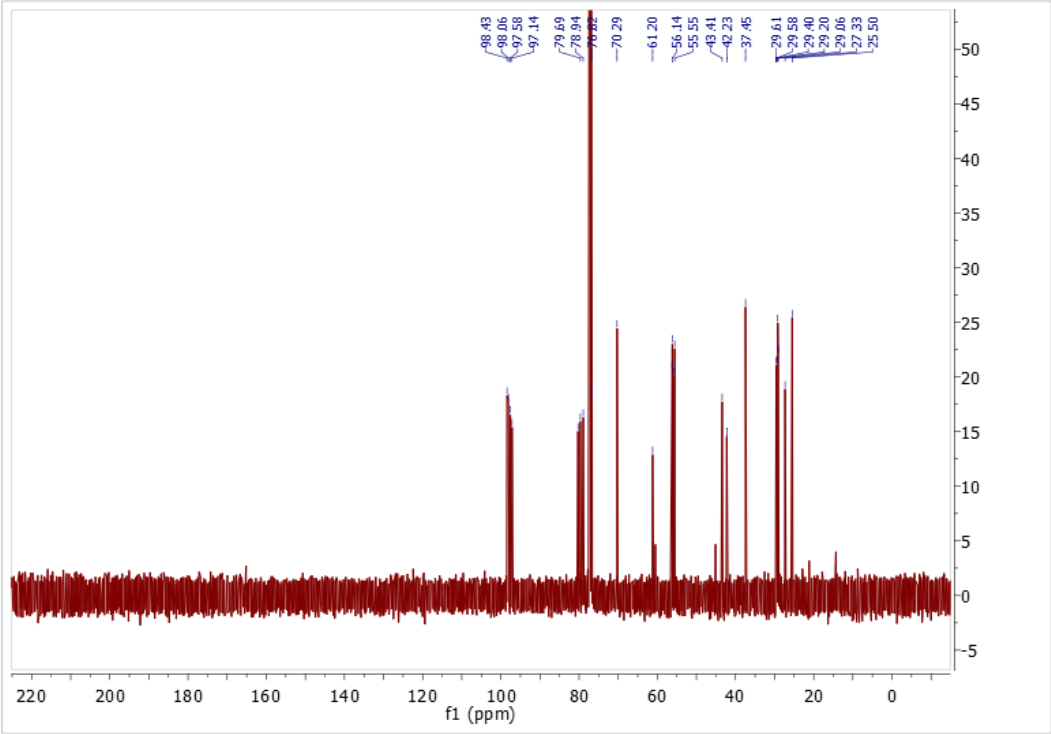

^{1}H NMR of Compound **38** in $CDCl_3$

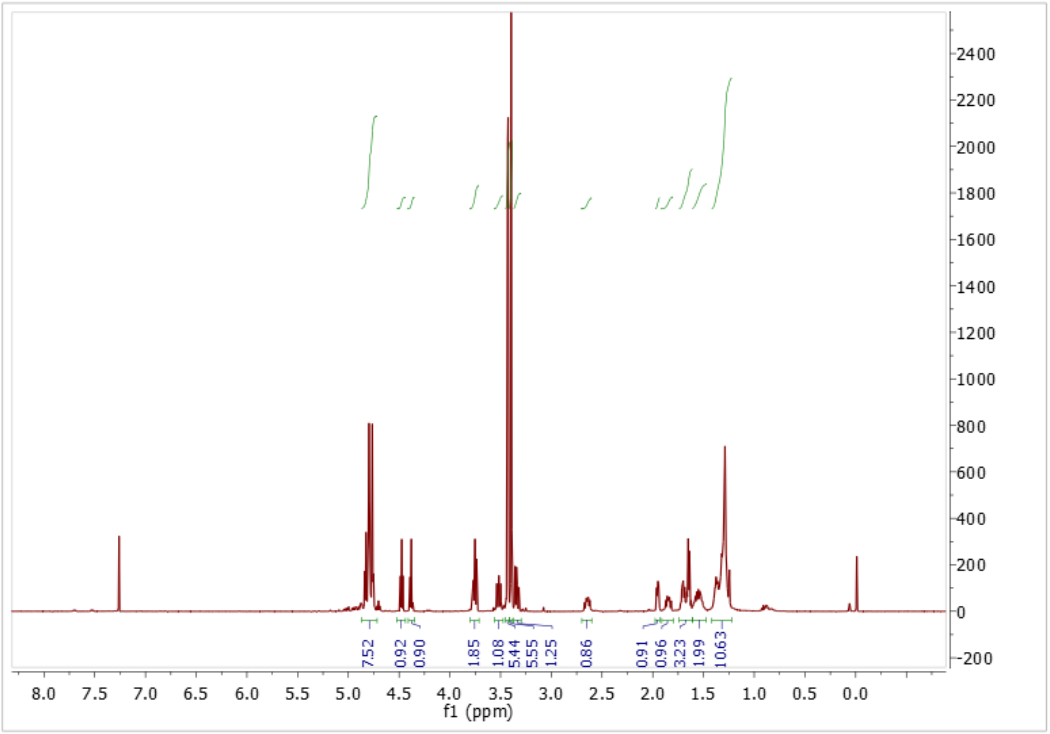

^{13}C NMR of Compound **38** in $CDCl_3$

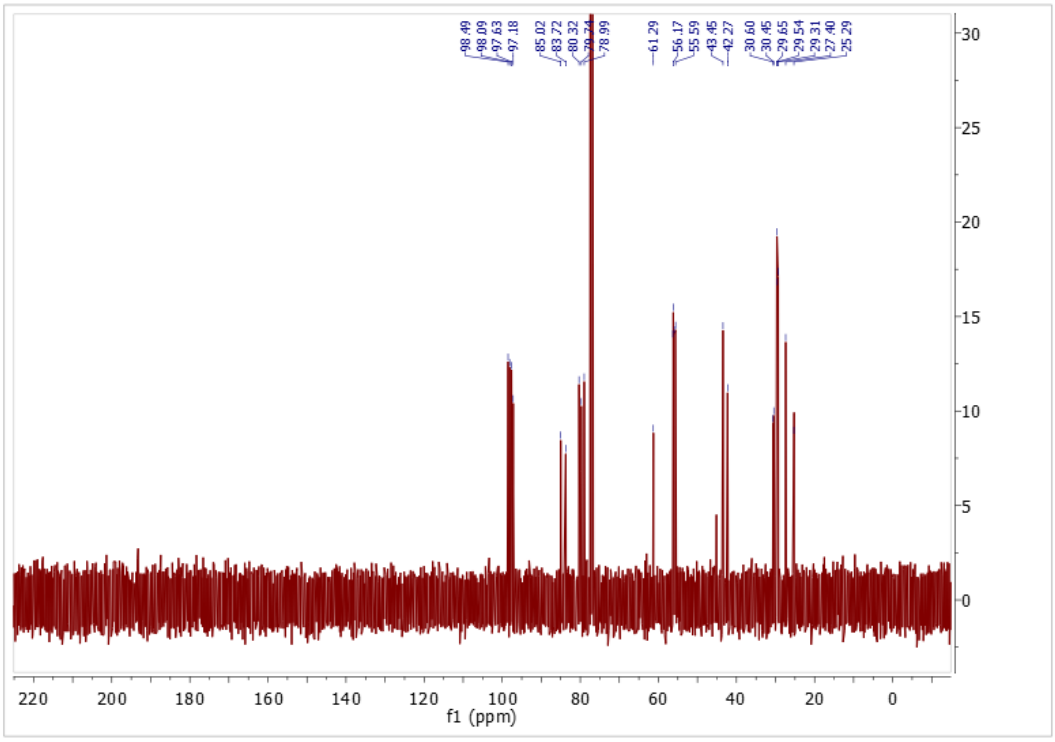

^{1}H NMR of Compound **39** in CD_3OD

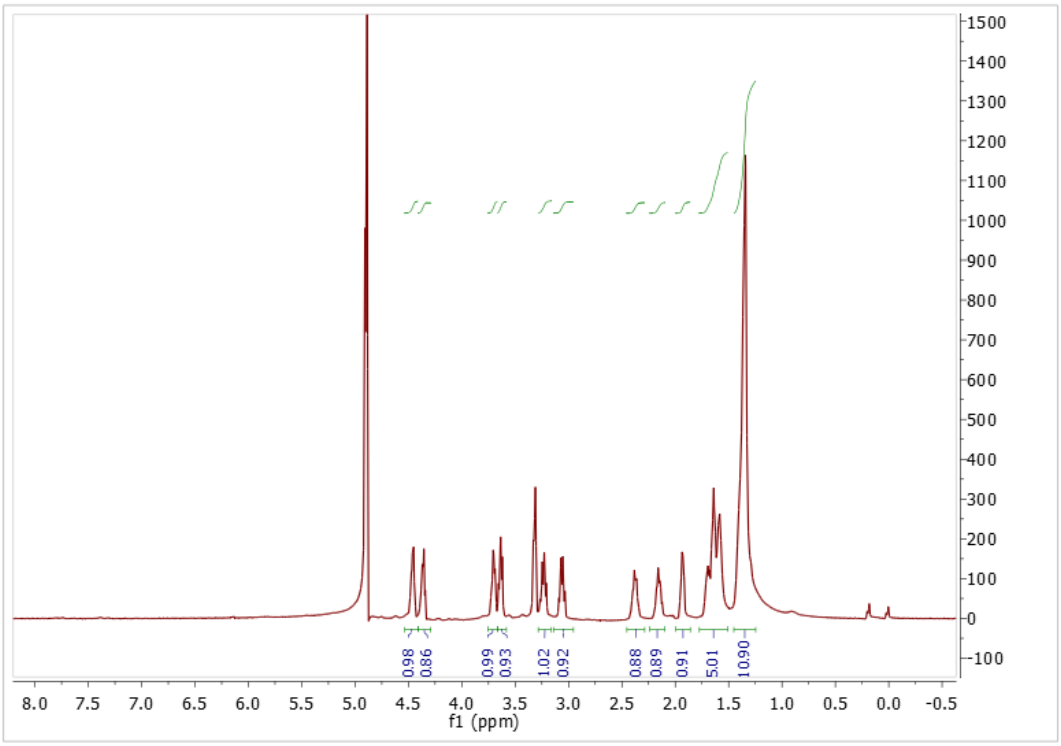

^{13}C NMR of Compound **39** in CD_3OD

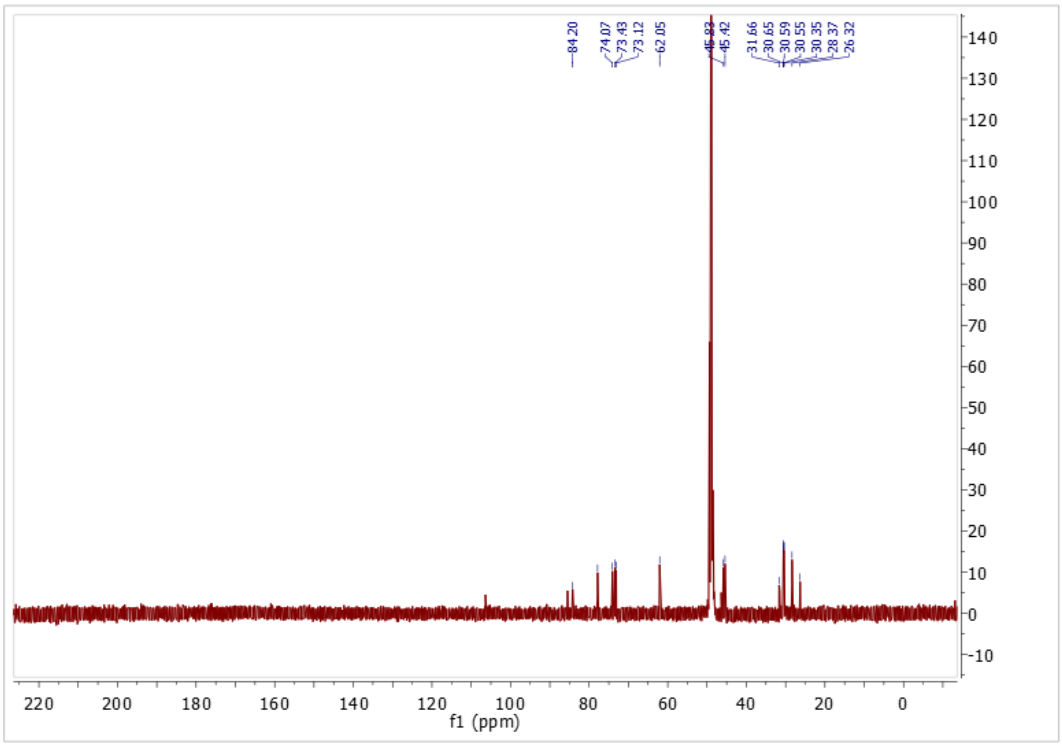

References

1. Lombard, V., Golaconda Ramulu, H., Drula, E., Coutinho, P. M., Henrissat, B. The carbohydrate-active enzymes database (CAZy) in 2013. *Nucleic Acids Res*. **2014**, 42, D490.
2. (a) Legler, G. Glycoside hydrolases: mechanistic information from studies with reversible and irreversible inhibitors. *Adv. Carbohydr. Chem. Biochem.* **1990,** 48**,** 319–384. 9. (b) Vocadlo, D. J., Davies, G. J., Laine, R. and Withers, S. G. Catalysis by hen egg-white lysozyme proceeds via a covalent intermediate. *Nature* **2001**, *412* (6849), 835-838. (c) Withers, S. G., Rupitz, K., Street, I. P., 2-DEOXY-2-FLUORO-D-GLYCOSYL FLUORIDES - A NEW CLASS OF SPECIFIC MECHANISM-BASED GLYCOSIDASE INHIBITORS. *Journal of Biological Chemistry* **1988**, *263* (17), 7929-7932.
3. Zechel, D. L., Withers, S. G., Glycosidase mechanisms: Anatomy of a finely tuned catalyst. *Accounts of Chemical Research,* **2000**, 33 (1), 11-18.
4. Premkumar, L., Sawkar, A. R, Boldin-Adamsky, S., Toker, L., Silman, I., Kelly, J. W., Futerman, A. H. and Sussman, J. L. X-ray Structure of Human Acid-β-Glucosidase Covalently Bound to Conduritol-B-Epoxide IMPLICATIONS FOR GAUCHER DISEASE. *J. Biol. Chem.* **2005**, 280 (25), 23815-23819.
5. Horowitz, M., Wilder, S., Horowitz, Z., Reiner, O., Gelbart, T., Beutler, E. The human glucocerebrosidase gene and pseudogene: structure and evolution. *Genomics*, **1989**, 4: 87–96.
6. Reczek, D., Schwake, M., Schroder, J., Hughes, H., Blanz, J., Jin, X., Brondyk, W., Van Patten, S., Edmunds, T. and Saftig, P. LIMP-2 is a receptor for lysosomal mannose-6-phosphate-independent targeting of beta-glucocerebrosidase. *Cell,* **2007**, 131, 770–83.
7. Siebert, M., Sidransky, E. and Westbroek, W. Glucocerebrosidase is shaking up the synucleinopathies. *Brain*. **2014**, 137, 1304-1322.
8. Jiang, J., Artola, M., Beenakker T. J. M., Schröder, S. P., Petracca, R., de Boer, C., Aerts, J. M., van der Marel, G. A., Codée, J. D. and Overkleeft. H. S. The Synthesis of Cyclophellitol-Aziridine and Its Configurational and Functional Isomers. *Eur. J. Org. Chem.* **2016**, 3671–3678.
9. (a) Soreghan, B., Thomas, S. N., Yang, A. J. Aberrant sphingomyelin/ceramide metabolic-induced neuronal endosomal/lysosomal dysfunction: potential pathological consequences in age-related neurodegeneration. *Adv. Drug Deliv. Rev.,* **2003**, 55, 1515–24. (b) Jana, A., Hogan, E. L., Pahan, K. Ceramide and neurodegeneration: susceptibility of neurons and oligodendrocytes to cell damage and death. *J. Neurol. Sci.,* **2009**, 278, 5–15. (c) Fortin, D. L., Troyer, M. D., Nakamura, K., Kubo, S., Anthony, M. D., Edwards, R.H. Lipid rafts mediate the synaptic localization of alpha-synuclein. *J. Neurosci*. **2004**, 24, 6715–23.
10. Kitatani, K., Idkowiak-Baldys, J., and Hannun, Y. A. The sphingolipid salvage pathway in ceramide metabolism and signaling. *Cell Signal,* **2008**, 20,1010–8.
11. Gillard, B.K., Clement, R. G., Marcus, D. M. Variations among cell lines in the synthesis of sphingolipids in de novo and recycling pathways. *Glycobiology*, **1998**, 8, 885–90. (b) Tettamanti, G., Bassi, R., Viani, P., Riboni, L. Salvage pathways in glycosphingolipid metabolism. *Biochimie*. **2003**, 85, 423–37.
12. Kennedy, D. The Living Cell. San Francisco and London, W.H. Freeman and Company, **1965.**
13. Sardia, S. P., Clarke, J., Viel, C., Chan, M., Tamsett, T. J., Treleaven, C. M., Bu, J., Sweet, L., Passini, M. A., Dodge, J. C., Yu, W. H., Sidman, R. L., Cheng, S. H. and Shihabuddin, L. S. Augmenting CNS glucocerebrosidase activity as a therapeutic strategy for parkinsonism and other Gaucher-related synucleinopathies. *PNAS.* **2013,** 110, 3537-3542.
14. Jmoudiak, M. and Futerman A. H. Gaucher disease: pathological mechanisms and modern management. *Brit. J. Haematol.* **2005,** 129, 178-188.

15. Grabowski, G. A., Lysosomal storage disease 1 - Phenotype, diagnosis, and treatment of Gaucher's disease. *Lancet,* **2008**, *372* (9645), 1263-1271.
16. Sawkar, A. R., Adamski-Werner, S. L., Cheng, W. C., Wong, C. H., Beutler, E., Zimmer, K. P., Kelly, J. W. Gaucher disease-associated glucocerebrosidases show mutation-dependent chemical chaperoning profiles. *Chemistry & Biology,* **2005**, 12 (11), 1235-1244.
17. Beutler, E. and Grabowski, G.A. (**2001**) Gaucher Disease. In: The Metabolic and Molecular Bases of Inherited Disease, Vol. II (ed. by C.R. Scriver, W.S. Sly, B. Childs, A.L. Beaudet, D. Valle, K.W. Kinzler & B. Vogelstein), pp. 3635–3668. McGraw-Hill Inc., Columbus, USA.
18. Tamargo, R. J., Velayati, A., Goldin, E., and Sidransky, E. The role of saposin C in Gaucher disease. *Mol. Genet. Metab.* **2012**, 106(3), 257-263.
19. Zimran, A. (ed.) (**1997**) Gaucher's Disease. Balliere Tindall, Cambridge, UK.
20. Goker-Alpan, O., Schiffmann, R., Park, J.K., Stubblefield, B.K., Tayebi, N. and Sidransky, E. Phenotypic continuum in neuronopathic Gaucher disease: an intermediate phenotype between type 2 and type 3. *Journal of Pediatrics*, **2003**, 143, 273–276.
21. Weinreb, N.J., Charrow, J., Andersson, H.C., Kaplan, P., Kolodny, E.H., Mistry, P., Pastores, G., Rosenbloom, B.E., Scott, C.R., Wappner, R.S. & Zimran, A. Effectiveness of enzyme replacement therapy in 1028 patients with type 1 Gaucher disease after 2 to 5 years of treatment: a report from the Gaucher Registry. *American Journal of Medicine*, **2002**, 113, 112–119.
22. (a) Dvir, H., Harel, M., McCarthy, A. A., Toker, L., Silman, I., Futerman, A. H. and Sussman, J. L. X-ray structure of human acid-betaglucosidase, the defective enzyme in Gaucher disease. *EMBO Reports*, **2003**, 4, 704–709. (b) Desnick, R.J. Enzyme replacement and enhancement therapies for lysosomal diseases. *Journal of Inherited Metabolic Disease*, **2004,** 27, 385–410. (c) Fan, J.Q. A contradictory treatment for lysosomal storage disorders: inhibitors enhance mutant enzyme activity. *Trends in Pharmacological Science*, **2003**, 24, 355–360.
23. Hoehn, M. M. and Yahr, M. D. Parkinsonism: onset, progression and mortality. *Neurology*, **1967**, 17, 427–442.
24. Kotzbauer, P. T., Tu, Z. and Mach, R. H. Current status of the development of PET radiotracers for imaging alpha synuclein aggregates in Lewy bodies and Lewy neurites. *Clin. Transl. Imaging*, **2017**, 5:3–14.
25. Spillantini, M. G., Crowther, R. A., Jakes, R., Hasegawa, M. and Goedert, M. (1998) alpha-Synuclein in filamentous inclusions of Lewy bodies from Parkinson's disease and dementia with lewy bodies. *Proc. Natl. Acad. Sci. USA*, **1998**, 95(11):6469–6473.
26. Bahr, B.A. and Bendiske, J. The neuropathogenic contributions of lysosomal dysfunction. *J. Neurochem.* **2002**, 83, 481–489.
27. Chinta, S. J., Andersen, J. K., Dopaminergic Neurons. *Int. J. Biochem. Cell B.* **2005**, 37, 942-946.
28. Hely, M. A., Reid, W. G., Adena, M. A., Halliday, G. M. and Morris, J. G. The Sydney multicenter study of Parkinson's disease: the inevitability of dementia at 20 years. *Mov. Disord.* **2008**, 23(6), 837–844.
29. Olanow, C.W, Hauser, R.A., Gauger, L., Malapira, T., Koller, W., Hubble, J., Bushenbark, K., Lilienfeld, D. and Esterlitz, J. The effect of deprenyl and levo-dopa on the progression of Parkinson's disease. *Ann. Neurol.,* **1995**, 38, 771–7.
30. Fahn, S., Oakes, D., Shoulson, I., *et al*. Levodopa and the progression of Parkinson's disease. New *Engl. J. Med*. **2004**, 351(24), 2498–2508.
31. Tveiten, O.V., Skeie, G.O., Haugarvoll, K., Muller, B., Larsen, J.P. and Tysnes, O.B. Treatment in early Parkinson's disease: the Norwegian Park West study. *Acta. Neurol. Scand.* **2013**, 128, 107–113.

32. Hughes, A.J., Ben-Shlomo, Y., Daniel, S.E. and Lees, A.J. What features improve the accuracy of clinical diagnosis in Parkinson's disease: a clinicopathologic study. *Neurology*, **1992**, 42(6), 1142–1146.
33. (a) Marsden, C.D. Parkinson's disease. *Lancet*. **1990**, 335, 948–952. (b) Ross, G.W., Petrovitch, H., Abbott, R.D., Nelson, J., Markesbery, W., Davis, D., Hardman, J., Launer, L., Masaki, K., Tanner, C. M. and White, L. R. Parkinsonian signs and substantia nigra neuron density in decedents elders without PD. *Ann. Neurol*. **2004**, 56, 532–539.
34. Skovronsky, D. M., Lee, V. M. and Trojanowski, J. Q. Neurodegenerative diseases: new concepts of pathogenesis and their therapeutic implications. *Annu. Rev. Pathol*. **2006**, 1151–170.
35. Booth, T. C., Nathan, M., Waldman, A. D., Quigley, A. M., Schapira, A. H., and Buscombe, J. The Role of Functional Dopamine-Transporter SPECT Imaging in Parkinsonian Syndromes, Part 1, *AJNR Am J Neuroradiol,* **2015,** 36, 229 –35.
36. Rosenbloom, B., Balwani, M., Bronstein, J. M., Kolodny, E., Sathe, S., Gwosdow, A. R., Taylor, J. S., Cole, J. A., Zimran, A. and Weinreb, N. J. The incidence of Parkinsonism in patients with type 1 Gaucher disease: Data from the ICGG Gaucher Registry. *Blood Cell. Mol. Dis.* **2011**, 46, 95–102.
37. (a) Neumann, J., Bras, J., Deas, E., O'Sullivan, S.S., Parkkinen, L., Lachmann, R. H., Li A, Holton, J., Guerreiro, R., Paudel, R., Segarane, B., Singleton, A., Lees, A., Hardy, J., Houlden, H., Revesz, T. and Wood, N. W. Glucocerebrosidase mutations in clinical and pathologically proven Parkinson's disease. *Brain,* **2009**, 132, 1783–94. (b) Sidransky, E., Nalls, M.A., Aasly, J. O., Aharon-Peretz, J., Annesi, G., Barbosa, E. R., Bar-Shira, A., Berg, D., Bras, J., Brice, A., Chen, C. M., Clark, L. N., Condroyer, C. De Marco, E. V. *et al*. Multicenter analysis of glucocerebrosidase mutations in Parkinson's disease. *N. Engl. J. Med.* **2009**, 361, 1651–61.
38. Lwin, A., Orvisky, E., Goker-Alpan, O., LaMarca, M. E. and Sidransky, E. Glucocerebrosidase mutations in subjects with parkinsonism. *Mol. Genet. Metab.* **2004**, 81, 70–73.
39. Goker-Alpan, O., Stubblefield, B. K., Giasson, B. I. and Sidransky, E. Glucocerebrosidase is present in a-synuclein inclusions in Lewy body disorders. *Acta Neuropathol.* **2010,** 120, 641–649.
40. Clark, L.N., Kartsaklis, L. A., Wolf Gilbert, R., Dorado, B., Ross, B. M., Kisselev, S., Verbitsky, M., Mejia-Santana, H., Cote, L. J., Andrews, H., Vonsattel, J. P., Fahn, S., Mayeux, R., Honig, L. S., Marder, K. Association of glucocerebrosidase mutations with dementia with Lewy bodies. *Arch. Neurol.* **2009**, 66(5), 578–583.
41. Bae, E., Yang, N. A., Lee, C., Lee, H., Kim, S., Sardi, S. P. and Lee, S. Loss of glucocerebrosidase 1 activity causes lysosomal dysfunction and α-synuclein aggregation. *Exp. Mol. Med.* **2015**, 47, 1-8.
42. Murphy, K. E., Gysbers, A. M., Abbott, S. K., Tayebi, N., Kim, W. S., Sidransky, E., Cooper, A., Garner, B. and Halliday, G. M. Reduced glucocerebrosidase is associated with increased a-synuclein in sporadic Parkinson's disease. *Brain.* **2014**, 137, 834-848.
43. Mazzulli, J.R., Xu, Y. H., Sun, Y., Knight, A. L., McLean, P. J., Caldwell, G. A., Sidransky, E., Grabowski, G. A. and Krainc, D. Gaucher disease glucocerebrosidase and alpha-synuclein form a bidirectional pathogenic loop in synucleinopathies. *Cell*, **2011**, 146, 37–52.
44. Walvoort, M. T. C., Kallemeijn, W. W., Willems, L. I., Witte, M. D., Aerts, J. M. F. G., van der Marel, G. A., Codée, J. D. and Overkleeft. H. S. Tuning the leaving group in 2-deoxy-2-fluoroglucoside results in improved activity-based retaining b-glucosidase probes. *Chem. Commun*., **2012**, 48, 10386–10388.
45. Willems, L. I., Jiang, J., Li, K., Witte, M. D., Kallemeijn, W. W., Beenakker T. J. M., Schröder, S. P., Aerts, J. M., van der Marel, G. A., Codée, J. D. and Overkleeft. H. S. From Covalent

Glycosidase Inhibitors to Activity-Based Glycosidase Probes. *Chem. Eur. J*. **2014**, 20, 10864 – 10872.
46. Adams, B. T., Niccoli, S., Chowdhury, M. A., Esarik, A. N., Lees, S. J., Rempel, B. P. and Phenix, C. P. *N*-Alkylated Conduritol Aziridines are Potent, Specific and Cell-permeable Covalent Inactivators of Human β-Glucocerebrosidase. *Chem. Commun. (Camb).* **2015**, 51(57), 11390-11393.
47. (a) Withers, S. G., Street, I. P., Bird, P. and Dolphin, D. H. *J. Am. Chem. Soc*., **1987**, 109, 7530. (b) Withers, S.G., Rupitz, K. and Street, I. P. *J. Biol. Chem*., **1988**, 263, 7929.
48. Phenix, C. P., Rempel, B. P., Colobong, K., Doudet, D. J., Adam, M. J., Clarke, L. A. and Withers, S. G. Imaging of enzyme replacement therapy using PET. *PNAS.* **2010**, 107, 10842-10847.
49. Ridley, C. M., Thur, K. E., Shanahan, J., Thillaiappan, N. B., Shen, A., Uhl, K., Walden, C. M., Rahim, A. A., Waddington, S. N., Platt, F. M. and van der Spoel, A. C. beta-Glucosidase 2 (GBA2) Activity and Imino Sugar Pharmacology. *J. Biol. Chem*. **2013**, 288, 26052-26066.
50. Witte, M. D., Kallemeijn, W. W., Aten, J., Li, K. Y., Strijland, A., Donker-Koopman, W. E., van den Nieuwendijk, A. M., Bleijlevens, B., Kramer, G., Florea, B. I., Hooibrink, B., Hollak, C. E., Ottenhoff, R., Boot, R. G., van der Marel, G. A., Overkleeft, H. S. and Aerts, J. M.. Ultrasensitive *in situ* visualization of active glucocerebrosidase molecules. *Nat. Chem. Biol.* **2010**, 6, 907-913.
51. (a) Walvoort, M. T. C., Kallemeijn, W. W., Willems, L. I., Witte, M. D., Aerts, J. M. F. G., van der Marel, G. A., Codée, J. D. and Overkleeft. H. S. Tuning the leaving group in 2-deoxy-2-fluoroglucoside results in improved activity-based retaining b-glucosidase probes. *Chem. Commun*., **2012**, 48, 10386–10388. (b) Li, K. Y., Jiang, J., Witte, M. D., Kallemeijn, W. W., Donker-Koopman, W. E., Boot, R. G., Aerts, J. M., Codée, J. D., van der Marel, G. A. and Overkleeft, H. S. Exploring functional cyclophellitol analogues as human retaining beta-glucosidase inhibitors. *Org. Biomol. Chem*., **2014**, 12, 7786. (c) Jiang J., Beenakker, T. J., Kallemeijn, W. W., van der Marel, G. A., van den Elst, H., Codée, J. D. Aerts, J. M. F. G., and Overkleeft. H. S. Comparing Cyclophellitol N-Alkyl and N-Acyl Cyclophellitol Aziridines as Activity-Based Glycosidase Probes. *Chem. Eur. J*. **2015**, 21, 10861 – 10869. (d) Willems, L. I., Jiang, J., Li, K., Witte, M. D., Kallemeijn, W. W., Beenakker T. J. M., Schröder, S. P., Aerts, J. M., van der Marel, G. A., Codée, J. D. and Overkleeft. H. S. From Covalent Glycosidase Inhibitors to Activity-Based Glycosidase Probes. *Chem. Eur. J*. **2014**, 20, 10864 – 10872. (e) Jiang, J., Artola, M., Beenakker T. J. M., Schröder, S. P., Petracca, R., de Boer, C., Aerts, J. M., van der Marel, G. A., Codée, J. D. and Overkleeft. H. S. The Synthesis of Cyclophellitol-Aziridine and Its Configurational and Functional Isomers. *Eur. J. Org. Chem.* **2016**, 3671–3678.
52. Kallemeijn, W. W., Li, K. Y., Witte, M. D., Marques, A. R., Aten, J., Scheij, S., Jiang, J., Willems, L. I., Voorn-Brouwer, T. M., van Roomen, C. P., Ottenhoff, R., Boot, R. G., van den Elst, H., Walvoort, M. T., Florea, B. I., Codée, J. D., van der Marel, G. A., Aerts, J. M. and Overkleeft, H. S. Novel Activity-Based Probes for Broad-Spectrum Profiling of Retaining β-Exoglucosidases In Situ and In Vivo. *Angew. Chem-Ger Edit.* **2012**, 51(50), 12529-12533.
53. Jiang J., Beenakker, T. J., Kallemeijn, W. W., van der Marel, G. A., van den Elst, H., Codée, J. D. Aerts, J. M. F. G., and Overkleeft. H. S. Comparing Cyclophellitol N-Alkyl and N-Acyl Cyclophellitol Aziridines as Activity-Based Glycosidase Probes. *Chem. Eur. J*. **2015**, 21, 10861 – 10869.
54. Green, T. W. and Wuts, P. G. M. Protective Groups in Organic Synthesis, Wiley-Interscience, New York, **1999**, 217-224, 716-719.
55. Smith, M.W. and Gumbleton, M. Endocytosis at the blood-brain barrier: from basic understanding to drug delivery strategies. *J. Drug Target*. **2006**, 14, 191–214.

56. (a) Yadav, A. K., Shen, D. L., Shan, X., He, X., Kermode, A. R., Vocadlo, D.J. Fluorescence-Quenched Substrates for Live Cell Imaging of Human Glucocerebrosidase Activity. *J. Am. Chem. Soc.,* **2015**, 137, 1181−1189. (b) Jiang J., Beenakker, T. J., Kallemeijn, W. W., van der Marel, G. A., van den Elst, H., Codée, J. D. Aerts, J. M. F. G., and Overkleeft. H. S. Comparing Cyclophellitol N-Alkyl and N-Acyl Cyclophellitol Aziridines as Activity-Based Glycosidase Probes. *Chem. Eur. J*. **2015**, 21, 10861 – 10869.
57. Schirrmacher, R., Bernard-Gauthier, V., Reader, A., Soucy, J. P., Schirrmacher, E., Wangler, B. and Wangler, C. Design of brain imaging agents for positron emission tomography: do large bioconjugates provide an opportunity for *in vivo* brain imaging? *Future Med. Chem.* **2013**, 5(14), 1621–1634.
58. Bruzzone, M.G., D'Incerti, L., Farina, L.L., Cuccarini, V. and Finocchiaro, G. CT and MRI of brain tumors. *Q. J. Nucl. Med. Mol. Imaging.* **2012**, 56, 112–137.
59. Van Paesschen, W., Dupont, P., Sunaert, S., Goffin, K. and Van Laere, K. The use of SPECT and PET in routine clinical practice in epilepsy. *Curr. Opin. Neurol.* **2007**, 20, 194–202.
60. Smith, M.W. and Gumbleton, M. Endocytosis at the blood-brain barrier: from basic understanding to drug delivery strategies. *J. Drug Target*. **2006**, 14, 191–214.
61. Holland, J. P., Cumming, P. and Vasdev, N. PET radiopharmaceuticals for probing enzymes in the *Brain Am. J. Nucl. Med. Mol. Imaging,* **2013**, 3(3), 194-216.
62. Surti, S., Kuhn, A., Werner, M. E., Perkins, A. E., Kolthammer, J. and Karp, J. S. Performance of Philips Gemini TF PET/CT Scanner with Special Consideration for Its Time-of-Flight Imaging Capabilities. *J. Nucl. Med*. **2007,** 48(3), 471-480.
63. Huang, B., Law, M. W. and Khong, P. L. Whole-Body PET/CT Scanning: Estimation of Radiation Dose and Cancer Risk. *Radiology,* **2009**, 251(1).
64. Bradberry, S. M., Dickers, K. J., Rice, P., Griffiths, G. D. and Vale, J. A. Ricin poisoning. *Toxicol. Rev*. **2003**, 22(1), 65-70.
65. Feng, Y.J., Chen, W.R., Sun, T.P., Duan, S.Y., Jia, B.S. and Zhang, H.L**.** Estimated cosmic radiation doses for flight personnel. *Space Med. Med. Eng.*, **2002,** 15(4), 265–269.
66. Desai, T., da Silva, A. A. T, da Silva, A. J. R., Tinoco, L. W., Almeida, R. V., de Alencastro, R. B., Simas, A. B. C. and Freire D. M. G. The synthesis and resolution of (±)-1,4-di-*O*-benzyl-2,3-*O*-isopropylidene-*myo*-inositol. *Carbohyd. Res.,* **1994**, 258, 135-144.
67. (a) Oda, Y., Hada, K., Miyata, M., Takahata, C., Hayashi, Y., Takahashi, M., Yajima, N., Fujinami, M. and Ishikawa, T. Guanidinium Ylide mediated aziridination from arylaldehydes: Scope and limitations in the formation of unactivated 3-arylaziridine-2-carboxylates. *Synthesis-Germany*. **2014**. 46(16), 2201-2219. (b) Yun, J. M., Sim, T. B., Hahm, H. S., Lee, W. K. and Ha, H. J. Efficient synthesis of enantiomerically pure 2-acylaziridines: Facile syntheses of N-Boc-safingol, N-Boc-D-erythro-sphinganine, and N-Boc-spisulosine from a common intermediate. *J. Org. Chem.* **2003**, 68(20), 7675-7680.
68. Chavan, S. P., Khairnar, L. B., Chavan, P. N., and Kalbhor, D. B. A short enantioselective total synthesis of (R)- and (S)-pipecolic acid. *Tetrahedron Asymmetry.* **2014.** 25(16), 1246-1251.
69. Patwardhan, A. P., Lu, Z., Pulgam, V. R., and Wulff, W. D. Novel Ozone-Mediated Cleavage of the Benzhydryl Protecting Group from Aziridinyl Esters. *Org. Lett.*, **2005**, 7 (11), 2201–2204.
70. Liu, H., J., and Yip, J. Reductive Cleavage of Benzyl Ethers with Lithium Naphthalenide. A Convenient Method for Debenzylation. *Tetrahedron. Lett.* **1997**, 38(13), 2253-2256.
71. Santra, A., Ghosh, T., and Misra, A. K. Removal of benzylidene acetal and benzyl ether in carbohydrate derivatives using triethylsilane and Pd/C. *Beilstein J. Org. Chem.* **2013,** *9,* 74–78.

72. Witte, M. D., Witte, M. D., Horst, D., Wiertz, E. J. H. J., van der Marel, G. A. and Overkleeft, H. S. Synthesis and biological evaluation of a chitobiose-based peptide VV-glycanase inhibitor library. *J. Org. Chem.* **2009,** 74, (2), 605-616.
73. Kronvall, G. and Myhre, E.B. Differential staining of bacteria in clinical specimens using acridine orange buffered at lowpH. *Acta Pathologica et Microbiologica Scandinavica - Section B, Microbiology* **1977,** 85, 249-254.
74. Garegg, P. J., and Lindberg, B. SYNTHESIS OF SOME BENZYL AND METHYL ETHERS OF *myo*-INOSITOL. *Carbohyd. Res.,* **1988**, 173, 205-216.
75. Way, J. D., Wang, M., Hamann, I., Wuest, M., Wuest, F. Synthesis and evaluation of 2-amino-5-(4-[^{18}F]fluorophenyl)pent-4-ynoic acid ([^{18}F]FPhPA): A novel ^{18}F-labeled amino acid for oncologic PET imaging. *Nucl. Med. Biol.,* **2014**, 660-669.
76. Way, J. D., and Wuest, F. Automated radiosynthesis of no-carrier-added 4 [^{18}F]fluoroiodobenzene: a versatile building block in ^{18}F radiochemistry. *J. Label Compd. Radiopharm.,* **2014,** 57, 104–109.
77. Brichard, L., Aigbirhio, F. I. An Efficient Method for Enhancing the Reactivity and Flexibility of [^{18}F]Fluoride Towards Nucleophilic Substitution Using Tetraethylammonium Bicarbonate. *Eur. J. Org. Chem.* **2014**, 28, 6145-6149.
78. (a) Briggs GE, H. J., A Note on the Kinetics of Enzyme Action. *Biochemical Journal* **1925**, *19* (2), 338-339; (b) Michaelis L, M. M., Die Kinetik der Invertinwirkung. *Biochemische Zeitschrift* **1913**, *49*, 333- 369; (c) Johnson, K. A.; Goody, R. S., The Original Michaelis Constant: Translation of the 1913 Michaelis– Menten Paper. *Biochemistry* **2011**, *50* (39), 8264-8269.
79. Fowler, J. S., MacGregor, R. R., Wolf, A. P., Arnett, C. D., Dewey, S. L., Schlyer, D., Christman, D., Logan, J., Smith, M., Sachs, H. Aquilonius, S. M., Bjurling, P., Halldin, C., Hartvig, P., Leenders, K. L., Lundqvist, H., Oreland, L., Stalnacke, C. G., Langstrom, B. Mapping Human-Brain Monoamine Oxidase-A and Oxidase-B With C-11 Labeled Suicide Inactivators and PET. *Science* **1987,** 235, 481-485.
80. Castro, J. C., Malakhov, A. and Burgess, K. Synthesis of Regioisomerically Pure 5-Functionalized 2¢,7¢-Dichlorofluoresceins. *Synthesis*, **2009**, 7, 1224–1226.
81. Agarwal, S., Jain, R., Pal, D., and Mitra, A. K. Functional Characterization Of Peptide Transporters In MDCKII - MDR1 Cell line As A Model For Oral Absorption Studies. *Int. J. Pharm.* **2007**, 332(1-2), 147–152.
82. (a) Slobbe, P., Windhorst, A. D., Walsum, M. S., Smit, E. F., Niessen, H. G., Solca, F., Stehle, S., van Dongen, G. A. M. S. and Poot, A. J. A comparative PET imaging study with the reversible and irreversible EGFR tyrosine kinase inhibitors [11C]erlotinib and [18F]afatinib in lung cancer-bearing mice. *EJNMMI Research*, **2015**, 5, 14. (b) Marquez, B. V. Ikotun, O. F., Parry, J. J., Rogers, B. E., Meares, C. F. and Lapi, S. E. Development of a Radiolabeled Irreversible Peptide Ligand for PET Imaging of Vascular Endothelial Growth Factor. *J. Nucl. Med.,* **2014**, 55, 1029–1034.
83. Cid, M. B., Alfonso, F., Alonso, I., and Martin-Lomas, M. On the origin of the regioselectivity in glycosylation reactions of 1,2-diols. *Org. Biomol. Chem.*, **2009**, **7**, 1471–1481.

Appendix

Appendix 1a: ^{1}H NMR in $CDCl_3$ of Compound isolated from cold reaction of 40 with KF, K222, K_2CO_3 in ACN at 90°C for 15 minutes

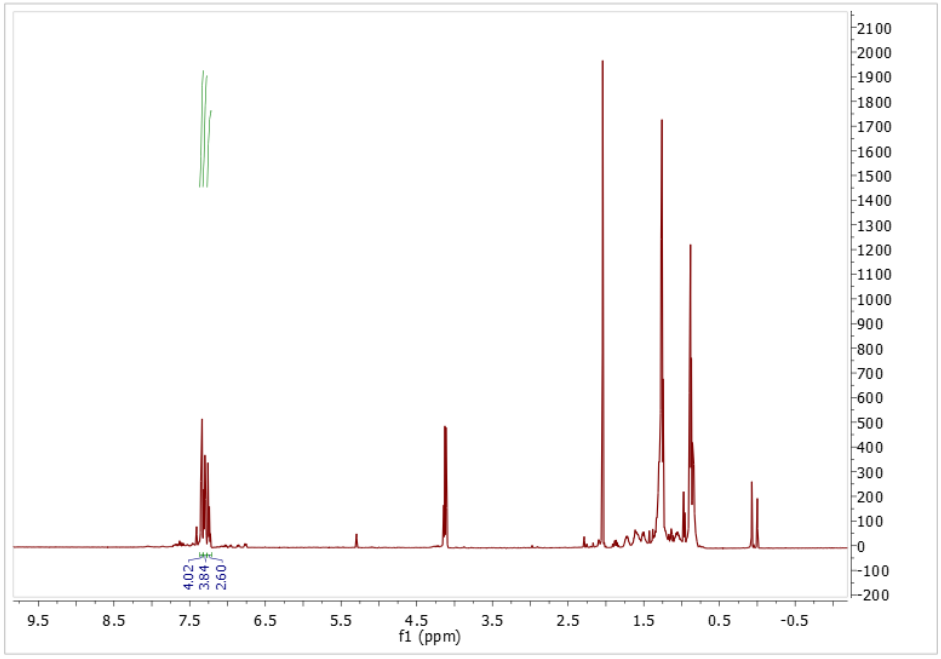

Appendix 1b: ^{1}H NMR in $CDCl_3$ of Compound isolated from cold reaction of 40 with KF, K222, K_2CO_3 in ACN at 90°C for 15 minutes